

Polimery w Medycynie

Polymers in Medicine

BIANNUAL ISSN: 0370-0747 e-ISSN: 2451-2699

polimery.umw.edu.pl

2025, Vol. 55, No. 1 (January–June)

Ministry of Science and Higher Education – 70 pts.
Index Copernicus (ICV) – 121.14 pts.



WROCLAW
MEDICAL UNIVERSITY

Polimery w Medycynie
Polymers in Medicine



Polimery w Medycynie

Polymers in Medicine

ISSN 0370-0747 (PRINT)

ISSN 2451-2699 (ONLINE)

polimery.umw.edu.pl

BIANNUAL
2025, Vol. 55, No. 1
(January–June)

“Polymers in Medicine” is an independent, multidisciplinary forum to exchange scientific and clinical information, which publishes original papers (technical, analytical, experimental, clinical), preliminary reports and reviews regarding the use of polymers (natural and synthetic) and biomaterials in different specialties of medicine (biochemistry, clinical medicine, pharmacology, dentistry, implantology), biotechnology and veterinary science.

Address of Editorial Office

Marcinkowskiego 2–6
50-368 Wrocław, Poland
Tel.: +48 71 784 11 33
E-mail: redakcja@umw.edu.pl

Editor-in-Chief

Prof. Witold Musiał

Deputy Editor

Dr. Konrad Szustakiewicz, DSc., Eng.

Statistical Editors

Wojciech Bombała, MSc
Anna Kopszak, MSc
Dr. Krzysztof Kujawa
Jakub Wronowicz, MSc
Maciej Wuczyński, MSc

Publisher

Wrocław Medical University
Wybrzeże L. Pasteura 1
50-367 Wrocław, Poland

Scientific Committee

Prof. Mirosława El-Fray
Prof. Franciszek Główka
Prof. Jörg Kreßler
Dr. Anna Krupa
Prof. Maciej Małecki
Prof. Bożena B. Michniak-Kohn

Prof. Wojciech Miltik
Prof. Masami Okamoto
Prof. Elżbieta Pamuła
Prof. Wiesław Sawicki
Prof. Szczepan Zapotoczny

Online edition is the original version of the journal

Section Editors

Dr. Tomasz Urbaniak
(synthesis, evaluation, medical use
of polymers, sensitive to environmental
factors, applied in controlled and targeted
drug delivery)

Dr. Monika Gasztych
(preparation, assessment and application
of polymers in pharmaceutical technology
and medical devices)

Dr. BEng., Agnieszka Gadomska-Gajadur
(synthesis and characterization of polymers
having biomedical potential, composites for
regenerative medicine)

Manuscript editing

Paulina Piątkowska, Marek Misiak

Editorial Policy

During the review process, the Editorial Board conforms to the "Uniform Requirements for Manuscripts Submitted to Biomedical Journals: Writing and Editing for Biomedical Publication" approved by the International Committee of Medical Journal Editors (<http://www.icmje.org/>). Experimental studies must include a statement that the experimental protocol and informed consent procedure were in compliance with the Helsinki Convention and were approved by the ethics committee.

For more information visit the following page: <https://polimery.umw.edu.pl>

Indexed in: Scopus, OCLC, WorldCat, PBL, EBSCO, MEDLINE, Index Copernicus

Typographic design: Monika Kołęda, Piotr Gil

Cover: Monika Kołęda

DTP: Wrocław Medical University Press

Printing and binding: Drukarnia I-BiS Bierońscy Sp.k.

Circulation: 11 copies

Contents

- 5 Preface
- 6 Wstęp

Original papers

- 7 Tioluwani Ibukun Adegbolagun, Olubusola Ayoola Odeniyi, Michael Ayodele Odeniyi
Native and pregelatinized starches of bitter yam as film formers for oral dissolving formulations
- 21 Tabarak S. Jassim, Sura S. Talib, Nawar R. Jaber, Dina H. Sahib, Rusul W. Ali, Bahaa Al-Rubaii
Impact of hepatitis C virus on *IFITM3* gene expression: A comprehensive analysis incorporating serological detection and viral load quantification via qPCR
- 31 Shams Ihssan Sadiq, Jenan Atiyah Ghafil
Polyhydroxybutyrate nanoparticle improving the sensitivity of *Pseudomonas aeruginosa* to ceftriaxone and reducing the biofilm formation in vitro
- 41 Maja Prajzner, Maria Twarda, Witold Musiał
The influence of selected polyoxyethylene glycols on the electrical conductivity of isosmotic and hyperosmotic sodium chloride solutions
- 49 Urszula Bąk-Kuciejda, Teresa Witczak, Mariusz Witczak, Anna Krupa
The impact of semisolid matrices on spreadability, rheology and celecoxib release rate

Reviews

- 59 Radosław Błok, Grzegorz Myszczyński, Artur Wiatrowski, Marek Tomiałowicz, Maria Pomorska, Jerzy Florjanski
Applications of biomaterials in reconstructive gynecology

Research letters

- 67 Agnieszka Gola, Adrianna Złocińska
Impact of polymerization reaction conditions on the stability of naproxen sodium

PREFACE

Dear Readers,

In this hot and sometimes difficult to analyze period of the history of our globe, we present following issue of the journal “Polimery w Medycynie – Polymers in Medicine”, which may contribute to a sense of good communication between scientists from all over the world, especially since our journal achieved a high CiteScore level for 2024, which now stands at 3.5.



This issue of “Polimery w Medycynie – Polymers in Medicine” includes articles from three continents: Africa, Asia and Europe. These publications were prepared by researchers from renowned universities, recognized worldwide and dynamically developing – University of Baghdad, University of Ibadan, Jagiellonian University, and Medical University of Wrocław. The work submitted from the first mentioned university, prepared in its Department of Biology, presents the beneficial effect of polymer nanoparticles based on polyhydroxybutyrate on the sensitivity of *Pseudomonas aeruginosa* bacteria to the antibiotic ceftriaxone and on the formation of an appropriate biofilm. An extremely interesting work from the second mentioned center, from its Department of Pharmaceutics and Industrial Pharmacy and the Department of Microbiology, describes the potential of bitter sweet potato as a pharmaceutical raw material for obtaining a modified polymer of natural origin for use in films covering solid forms of drugs.

Among papers from Europe, I would like to draw your attention to an original article from the Jagiellonian University, in which the authors took up a very important problem from the point of view of, i.e., oncological patients, i.e., the development of the issue of dermatological formulation of celecoxib. The Wrocław center can boast an interesting work on classical and innovative polymeric bioconstructive materials used in gynecology. Other articles were also highly rated by the review team. They present current issues of polymer science applied in medicine: quantitative DNA polymerase chain reaction in studies of the effect of the hepatitis C virus on the expression of the *IFITM3* gene, and the synthesis and studies of the properties of polymers as carriers of medicinal substances, including naproxen.

On behalf of the entire editorial team, I wish you a good and fruitful reading of the presented articles, but also peaceful holidays. I encourage you to send in more manuscripts (original papers and reviews), and I hope that our joint work, even to a minimal extent, will influence the further development of international cooperation between researchers from different countries. I would also like to thank my colleagues – editors and reviewers – for their undeniable contribution to the creation of this edition of “Polimery w Medycynie – Polymers in Medicine”.

Witold Musiał, PhD, DSc, Prof.
Editor-in-Chief
Polimery w Medycynie – Polymers in Medicine

WSTĘP

Drodzy Czytelnicy,

w tym gorącym i czasem trudnym w analizie okresie historii naszego globu przedstawiamy kolejny numer czasopisma „Polimery w Medycynie – Polymers in Medicine”, który być może przyczyni się do poczucia dobrej łączności pomiędzy naukowcami z całego świata – tym bardziej, że nasze czasopismo uzyskało za rok 2024 wysoki poziom wskaźnika CiteScore i wynosi on teraz 3.5.



Prezentowany Państwu numer „Polimerów w Medycynie – Polymers in Medicine” zawiera artykuły z trzech kontynentów: Afryki, Azji i Europy. Publikacje zostały przygotowane przez badaczy z uznanych uczelni, z ośrodków uniwersyteckich rozpoznawanych na całym świecie i dynamicznie rozwijających się – Uniwersytetu w Bagdadzie, Uniwersytetu w Ibadanie, Uniwersytetu Jagiellońskiego czy Uniwersytetu Medycznego we Wrocławiu. Nadesłana z pierwszej wymienionej uczelni praca, przygotowana w tamtejszym Zakładzie Biologii, przedstawia korzystny wpływ polimerowych nanocząstek na bazie polihydroksymaślanu na wrażliwość bakterii *Pseudomonas aeruginosa* na antybiotyk ceftriakson oraz na tworzenie się odpowiedniego biofilmu. Niezwykle ciekawa praca z drugiego wymienionego ośrodka, z Zakładu Farmacji Przemysłowej oraz Zakładu Mikrobiologii, opisuje potencjał gorzkiego batatu jako surowca farmaceutycznego do otrzymywania zmodyfikowanego polimeru pochodzenia naturalnego w celu zastosowania w filmach pokrywających stałe postacie leku.

Wśród prac z Europy chciałbym zwrócić Państwa uwagę na artykuł oryginalny z Uniwersytetu Jagiellońskiego, w którym autorzy podjęli się problemu bardzo ważnego z punktu widzenia m.in. pacjentów onkologicznych, tj. opracowania zagadnienia dermatologicznej formułacji celekoksylu. Ośrodek wrocławski może pochwalić się ciekawą pracą nt. klasycznych i najnowszych polimerowych materiałów biorekonstrukcyjnych stosowanych w ginekologii. Również pozostałe artykuły zostały wysoko ocenione przez zespół recenzencki. Prezentują one bowiem aktualne zagadnienia nauki o polimerach zastosowane w medycynie: ilościową reakcję łańcuchową polimerazy DNA w badaniach wpływu wirusa zapalenia wątroby typu C na ekspresję genu *IFITM3*, oraz syntezę i badania właściwości polimerów jako nośników substancji leczniczych, w tym naproksenu.

Życzę Państwu, w imieniu całego zespołu redakcyjnego, dobrej i owocnej lektury przedstawianych artykułów oraz spokojnych wakacji. Zachęcam do nadsyłania kolejnych manuskryptów oryginalnych i przeglądowych oraz mam nadzieję że nasza wspólna praca choćby w minimalnym stopniu wpłynie na dalszy rozwój współpracy międzynarodowej badaczy z różnych krajów. Przy okazji dziękuję współpracownikom – redaktorom i recenzentom – za niezaprzeczalny wkład w powstanie tego wydania „Polimerów w Medycynie – Polymers in Medicine”.

Prof. dr hab. Witold Musiał
Redaktor naczelny
Polimery w Medycynie – Polymers in Medicine

Native and pregelatinized starches of bitter yam as film formers for oral dissolving formulations

Tioluwani Ibukun Adegbolagun^{1,B–D,F}, Olubusola Ayoola Odeniyi^{2,B,C,E,F}, Michael Ayodele Odeniyi^{1,A,C–F}

¹ Department of Pharmaceutics and Industrial Pharmacy, University of Ibadan, Nigeria

² Department of Microbiology, University of Ibadan, Nigeria

A – research concept and design; B – collection and/or assembly of data; C – data analysis and interpretation;

D – writing the article; E – critical revision of the article; F – final approval of the article

Polymers in Medicine, ISSN 0370-0747, eISSN 2451-2699

Polim Med. 2025;55(1):7–19

Address for correspondence

Michael Ayodele Odeniyi

E-mail: deleodeniyi@gmail.com

Funding sources

None declared

Conflict of interest

None declared

Received on January 31, 2025

Reviewed on March 13, 2025

Accepted on March 14, 2025

Published online on June 30, 2025

Cite as

Adegbolagun TI, Odeniyi OA, Odeniyi MA. Native and pregelatinized starches of bitter yam as film formers for oral dissolving formulations. *Polim Med.* 2025;55(1):7–19. doi:10.17219/pim/202946

DOI

10.17219/pim/202946

Copyright

Copyright by Author(s)

This is an article distributed under the terms of the Creative Commons Attribution 3.0 Unported (CC BY 3.0) (<https://creativecommons.org/licenses/by/3.0/>)

Abstract

Background. Oral dissolving films are portable dosage forms that consist of active pharmaceutical ingredients incorporated into film-forming polymers such as starch. Starches obtain optimum filmogenic properties by gelatinization and blending with other polymers. The high starch content of bitter yam (*Dioscorea dumetorum* Pax) gives it yet unexplored potential for orodispersible films.

Objectives. This study aimed to investigate the effect of pregelatinization on the physicochemical properties of bitter yam starch. Additionally, our objective was to evaluate the potential of both native starch (NS) and pregelatinized starch (PS), incorporated into polymer blends, as biopolymeric materials for use in orally dissolving films (ODFs).

Materials and methods. Native and pregelatinized wild *Dioscorea dumetorum* Pax (bitter yam) starch were prepared and characterized using physicochemical, microscopic and rheological methods, Fourier-transform infrared spectroscopy, X-ray diffractometry (XRD), and differential scanning calorimetry (DSC). Oral dissolving films with varying hydroxylpropylmethyl cellulose (HPMC)-to-starch ratios (1:1, 1:2 and 2:1) were formulated and evaluated based on organoleptic properties, surface morphology, folding endurance, weight and thickness, pH, and disintegration time.

Results. Pregelatinization improved the swelling, solubility and hydration capacity of the starch. Although no changes were observed in the crystalline nature upon gelatinization, DSC analysis revealed remarkable changes in the thermal behavior of the NS after pregelatinization. Both NS and PS did not produce continuous films without HPMC. Flexibility of the starch increased with increasing HPMC concentration films, and PS-based films had higher folding endurance compared to NS films. Native starch-based films had smoother surfaces and higher thicknesses than PS films. All the starch films demonstrated disintegration times longer than 15 min, and slightly acidic pH values.

Conclusions. Pregelatinization of bitter yam starch, followed by blending with HPMC at a 2:1 ratio, resulted in the most effective oral film formulation. Further studies focusing on optimizing disintegration rates and pH would help confirm the suitability of this starch for use in ODF formulations.

Key words: starch pregelatinization, bitter yam, orodispersible films, film formers

Background

As the most abundant polysaccharide and the 2nd most abundant renewable polymer in nature, starch is a biopolymer that has found vast applications in several industries.^{1,2} Starch is utilized in the manufacturing of food, textiles, paper, and cosmetics as an adhesive, thickening, stabilizing, and gelling agent. In the pharmaceutical industry, starch is considered to be in the top 10% of excipients used in drug formulations as a multifunctional excipient in tablet formulations as a binder, disintegrant, filler, and/or lubricant.^{3,4}

Dioscorea dumetorum Pax (bitter yam) is one of the most economically valuable species in the *Dioscorea* genus and *Dioscoreaceae* family.⁵ It typically has white or lemon-colored tubers. The wild form is sometimes used as animal poison when mixed with bait.⁵ Although the tubers from edible or wild varieties are usually boiled before consumption, the wild-type tubers have to be soaked in running water for several days after cutting to remove toxic or bitter compounds.⁶ In past studies, bitter yam starch has been modified by acetylation and pregelatinization to improve its tableting properties.^{6,7}

Native starches (NS) have limited application potential in the pharmaceutical industry due to poor thermal stability, high brittleness, high viscosity, and poor solubility.⁷ As such, they have to be modified to improve their functional properties. Pregelatinization is achieved by a combination of heating and mechanical shearing activities, followed by drying and grinding. The resultant modified starch has higher cold-water solubility and swellability, thickening/gelling capabilities, and improved flowability.⁸ Consequently, pregelatinized starches (PS) are widely utilized in the pharmaceutical industry as a multifunctional versatile excipient, functioning as a binder, disintegrant and filler in formulations.⁹

Oral dissolving films (ODFs) are small flat dosage forms made from hydrophilic polymers that incorporate active pharmaceutical ingredients. They are designed to dissolve in the mouth and release drugs rapidly within 60 s without chewing.¹⁰ Their large surface area and thin design facilitate rapid disintegration, drug release and absorption through the oral mucosa. This allows for direct systemic absorption, bypassing pre-systemic metabolism and gastrointestinal degradation. Additionally, they offer convenience for patients who experience difficulty swallowing.^{10,11}

Polymers serve as film formers for ODFs and provide the mechanical strength required for film integrity.¹¹ Various native and modified starches, as well as gums, have been utilized in the formulation of films for drugs such as diclofenac,¹² chlorpheniramine,^{13,14} amlodipine,¹⁵ buspirone hydrochloride,¹⁶ and even plant extracts like *Zingiber officinale* (ginger).¹⁷ To function effectively as film formers in ODFs, starches must be gelatinized and plasticized to develop suitable filmogenic properties, an effect that can also be achieved by blending them with other polymers.¹⁵

Objectives

Although extensive studies have been carried out on the suitability of various starch forms as biopolymers for oral dissolving films, the suitability of starches from bitter yam remains largely unexplored. In this study, we identify the effect of pregelatinization on the physical, chemical and pasting properties of bitter yam starch. We further investigate the applicability of both starch forms in hydroxyl-propylmethyl cellulose (HPMC)-starch blends as film formers for oral dissolving films.

Materials and methods

Materials

The major materials used include tubers of bitter yam (sourced from Aawe, Oyo Town, Nigeria), sodium hydroxide, and hydrochloric acid (BDH Chemicals Limited, Poole, UK), sodium chloride (BDH Chemicals Limited) and distilled water (Department of Pharmaceutics and Industrial Pharmacy Laboratory, University of Ibadan, Nigeria). The phosphate buffers were prepared from 2 packages containing disodium hydrogen phosphate dehydrate and potassium dihydrogen phosphate (BDH Chemical Limited).

Methods

Collection of bitter yam and extraction of starch

The tubers were washed, peeled and cut into smaller sizes using a knife. The cut pieces were soaked in distilled water for 48 h and milled using a local grinding machine. The formed slurry was strained through a muslin cloth and the filtrate was left to stand for 24 h. The sediment was washed twice daily for 4 days with distilled water and the remaining residue was dried to a constant weight at 50°C in a hot-air oven (Gallenkamp BS 250 size 1; Gallenkamp Labs, London, UK). The dried flakes were milled using a laboratory mill (Panasonic MX-AC400; Panasonic, Tokyo, Japan) and passed through a sieve of pore size of 250 µm.¹⁸

Pregelatinization of bitter yam starch

Quantities (100 g) of NS were dispersed in 100 mL of distilled water and heated at 55°C with slow constant stirring for 10 min. The resultant starch pastes were spread into thin films on clean ceramic tile and dried in a hot-air laboratory oven (TT-9083; Techmel & Techmel Ltd, Onitsha, Nigeria) at 60°C for 24 h. After this, the dried flakes were comminuted using a laboratory mill (Panasonic MX-AC400; Panasonic) and screened through a sieve of pore size of 250 µm.^{19,4}

Characterization of the starches

Particle size and morphology

Samples of the starches were thinly spread on microscope slides of a digital microscope (VJ-2005 DN model Bio-microscope®; WanTong Precision Instruments, Wuhan, China) and examined at $\times 400$ magnification. The particle diameters of 100 particles were measured using TS View CX Image® software (v. 6.2.4.3) and Motic Image 2000 (Motic China Group Co., Ltd., Xiamen, China). The mean particle size and standard deviation (SD) for each starch were determined using GraphPad Prism v. 8.0.1 (GraphPad Software, San Diego, USA) and recorded.

Determination of pH

Starch dispersions of 1.0%, 2.5%, 5.0%, 7.5%, and 10.0% w/v concentrations were prepared and allowed to hydrate for 2 h. The pH values of the dispersions were measured with a pH meter (FiveEasy FP20-Meter; Mettler-Toledo GmbH, Greifensee, Switzerland).^{4,18}

Determination of solubility in water

Quantities (1.0 g) of starch were dispersed in 15 mL of distilled water, stirred for 5 min, and then heated at around 80°C on a steam bath with constant stirring. The slurry was transferred to a centrifuge tube and distilled water was added to make up to 30 mL. The mixture was separated with a centrifuge (Biobase TDL-50 Electric Centrifuge; Biobase Group, Jinan, China) at 4,000 rpm for 20 min, and the supernatant was decanted into a weighed glass petri dish (w_2) and dried in a hot-air oven (Techmel and Techmel TT-9083; Techmel & Techmel Ltd) to a constant weight (w_3) at 100°C. The percent solubility was calculated using the following formula¹⁹:

$$\% \text{Solubility} = \frac{(w_3 - w_2)}{w} \times 100$$

Determination of moisture content

Two grams (2 g) samples of each starch were separately weighed and placed on the weighing balance/heating plate of an infrared moisture analyzer (MX-50; A&D, Wood Dale, USA) and dried till their weights were constant. The determination was done in triplicates.¹⁸

Determination of swelling capacity

Ten-gram (10 g) quantities of NS and PS were weighed into clean 100-mL measuring cylinders and their tapped volumes (V_a) were determined and recorded. Subsequently, the starches were dispersed in 50 mL quantities of the media solutions (distilled water, 0.1 M hydrochloric acid (HCl), pH 6.8 phosphate-buffered saline (PBS) and pH 7.4 phosphate

buffer); next, the volumes were made up to 100 mL with the respective solvents. The cylinders were sealed and left to stand on the shelf for 24 h, after which the volumes of the sediments (V_b) were measured. The swelling indices of the starches in the mediums were calculated with the formula⁴:

$$SI = \frac{V_b}{V_a}$$

Determination of hydration capacity

One gram quantities of the starch powders were transferred into pre-weighed 50 mL centrifuge tubes (w_1), and the tubes were reweighed to determine the total weight (w_2). Ten milliliters of distilled water were added to the tube, which was then shaken for 2 min and allowed to stand for 10 min, with intermittent shaking at the 5-min and 10-min marks. The samples in tubes were centrifuged at 4,000 rpm for 10 min, after which the supernatant was carefully to leave the sediment and the tube was weighed again (w_2). The hydration capacity was calculated as the percentage ratio of sediment weight ($w_2 - w_1$) to the dry starch weight⁵:

$$HC = \frac{(w_2 - w_1)}{w}$$

Determination of particle density

A clean, empty 50-mL pycnometer bottle was weighed (w), then completely filled with xylene in a well-ventilated area and sealed with its lid; any excess liquid was carefully wiped off. The pycnometer with its content was weighed again (w_1). A 5 g quantity of the starch was weighed (w_3) into the pycnometer. The excess xylene was wiped off and the bottle was re-weighed (w_4). The particle density was calculated using the equation below²⁰:

$$\text{Particle density} = \frac{w \times w_3}{50(w_3 - w_4 + w_2 + w)}$$

Determination of bulk density, tapped density and porosity

Bulk density of each starch sample was determined by pouring 10 g of starch into a 100-mL graduated cylinder (25 mm in diameter) through a short-stemmed glass funnel positioned at a 45° angle. The height reached by the powder was measured and the volume was calculated. In measuring the tapped density (pt), the starch sample in the measuring cylinder was subjected to 100 taps at a metronome-controlled pace of 38 taps per minute from a height of 2.54 cm. The resultant height was measured and used to calculate the tapped volume. The bulk density (pb) and tapped density (pt) were calculated as the ratios of the mass of starch to the respective volumes calculated.^{7,21} The formulas used in calculating the volume and density are stated below:

$$\text{Volume} = \pi r^2 h,$$

where:

r – radius of the measuring cylinder;

h – height of the sample in the measuring cylinder.

$$\text{Density} = \frac{\text{mass}}{\text{volume}}$$

The powder porosity (e) was further calculated using the equation below²²:

$$e = \left(1 - \frac{\rho_b}{\rho_s} \times 100\%\right)$$

Determination of angle of repose

A 5 g quantity of starch powder was weighed and allowed to flow freely through a funnel under the influence of gravity into an open-ended cylinder with a known diameter, positioned on a cork base resting on a horizontal surface. The height of the conical heap formed was measured and used with dimension of the cylinder to calculate the angle of repose (θ), using the formula below²³:

$$\tan \theta = \frac{h}{r},$$

where: h – height of powder heap;

r – radius of the open-ended cylinder used.

Determination of Hausner ratio and compressibility index

The Hausner ratio of each starch density determination was calculated as ratio of the tapped density (ρ_t) to the bulk density (ρ_b), while the Carr compressibility index was calculated using the equation below²¹:

$$\text{Carr's index} = \frac{(\rho_t - \rho_b)}{\rho_t} \times 100\%$$

$$\text{Hausner ratio} = \frac{\rho_t}{\rho_b}$$

Pasting properties of the starches

The pasting properties of the NS and PS were determined using a heating and cooling viscometer (Rapid Visco Analyzer (RVA) model Super 4; Newport Scientific, Warriewood, Australia), and viscosity profile in the form of an amylograph was generated using Thermocline for Windows (Newport Scientific).⁴ Three-gram (3 g) samples of each starch type were dispersed in 30 mL of water within the sample holding can, using the RVA paddle for mixing. Each analysis ran for 13 min; the stirring speed was set at 960 rpm for the first 8 s, after which it was maintained at 160 rpms for the rest of the analysis. The temperature was initially set to 50°C and held for 1 min, then gradually increased to 95°C over 3 min. It was maintained at 95°C for 4 min, then reduced back to 50°C over another 3 min, and held at 50°C for the final 2 min.²⁴ Viscoamylographs were generated and used to determine various pasting parameters, including peak viscosity,

final viscosity, setback viscosity, breakdown viscosity, and peak temperature.¹⁸

Fourier transform infrared spectroscopy

The Fourier transform infrared (FT-IR) spectra were obtained at room temperature using an FT-IR spectrophotometer (PerkinElmer SpectrumTwo UATR Two; PerkinElmer, Waltham, USA) with the attenuated total reflection (ATR) mode.²⁵ Minute starch powder samples were loaded onto the diamond crystal sample stage, pressed using the apparatus clamp, and analyzed at a resolution of 4 cm⁻¹ across the wavelength range of 400–4,000 cm⁻¹.

X-ray diffractometry

The analysis was done at ambient temperature using an X-ray diffractometer (Rigaku Miniflex 600; Rigaku, Tokyo, Japan). The samples were finely homogenized and compressed into a flat, smooth surface in the flat sample holder, and mounted on the sample stage. The samples were analyzed using on the reflection–transmission spinner stage at the theta–theta settings. The equipment was operated at an accelerating potential of 30 kV and a current of 40 mA, using a programmable divergent slit with a 5 mm-wide mask and a goni scan. The diffraction angle (2θ) ranged from 3° to 70°, with a step size of 0.02° and a dwell time of 1.0 s per step. A CuK α radiation was generated by the anode and the intensity of diffracted X-rays was continuously recorded as the sample and detector rotated through their respective angles. Using Origin software v. 6.0 (Microcal Software Inc., Northampton, USA), the results (diffractograms) were presented as X–Y plots of peak positions at 2θ vs X-ray intensity (counts).¹⁸

Differential scanning calorimetry

Thermal analysis of the starches was done using a Differential Scanning Calorimeter (Mettler-Toledo DSC; Mettler-Toledo, Columbus, USA). Sample quantities were weighed into hermetic aluminum pans and sealed tightly, while a tightly sealed empty pan was used as the reference. Both pans were placed in their allocated slots in the calorimeter. The nitrogen gas tank was turned on and maintained at a pressure of 20 psi and flow rate of 50 mL/min. Under nitrogen gas atmosphere, the sample and reference pans were heated at a rate of 10°C/min from 35°C to 250°C. Differential thermograms of the starch samples, reflecting their thermal responses, were generated using STARe SW 13.00 software (Mettler-Toledo). The differential thermograms were normalized to the mass of starches used for the analysis.

Formulation of ODFs of the starches

Blends of NS and PS with hydroxypropyl methylcellulose (HPMC) were prepared in 5 different ratios (1:0, 1:1, 1:2, 2:1, and 0:1) using a mortar and pestle. Three grams of each polymer, both starch and starch–polymer blends, were individually dispersed in 30 mL of distilled water and stirred using a magnetic stirrer (Bante Instruments MS300; Bante Instruments, Shanghai, China) at 400 rpm. Subsequently, 0.3 mL of glycerol was added to each mixture. The resulting solutions were further stirred for 10 min. The final solutions were poured into clean Petri dishes and left to stand overnight to remove bubbles. Afterward, the Petri dishes were dried in a laboratory oven (TT-9083; Techmel & Techmel) at 60°C for 24 h. The films were carefully removed from the plates, cut into intact 2 × 2 cm pieces, and stored in an airtight container.¹⁵ Table 1 shows the formulae of the oral dissolving films.

Evaluation of oral dissolving films of the starches

Organoleptic test

The organoleptic properties of film samples were evaluated by visually observing their color, texture and transparency.¹⁷ The surface textures of the films were examined by rubbing the films between a clean thumb and index finger.¹⁵

Evaluation of surface morphology

The surface morphology of the films was examined using a light microscope (Zeiss Axioskop 40; Carl Zeiss AG, Oberkochen, Germany) fitted with a digital camera (Canon PowerShot A620; Canon, Tokyo, Japan), which was used to take photomicrographs. Cut samples of 1 × 1 cm were placed on microscope slides using a forceps and viewed at ×10 magnification.

Determination of weight and thickness variation

Five films from each batch of films were weighed and the mean weight of each batch was calculated; the deviation from the mean was determined as the weight variation.¹⁴ The thickness of sample films was measured using a digital micrometer screw gauge at the 4 corners and the center of the films.¹⁶

Determination of film pH

Cut samples from each formulation batch were dissolved in 10 mL of distilled water and the pH was determined using a pH meter (FiveEasy FP20-Meter; Mettler-Toledo).¹⁴

Determination of the folding endurance

Film strips from each batch were repeatedly folded at the same point across a 180° angle until they broke; the number of folds endured before breakage was recorded as the folding endurance value.¹⁶

In vitro disintegration test

Selected films from each batch were cut into 1 × 1 cm samples and placed on 2 mL of water in a Petri dish. The average time taken for 3 films from each batch to completely disintegrate was determined as the disintegration time for the entire batch.¹⁵

Statistical analyses

Determinations were done in triplicates; the average and standard deviation values were calculated. Data obtained from the various studies were subjected to statistical analysis via Students' t-test and analysis of variance (ANOVA) at $p < 0.05$ significance limit using GraphPad Prism 8.0.1 (GraphPad Software).

Table 1. Formulation composition of starch oral dissolving films

Formulation No.	Formulation codes	HMPc:starch ratio	Quantity of film former [g]			Volume of glycerin [mL]	Volume of distilled water [mL]
			HPMC	NS	PS		
1.	HP	1:0	3	–	–	0.3	30
2.	NS	0:1	–	3	–	0.3	30
3.	PS	0:1	–	–	3	0.3	30
4.	NS-a	1:2	1	2	–	0.3	30
5.	NS-b	1:1	1.5	1.5	–	0.3	30
6.	NS-c	2:1	2	1	–	0.3	30
7.	PS-a	1:2	1	–	2	0.3	30
8.	PS-b	1:1	1.5	–	1.5	0.3	30
9.	PS-c	2:1	2	–	1	0.3	30

HPMC – hydroxypropylmethyl cellulose; NS – native starch; PS – pregelatinized starch.

Results

The results of the characterization of these formulations are summarized in Table 2 and presented in this section.

Characterization of native and pregelatinized starches

Particle size, and morphology

The result of particle size analysis as shown in Table 2 revealed a significant ($p < 0.05$) increase in mean particle size from $0.83 \pm 0.33 \mu\text{m}$ (NS) to $25.27 \pm 11.07 \mu\text{m}$ (PS). The photomicrograph (Fig. 1) of the NS and PS at $\times 400$ magnification showed a distinct morphological change after pregelatinization.

Native starch particles appeared smaller with smoother spherical shapes and relatively uniform distributions, while PS particles were larger, with fragmented irregular shapes and heterogenous size distribution.

pH and swellability

Both starches had acidic pH values, but the PS was more acidic. The swelling indices were significantly ($p < 0.05$)

Table 2. Physicochemical and flow properties of native and pregelatinized bitter yam starch

Evaluation parameter		Starch form	
		NS	PS
Mean particle size [μm]		0.83 ± 0.33	25.27 ± 11.07
pH values	1.0%	3.09 ± 0.01	2.63 ± 0.40
	2.5%	2.75 ± 0.06	2.55 ± 0.02
	5.0%	2.69 ± 0.02	2.24 ± 0.02
	7.5%	2.63 ± 0.03	1.87 ± 0.19
	10.0%	2.57 ± 0.02	2.28 ± 0.07
Solubility [%]		8.50 ± 0.16	10.56 ± 0.15
Moisture content [%]		13.36 ± 0.15	12.10 ± 0.84
Water absorption index		2.22 ± 0.03	3.59 ± 0.14
Swelling index	Water	1.38 ± 0.03	2.92 ± 0.24
	0.1M HCl	1.19 ± 0.01	3.03 ± 0.52
	6.8 phosphate buffer	1.43 ± 0.04	3.48 ± 0.21
	7.4 phosphate buffer	1.33 ± 0.04	3.93 ± 0.38
Particle density [g/cm^3]		1.47 ± 0.01	1.52 ± 0.02
Bulk density [g/cm^3]		0.40 ± 0.02	0.64 ± 0.03
Tapped density [g/cm^3]		0.60 ± 0.02	0.72 ± 0.02
Porosity [%]		72.76	58.15
Hausner ratio		1.51 ± 0.08	1.14 ± 0.06
Carr compressibility index		33.63 ± 3.63	12.18 ± 4.71
Angle of repose [$^\circ$]		57.18 ± 4.47	43.78 ± 0.77

mean \pm standard deviation; NS – native starch; PS – pregelatinized starch.

higher in PS across all media. Swelling index values ranged from 1.19 to 1.43 and from 2.92 to 3.93 for the NS and PS, respectively.

Solubility, moisture content and hydration capacity

Overall, PS demonstrated higher solubility (10.56% vs 8.50%), lower moisture content (12.10% vs 13.40%) and higher hydration capacity (3.6 vs 2.2) than NS.

Particle density, tapped density and bulk density

There was a general increase in all forms of density post-gelatinization. For particle density, PS had a value of $1.52 \text{ g}/\text{cm}^3$ and NS had $1.47 \text{ g}/\text{cm}^3$. The increase in the tapped and bulk densities was more significant ($p < 0.05$), as shown by PS having 0.64 and $0.72 \text{ g}/\text{cm}^3$ bulk and tapped density respectively, and the NS having 0.40 and $0.60 \text{ g}/\text{cm}^3$ bulk and tapped density, respectively.

Hausner ratio, Carr compressibility index, porosity, and angle of repose

Table 2 shows a significant ($p < 0.05$) reduction in Hausner ratio (1.14 vs 1.51) and Carr compressibility index (12.18% vs 33.63%) after pregelatinization. The angle of repose decreased from 57.18° in NS to 43.78° in PS, and the porosity of NS decreased from 72.76% to 58.15% in PS.

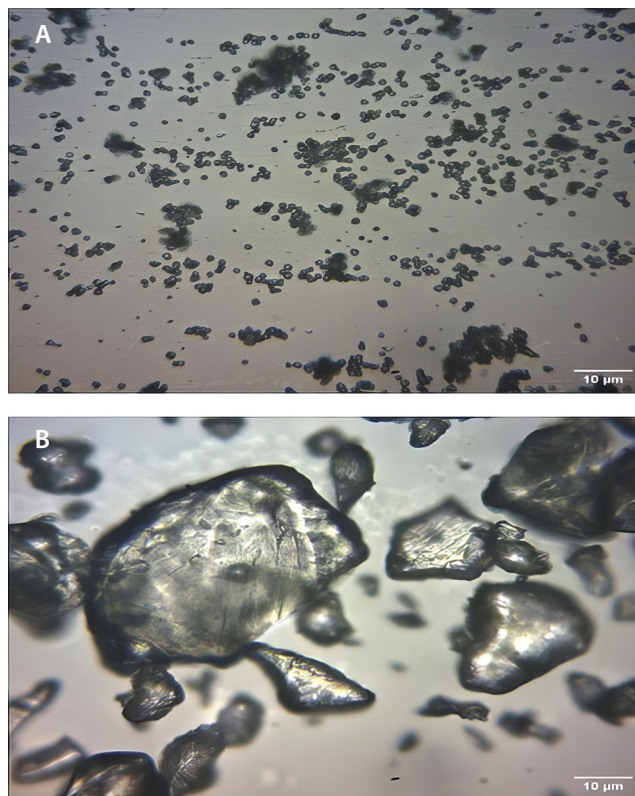


Fig. 1. Photomicrographs of (A) native and (B) pregelatinized bitter yam starch ($\times 400$ magnification)

Pasting properties of the starches

In Table 3 and Fig. 2, NS exhibited a higher peak viscosity (4204 cP vs 3655 cP) and higher breakdown viscosity (1048 cP vs 379 cP) compared to PS. Although both forms exhibited the same peak time of 6.07 min, PS presented a lower pasting temperature (78.25°C vs 84.10°C) and higher final viscosity (4638 cP vs 3635 cP).

Fourier transform infrared spectroscopy

The FT-IR spectra (Fig. 3) showed that the NS had pronounced absorption peaks around 3200 cm⁻¹ (O-H stretching) and in the fingerprint region below 1200 cm⁻¹

(C-O stretching and C-O-H bending). In contrast, the PS exhibited lower absorption peaks.

X-ray diffractometry

As seen in the X-ray diffractograms (Fig. 4), the native and pregelatinized bitter yam starch showed no difference in their crystalline nature.

Differential scanning calorimetry

In the differential thermograms (Fig. 5), NS showed a single, sharp endothermic peak around 100°C and a smooth, continuous curve from 40°C to 93°C, whereas PS showed

Table 3. Pasting properties of native and pregelatinized bitter yam starch

Starch form	Peak viscosity [cP]	Trough viscosity [cP]	Breakdown [cP]	Final viscosity [cP]	Setback from trough [cP]	Peak time [min]	Pasting temp [°C]
Native	4204	3156	1048	3635	479	6.07	84.10
Pregelatinized	3655	3276	379	4638	1362	6.07	78.25

cP – centipoise.

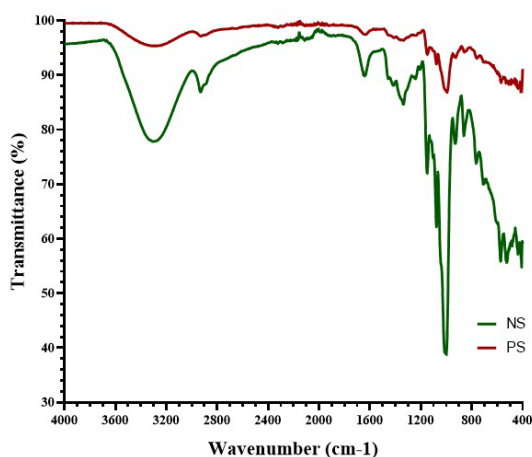


Fig. 2. Combined viscoamylograph of NS and PS

NS – native starch; PS – pregelatinized starch.

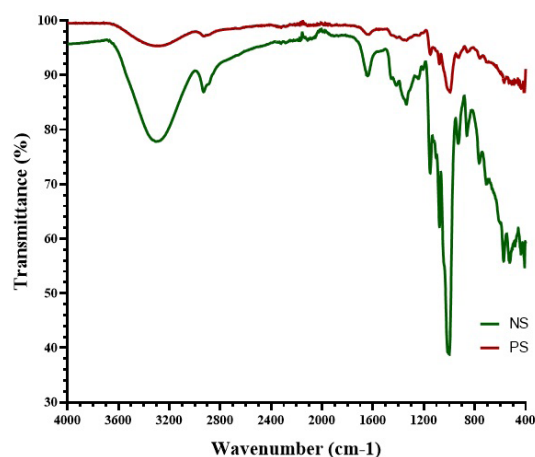


Fig. 3. Combined FT-IR spectra of NS and PS

NS – native starch; PS – pregelatinized starch.

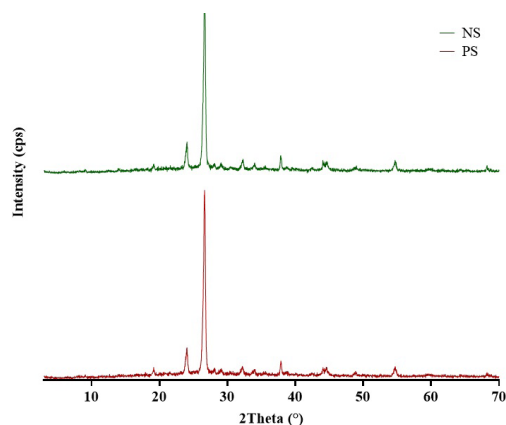


Fig. 4. Combined X-ray diffractograms of NS and PS

NS – native starch; PS – pregelatinized starch.

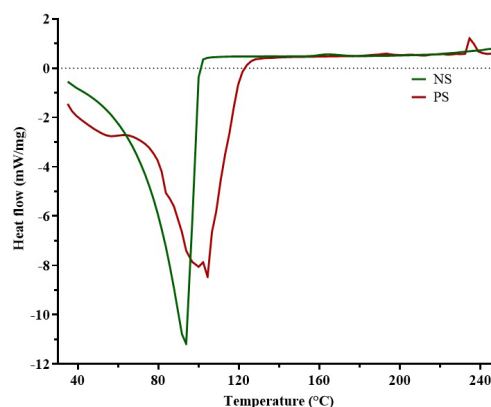


Fig. 5. Combined differential thermograms of NS and PS

NS – native starch; PS – pregelatinized starch.

a broader endothermic region around 80–120°C, multiple peaks in the endothermic region, and a small exothermic peak near 240°C.

Evaluation of oral dissolving films of the starches

Organoleptic properties and surface morphology of starch ODFs

The color shade differed depending on which starch type blended with HPMC, whether NS or PS, and color intensity decreased across the starch-to-HPMC ratios. The NS–HPMC 1:1 (NS-b) and PS–HPMC 1:2 (PS-c) samples were the most transparent among the characterized oral films of NS and PS.

Table 4 provides more information on the surface texture and transparency of the films. The NS films NS-a and NS-b showed dual coloring with brown and off-white colors at the tops and bottom surfaces of the films, respectively. While HP (the film formulation at HPMC–starch ratio 1:0) was the most transparent film, the NS films were the most translucent. Hydroxypropylmethyl cellulose, NS-a and NS-b films had smooth surface textures on both sides, while PS films (PS-a, PS-b and PS-c) exhibited smooth and rough surface textures on their top and bottom surfaces, respectively.

The photomicrograph in Fig. 6 shows the surface morphologies of the films on a microscopic level. The HP showed a relatively smooth and uniform surface, and NS-a and NS-b revealed cracks with granular structures on their bottom surfaces. The PS-a, PS-b and PS-c films had irregular surface appearances with numerous surface irregularities and micro-cavities.

Table 4. Organoleptic properties of the formulated oral dissolving films

Film	Color	Clarity	Surface texture
HP	pale yellow on both sides	transparent	smooth on both sides
NS	***	***	***
PS	***	***	***
NS-a	top – brown bottom – off-white	translucent	smooth on both sides
NS-b	top – brown bottom – off-white	translucent	smooth on both sides
NS-c	---	---	---
PS-a	brown on both sides	translucent	top – smooth bottom – rough
PS-b	brown on both sides	translucent	top – smooth bottom – rough
PS-c	brown on both sides	translucent	top – smooth bottom – rough

*** – films did not form; --- – films did not separate intact from the Petri dish.

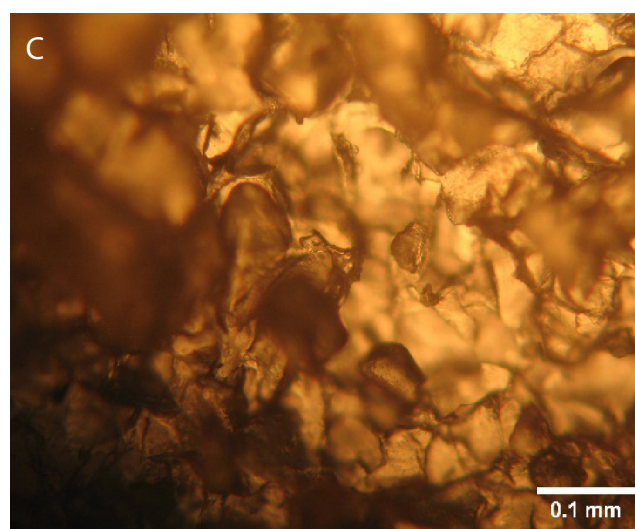
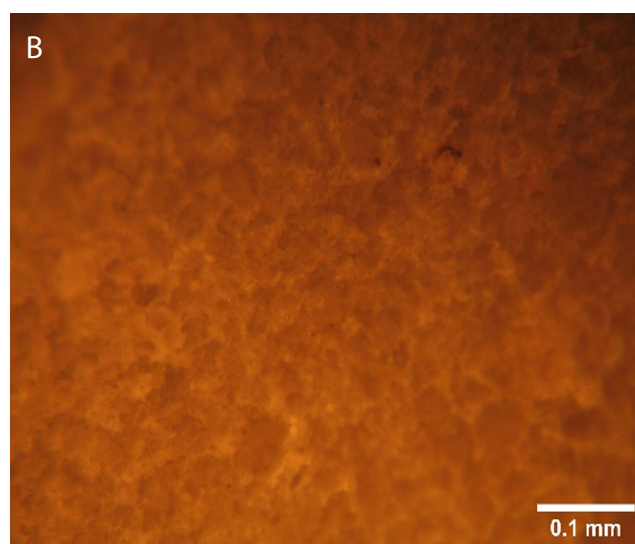
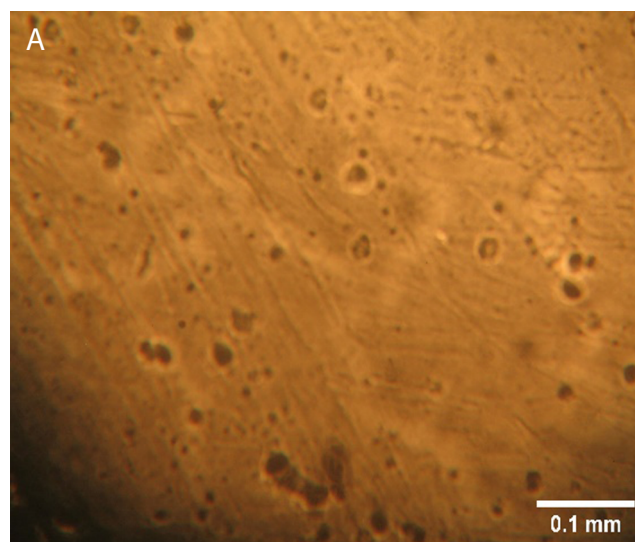


Fig. 6. Photomicrographs of the bottom surfaces of (A) HP, (B) NS-b and (C) PS-b (×10 magnification)

Weight and thickness uniformity

According to Table 5, HP exhibited the lowest weight (0.25 ± 0.03 g), while NS-a showed the highest (0.36 ± 0.03 g). All the PS films exhibited lower film weights than those of NS, with weight in the narrow range of 0.26–0.28 mg. Similarly, HP had the lowest thickness (0.44 ± 0.04 mm), while the starch-based films exhibited higher thicknesses ranging from 0.53 to 0.60 mm, with PS-b showing the highest thickness (0.69 ± 0.16 mm).

Film pH, folding endurance and disintegration time

Table 5 shows that the pH values of the films ranged from 4.89 to 6.11; HP had the highest pH (6.11) and the starch-ODFs had lower pH values, within a narrow range of 4.89–5.1. Among the starch-containing films, PS-c had the highest pH (5.10). The folding endurance values ranged from 1 to 10, with NS-a and HP showing the highest and lowest values, respectively. The PS ODFs (PS-a, PS-b and PS-c) had relatively higher values (5–8). All the ODFs had disintegration times greater than 15 min.

Discussion

Characterization of the native and pregelatinized starches

Particle size and morphology

Microscopic analysis was employed to identify differences in the characteristic morphology of the particles of both starches. The analysis of samples of the bitter yam starch forms showed distinct morphological changes following pregelatinization. A comparison of the photomicrographs obtained for native and modified starches revealed that pre-gelatinization disrupted the granular structure of the NS.⁷

Light microscopy revealed that the NS granules had smooth, intact surfaces with a well-defined ovoid/spherical shape. The granules were observed as loosely packed aggregates, indicative of minimal structural disruption. Pregelatinization led to visible fragmentation and rough, irregular particle shapes with significant structural changes. These alterations align with the typical effects of heat and moisture on starch granules, which disrupt crystallinity and create a more amorphous structure. Studies such as those by Okunola et al. report similar findings, where pregelatinization causes granule swelling, fusion and eventual breakdown, resulting in particles that lose their organized, compact structures.⁷

The increase in particle size following the pregelatinization of bitter yam starch can be attributed to the swelling and fusion of granules. This change is consistent with

Table 5. Properties of the oral dissolving film formulations

Film	Average weight [g]	Average thickness [mm]	pH	Folding endurance value	Disintegration time
HP	0.25 \pm 0.03	0.44 \pm 0.04	6.11	10 \pm 0.82	>15 min
NS-a	0.36 \pm 0.03	0.61 \pm 0.01	4.89	1 \pm 0.47	>15 min
NS-b	0.29 \pm 0.05	0.62 \pm 0.11	5.10	4 \pm 0.47	>15 min
PS-a	0.28 \pm 0.03	0.67 \pm 0.09	4.97	5 \pm 0.94	>15 min
PS-b	0.28 \pm 0.06	0.69 \pm 0.16	4.89	6 \pm 0.47	>15 min
PS-c	0.26 \pm 0.03	0.53 \pm 0.07	5.10	8 \pm 1.70	>15 min

HP: HPMC–starch ratio 1:0; NS: HPMC–starch ratio 0:1; PS: pregelatinized starch–HPMC ratio 0:1; NS-a: native starch–HPMC ratio 1:2; NS-b: Native starch–HPMC ratio 1:1; NS-c: native starch–HPMC ratio 2:1; PS-a: pregelatinized starch–HPMC ratio 1:2; PS-b: pregelatinized starch–HPMC ratio 1:1; PS-c: pregelatinized starch–HPMC ratio 2:1. HPMC – hydroxypropylmethyl cellulose.

findings that heating starch in the presence of moisture causes granules to absorb water and expand. The variation in particle size across samples is likely due to inconsistencies in how individual granules fracture, fuse or swell under thermal treatment, leading to a broader particle size distribution.¹ The larger particle size observed is similar to the result obtained by Okunola et al., and Omoteso and Odeniyi in the particle size analysis of PS of bitter yam, among other plant sources.^{7,4}

pH and swellability

The pH results indicate that both the native and pregelatinized bitter yam starch samples fall below the ideal pH range for pharmaceutical applications, as stated by Rowe et al. For pharmaceutical starch excipients, a pH range between 4.0 and 8.0 is typically recommended, with PS ideally between 4.5 and 7.0, as these ranges ensure compatibility with most active pharmaceutical ingredients (APIs) and ensure formulation stability.²⁶ Since most drugs are weak acids or bases, the use of these starches may induce stability problems for pH-sensitive drugs and potentially lead to irritation in certain drug delivery routes such as buccal and gastrointestinal. For excipient applications these bitter yam starches may require further processing steps or pH adjustments by neutralization or buffering to bring the pH closer to the desired range, enhancing its compatibility with APIs and reducing potential issues in formulations.

The PS exhibited a significantly ($p < 0.05$) higher swelling index compared to NS in all tested media, including water, 0.1 M hydrochloric acid, 6.8 phosphate buffer and 7.4 phosphate buffer. During pregelatinization, the granular structure of starch is disrupted, enhancing its hydrophilicity and allowing it to absorb more water.

Gelatinization breaks intramolecular hydrogen bonds that link starch molecules, which not only loosens the starch structure to reduce restrictions to swelling, but also creates new opportunities for hydrogen bonding with water molecules. As a result, PS has a greater affinity for water, leading to an increased ability to swell.¹⁹ The higher swelling observed in the phosphate buffers (pH 6.8 and 7.4) suggests that PS may be beneficial for applications in buccal or gastrointestinal drug delivery, where rapid hydration is desired to facilitate the release and absorption of active ingredients.⁴

Solubility, moisture content and hydration capacity

Also, PS demonstrated higher solubility and hydration capacity than NS. These improved values stem from the structural modifications during the gelatinization process. Increased interaction with water facilitates both dissolution and dispersion in aqueous solutions, aiding the overall hydration process.⁴ The improved hydration capacity of PS is particularly advantageous for applications where rapid water absorption is needed, such as in oral dissolving films. The moisture content of both NS and PS fell within the official acceptable threshold of 14% for pharmaceutical materials.²⁶ Pregelatinized starch exhibited a lower moisture content compared to NS, suggesting enhanced stability under storage conditions. Lower moisture content is desirable for extended shelf life, as it minimizes the risk of microbial growth and reduces the likelihood of spoilage, caking and the development of off-flavors or unwanted odors.⁵

Particle density, tapped density and bulk density

The results of this aspect of the study show that pregelatinization has a significant ($p < 0.05$) effect on the particle density, bulk density and tapped density of bitter yam starch. The marginally higher particle density of the modified starch is because the heat and water treatment disrupt the crystalline nature of the NS granule, resulting in the partial breakdown of intramolecular bonds of the starch and a rearrangement into a denser form.¹

A more significant ($p < 0.05$) increase was observed with the bulk and tapped starch densities. Bulk density measures how well starch particles pack together without tapping or compression, while tapped density indicates how well they pack under tapping or vibration, which allows the particles to settle. The bulk density of a powder determines its packing behavior during the various tableting unit operations such as die filling, mixing, granulation, and compression.²⁷ High bulk density is preferable mostly because it reduces the fill volume of the die; it contributes to better flow characteristics. The differences observed in the bulk density values could be due to the difference in particle shapes and sizes between the 2 starch forms which affected the packing arrangement of the powder particles.²³

Porosity, Hausner ratio, Carr compressibility index, and angle of repose

Porosity is a crucial parameter that determines powder flow and pack behavior. The lower porosity of PS indicates that the particles can pack more densely with reduced inter-particle spaces; this confirms the observation of higher tapped density. This compact packing is beneficial for applications that require uniform density such as in tablet compression. The decrease in porosity is due to the changes in the chemical and physical nature of starch granules from the rearrangement of intra- and intermolecular bonds.²⁸

These results show that pregelatinization improved the flow characteristics of the bitter yam starch, as evidenced by the decreased Hausner ratio, Carr index and angle of repose compared to the NS. Hausner ratio indicates the degree of densification that could occur during tableting; higher values predict significant densification of powders.²⁷ A lower Hausner ratio typically indicates better flow properties, as values closer to one suggest reduced cohesiveness via minimal inter-particle friction.²³ Carr compressibility index simultaneously measures the flowability and compressibility of a powder; the lower values indicate better flowability, but poorer compressibility due to reduced inter-particle interactions.²⁸ Carr index below 15% suggests good flow, while values above 25% indicate poor flow properties.²⁹

The angle of repose is a qualitative measure of the cohesiveness or the tendency of powdered or granulated materials to flow from hoppers through the feed frame into tableting machines. An angle of repose above 50° is defined as poor flow, while values between 25° and 45° signify fair flow.²⁹ The substantial reduction in the angle of repose in the PS is consistent with the flow improvements shown by Hausner ratio and Carr index.

Pasting properties of the starches

The pregelatinization process impacts the pasting properties of bitter yam starch, suggesting considerable changes in its functional behavior under heat and shear. Peak viscosity reflects the water-holding capacity and its ability to swell before granule disruption. The higher peak viscosity observed in NS compared to PS implies that NS granules retain their integrity better initially, resulting in greater initial viscosity.¹⁹ Conversely, PS, having undergone partial gelatinization, shows a lower peak viscosity, which is consistent with its increased solubility and faster hydration, previously observed.^{19,4}

The lower pasting temperature of PS indicates that it gelatinizes at a lower temperature, likely due to structural changes from pregelatinization that make starch granules more receptive to water absorption and swelling at lower temperatures.³⁰ This quality makes pregelatinized bitter yam starch suitable for processes requiring lower energy inputs or faster gelatinization, which is also beneficial

in energy-saving applications, providing a cost-effective alternative for industrial processing.¹

Fourier transform infrared spectroscopy

Characteristic peaks associated with starch molecules – including hydroxyl (O–H), C–H and carbonyl (C=O) groups – were detected in both starch forms, although with varying transmittance levels.¹⁹ For NS, the broad O–H stretching peak at 3305.13 cm⁻¹ reflects hydroxyl groups engaged in hydrogen bonding. C–H stretching, linked to aliphatic C–H bonds, appears at 2928.1 cm⁻¹, while C=O stretching bands, related to C=O and C–O–C glycosidic linkages integral to starch structure, are found at 1077.12 cm⁻¹ and 1150.45 cm⁻¹. A strong peak at 1647.8 cm⁻¹, attributed to O–H bond scissoring from absorbed water molecules is also present. Additional peaks at 859.37 cm⁻¹ and 524.76 cm⁻¹, unique to the NS, occur due to stretching vibrations of the polymer skeletal structure.²⁷ In PS, no remarkable changes in FT-IR peak positions were noted, though less pronounced peaks were observed. This signifies that pregelatinization may weaken some intra- and intermolecular bonds within the NS, resulting in broader peaks with reduced intensity.³¹

A strong peak at 1647.8 cm⁻¹, attributed to O–H bond scissoring from absorbed water molecules is also present. Additional peaks at 859.37 cm⁻¹ and 524.76 cm⁻¹, unique to the NS, are due to stretching vibrations of the polymer skeletal structure.²⁷ In PS, no remarkable changes in FT-IR peak positions were noted, though less pronounced peaks were observed. The pregelatinization process appears to weaken some intra- and intermolecular bonds within the NS, resulting in a more amorphous structure with reduced peak intensity.³²

X-ray diffractometry

The XRD patterns provide a “fingerprint” of the crystalline structure to assess the structural impact of modification processes like pregelatinization.¹⁹ Both NS and PS exhibit well-defined, sharp peaks, which suggest that the starch granules retained their crystalline structure after the modification process. The prominent peaks at approx. 27° 2θ are characteristic of the A-type crystalline pattern commonly observed in cereal starches, reflecting an ordered molecular arrangement within the granules. Additionally, minor peaks at around 24° 2θ further support the presence of crystalline regions.³²

Differential scanning calorimetry

In this study, DSC was utilized to investigate phase transitions and reveal distinct thermal behavior patterns between the NS and PS.³³ The thermal profiles demonstrated that pregelatinization altered the thermal properties of bitter yam starch, with PS exhibiting more complex

thermal behavior. The NS sample exhibited a single endothermic peak at 93.79°C, whereas the PA displayed multiple peaks, with the major endothermic transition occurring at 102.11°C. The endothermal peak indicates heat absorption by the samples and may be associated with processes such as melting and vaporization of water molecules within the starch polymer. Prior to the melting phase, the PS underwent glass transition at ~70°C. Higher melting temperatures and glass transition temperatures are commonly observed with increased amylose content, a characteristic property of PS.³⁴ At elevated temperatures, reactions such as oxidation facilitates the breakage of chemical bonds within starch molecules. This reaction, coupled with the re-crystallization of decomposed starch polymers, results in the release of heat which is observed as the exothermic peak at 240°C of PS.³⁵

Evaluation of oral dissolving films of the starches

Organoleptic properties and surface morphology

The pure HPMC film (HP) exhibited uniform, transparent and smooth textures, which are highly desirable in oral applications for consistent texture, clarity and a pleasant mouthfeel. The transparency suggests a well-formed, uniform structure with minimal internal scattering due to the absence of large particles and air bubbles.¹⁴ The inability of NS and PS alone to form films, despite the addition of glycerol as a plasticizer, points to their insufficient binding properties, which could lead to brittleness after drying. This outcome aligns with the findings of Ayorinde et al., who observed that starches alone exhibit poor film-forming properties, but show significant improvement when combined with HPMC in appropriate ratios.¹⁵

Native starch ODFs presented a 2-toned appearance, with brown and off-white layers, possibly due to oxidation or drying effects from environmental exposure. In contrast, PS ODFs displayed a uniform brown color, suggesting a more homogeneous film formation. The NS films were translucent, indicating partial light transmission, likely due to the opacity and limited solubility of NS. Pregelatinized starch films, on the other hand, had a semi-clear, less opaque appearance, possibly due to the increased solubility and cohesive properties of PS.³⁰ Native starch films also showed pronounced crack patterns, indicating high crystallinity and brittleness.⁷

Surface texture analysis indicated that the HP films were smoothest on both sides. Native starch blends retained this smoothness, while the PS films displayed smoother tops and rougher bottoms. This roughness may impact the films' dissolution and drug release rates, as smoother films likely dissolve more uniformly.¹⁷ Microscopic analysis revealed that HP films had a highly uniform surface, with no visible cracks or irregularities, demonstrating

strong cohesive interactions in the polymer matrix. Starch-containing films, particularly those with higher starch content, displayed rougher textures. Pregelatinized starch ODFs were rougher on the top surface than NS films, likely due to larger particle sizes and high swelling properties of PS particles.³⁶ Hydroxypropylmethyl cellulose enhances the smoothness of ODFs, while the starches contribute to textural variability, which may influence film dissolution and drug release. The choice and ratio of HPMC and starch are critical in optimizing the organoleptic and functional properties of ODFs.^{37,38}

Weight and thickness uniformity

Weight variation is a crucial parameter in oral dissolving films for ensuring dose consistency, as it reflects the even distribution of active ingredients and excipients within the film.^{14,16} In this study, the weight variations of the film formulations ranged from 0.03 to 0.06 g, indicating good uniformity within each batch. This consistency also reflects the efficiency of the formulation method used. The HP film had the lowest average weight, suggesting that the presence of starches increased the bulk of the ODFs.¹⁷ Native starch films exhibited greater average weights, potentially due to the higher solubility and swelling capacity of PS.¹²

The low standard deviation in film thickness across formulations further confirmed the consistency and reliability of the method used.¹⁵ The inclusion of starch increased the thickness of the films substantially, likely due to the differing viscosities of the polymers used.¹⁷ The higher swelling ability of PS could explain why its ODFs generally exhibited slightly greater thicknesses compared to those with NS. An increase in thickness was observed with higher HPMC content in the starch films, which aligns with findings from Balogun-Agbaje et al. in their study of HPMC/potato starch ODF blends.¹⁴

Film pH, folding endurance, and disintegration time

The surface pH of ODFs is a key factor in ensuring patient compliance, as it helps predict potential in vivo adverse effects. To minimize the risk of oral mucosal irritation, the pH of these films should be near 7.0.¹⁶ The slightly acidic starch ODFs can be attributed to the intrinsic acidity of starch. This may affect the film stability and compatibility with pH-sensitive drugs and excipients. The mechanical strength of the films was evaluated by assessing folding endurance, which measures film flexibility or brittleness.¹⁶ Generally, a folding endurance value of approx. 300 folds is recommended for ideal flexibility.³⁹ However, all films in this study exhibited folding endurance values well below this threshold. The HP films displayed higher folding endurance than starch-based formulations, indicating greater flexibility. Films formulated with NS (NS-a and NS-b) exhibited low folding endurance, reflecting the brittleness and rigid crystalline structure characteristic of NS. In contrast, PS films demonstrated better folding ability

due to the amorphous nature of PS.¹¹ Both NS and PS ODFs showed increased flexibility with increasing HPMC concentrations. Disintegration time is important for formulations that require rapid drug release applications. The ideal disintegration time is between 5 s and 30 s.¹³ All ODFs displayed disintegration times exceeding 15 min. Adjustments to the starch-to-HPMC ratio or the addition of super disintegrants could be a way to reduce disintegration times.

Conclusions

Pregelatinization of bitter yam starch improves physicochemical properties such as swelling, solubility and hydration capacity. This modification method also remarkably improves the flow and pasting properties of bitter yam starch as well as its surface morphology and thermal characteristics. Both starch forms of bitter yam produced thicker and heavier ODFs, which could potentially impact patient acceptability and ease of use. Pregelatinized starch ODFs have better mechanical strength and flexibility compared to NS ODFs. The acidic pH values of the starch ODFs pose a risk of mucosal irritation and reduced stability of pH-sensitive drugs and excipients. The use of bitter yam starches as film formers for ODFs would require additional formulation modifications to meet the mechanical strength, rapid dissolution and pH criteria for ODFs.

Data availability

The datasets generated and/or analyzed during the current study are available from the corresponding author on reasonable request.

Consent for publication

Not applicable.


Use of AI and AI-assisted technologies

Not applicable.

ORCID iDs

Tioluwani Ibukun Adegbolagun  <https://orcid.org/0000-0002-9442-2639>

Olubusola Ayoola Odeniyi  <https://orcid.org/0000-0002-0826-791X>

Michael Ayodele Odeniyi  <https://orcid.org/0000-0002-9918-4377>

References

1. Krithika PL, Ratnamala KV. Modification of starch: A review of various techniques. *Int J Res Anal Rev.* 2019;6(1):32–45. https://ijrar.com/upload_issue/ijrar_issue_20543116.pdf.
2. Odeniyi MA, Omoteso OA, Adepoju AO, Jaiyeoba KT. Starch nanoparticles in drug delivery: A review. *Polim Med.* 2019;48(1):41–45. doi:10.17219/pim/99993
3. Ayorinde JO, Odeniyi MA, Oyeniyi YJ. Material and compression properties of native and modified plantain starches. *Farmacia.* 2013;61(3):574–590. <https://farmaciajournal.com/wp-content/uploads/2013-03-art.16.ayorinde-574-590small.pdf>.

4. Omoteso OA, Odeniyi MA. Physical/chemical modifications of *Oryza glaberrima* and *Digitaria exilis* starches: Effect on packing and compression properties of ibuprofen tablet formulations. *Acta Pharm Sci.* 2024;62(1):122. doi:10.23893/1307-2080.APS6208
5. Oluwasina OO, Wahab OJ, Umunna QC, Nwosa OC. *Dioscorea dumetorum* Pax as an alternative starch source for industrial applications. *IOSR J Appl Chem.* 2017;10(5):5–13. doi:10.9790/5736-1005020513
6. Agbo UI, Odo GE. Evaluation of the effect of acetylation and oxidation on some functional properties of starch isolated from *Dioscorea dumetorum* (Wild). *Bioresearch.* 2010;8(1):588–592. doi:10.4314/br.v8i1.62538
7. Okunlola A, Adebayo S, Adeyeye MC. Solid state characterization of two tropical starches modified by pregelatinization and acetylation: Potential as excipients in pharmaceutical formulations. *Br J Pharm Res.* 2015;5(1):58–71. doi:10.9734/BJPR/2015/13445
8. Hong Y, Liu X. Pre-gelatinized modification of starch. In: Sui Z, Kong X, eds. *Physical Modifications of Starch.* Singapore: Springer Singapore; 2018:51–61. doi:10.1007/978-981-13-0725-6_4
9. Abdallah DB, Charoo NA, Elgorashi AS. Assessment of pregelatinized sorghum and maize starches as superior multi-functional excipients. *J Pharm Innov.* 2016;11(2):143–155. doi:10.1007/s12247-016-9247-8
10. Effiong DE, Umoh RA, Akpabio AE, Sunday NAI, Uko AI. The oral film delivery: Application of nanotechnology and potential in medication adherence. *GSC Biol Pharm Sci.* 2020;11(3):34–51. doi:10.30574/gscbps.2020.11.3.0154
11. Muruganantham S, Kandasamy R, Alagarsamy S. Nanoparticle-loaded oral fast-dissolving film: New realistic approach of prospective generation in drug delivery: A review. *Crit Rev Ther Drug Carrier Syst.* 2021;38(1):1–35. doi:10.1615/CritRevTherDrugCarrierSyst.2020034002
12. Tamanini F, Moraes BS, Amaral CST, Carvalho AJF, Trovatti E. Starch-based orodispersible film for diclofenac release. *Braz J Pharm Sci.* 2023;59:e211019. doi:10.1590/s2175-97902023e211019
13. Ayorinde JO, Effiong DE, Odeniyi MA. Design and evaluation of oral dissolving films of chlorpheniramine from native and modified *Enterolobium cyclocarpum* gum. *Afr J Biomed Res.* 2018;21(2):175–182. <https://www.ajol.info/index.php/ajbr/article/view/178865>.
14. Balogun-Agbaje OA, Babalola OC, Yusuff AA, Lateef R. Formulation and evaluation of chlorpheniramine maleate oral dissolving films using blends of pregelatinized potato starch and hydroxypropyl cellulose. *FUW Trends Sci Technol J.* 2024;9(1):135–141. <https://ftst-journal.com/Digital%20Library/91%20Article%2071.php>.
15. Ayorinde JO, Odeniyi MA, Balogun-Agbaje O. Formulation and evaluation of oral dissolving films of amlodipine besylate using blends of starches with hydroxypropyl methyl cellulose. *Polim Med.* 2016;46(1):45–51. doi:10.17219/pim/65098
16. Bharti K, Mittal P, Mishra B. Formulation and characterization of fast dissolving oral films containing buspirone hydrochloride nanoparticles using design of experiment. *J Drug Deliv Sci Technol.* 2019;49:420–432. doi:10.1016/j.jddst.2018.12.013
17. Daud A, Bonde M, Sapkal N. Development of *Zingiber officinale* in oral dissolving films: Effect of polymers on in vitro, in vivo parameters and clinical efficacy. *Asian J Pharm.* 2011;5(3):183. doi:10.4103/0973-8398.91995
18. Balogun-Agbaje OA, Odeniyi MA. Characterization and drug release properties of curcumin loaded native and nano-sized starches of pigeon pea (*Cajanus cajan*) and bambara nut (*Vigna subterranean*). *Starch Stärke.* 2024;76(9–10):2400022. doi:10.1002/star.202400022
19. Lawal MV, Odeniyi MA, Itiola OA. Material and rheological properties of native, acetylated, and pregelatinized forms of corn, cassava, and sweet potato starches. *Starch Stärke.* 2015;67(11–12):964–975. doi:10.1002/star.201500044
20. Bamiro OA, Bakre LG, Adeleye OA. Assessment of compression-al, mechanical and release properties of terminalia randii gum in paracetamol tablet formulation. *Acta Pharm Sci.* 2023;61(3):317. doi:10.23893/1307-2080.APS6121
21. Akin-ajani OD, Ajala TO, Okoli UM, Okonta O. Development of directly compressible excipients from *Phoenix dactylifera* (date) mucilage and microcrystalline cellulose using co-processing techniques. *Acta Pharm Sci.* 2018;56(3):7. doi:10.23893/1307-2080.APS.05615
22. Adetunji OA, Kolawole O. The influence of phosphate modified and pregelatinized plantain (*Musa paradisiaca*, family: Musaceae) starches as disintegrants in paracetamol tablet formulations. *Niger J Pharm Res.* 2018;14(1):15–24. <https://www.ajol.info/index.php/njpr/article/view/175419>.
23. Adeola A, Asare-Addo K, Odeniyi MA, Omoteso OA, Kaialy W. Effect of pregelatinization and carboxymethylation on starches from African rice and Fonio: Influence on release of low melting-point drug starch modifications for drug release. *Br J Pharm.* 2019;4(2):304–372. doi:10.5920/bjpharm.645
24. Karrila SJ, Nga LH, Karrila TT. Effect of blending and pregelatinizing order on properties of pregelatinized starch from rice and cassava. *Food Res.* 2019;4(1):102–112. doi:10.26656/fr.2017.4(1).245
25. Fonseca-Santos B, Chorilli M, Palmira Daflon Gremião M. Nanotechnology-based drug delivery systems for the treatment of Alzheimer's disease. *Int J Nanomed.* 2015;10:4981. doi:10.2147/IJN.S87148
26. Rowe RC, Sheskey PJ, Quinn ME, eds. *Handbook of Pharmaceutical Excipients.* 6th ed. London, UK: APHA, (PhP) Pharmaceutical Press; 2009. ISBN: 978-1-58212-135-2, 978-0-85369-792-3, 978-0-85369-794-7.
27. Gbenga BL, Olakunle O, Adedayo AM. Influence of pregelatinization on the physicochemical and compressional characteristics of starches obtained from two local varieties of *Dioscorea rotundata*. *IOSR J Pharm.* 2014;4(6):24–32. doi:10.9790/3013-040602024032
28. Odeku OA, Picker-Freyer KM. Analysis of the material and tablet formation properties of four *Dioscorea* starches. *Starch Stärke.* 2007;59(9):430–444. doi:10.1002/star.200700619
29. Sen DJ, Nandi K, Patra F, Nandy B, Bera K, Mahanti B. Angle of repose walks on its two legs: Carr index and Hausner ratio. *World J Pharm Pharm Sci.* 2020;9(5):1565–1579. https://www.wjpps.com/Wjpps_controller/abstract_id/12321.
30. Compant J, Singh A, Fettke J, Apriyanto A. Customizing starch properties: A review of starch modifications and their applications. *Polymers (Basel).* 2023;15(16):3491. doi:10.3390/polym15163491
31. Fahelelbom KM, Saleh A, Al-Tabakha MMA, Ashames AA. Recent applications of quantitative analytical FTIR spectroscopy in pharmaceutical, biomedical, and clinical fields: A brief review. *Rev Anal Chem.* 2022;41(1):21–33. doi:10.1515/revac-2022-0030
32. Subroto E. Review on the analysis methods of starch, amylose, amylopectinin food and agricultural products. *Int J Emerg Trends Eng Res.* 2020;8(7):3519–3524. doi:10.30534/ijeter/2020/103872020
33. Barzinjy AA, Azeez HH. Green synthesis and characterization of zinc oxide nanoparticles using *Eucalyptus globulus* Labill. leaf extract and zinc nitrate hexahydrate salt. *SN Appl Sci.* 2020;2(5):991. doi:10.1007/s42452-020-2813-1
34. Wang H, Zhu Q, Wu T, Zhang M. Glass transition temperature, rheological, and gelatinization properties of high amylose corn starch and waxy cassava starch blends. *J Food Process Preserv.* 2020;44(9):e14682. doi:10.1111/jfpp.14682
35. Rashid I, Omari MHA, Leharne SA, Chowdhry BZ, Badwan A. Starch gelatinization using sodium silicate: FTIR, DSC, XRPD, and NMR studies. *Starch Stärke.* 2012;64(9):713–728. doi:10.1002/star.201100190
36. Alebiowu G, Itiola OA. Compressional characteristics of native and pregelatinized forms of sorghum, plantain, and corn starches and the mechanical properties of their tablets. *Drug Dev Ind Pharm.* 2002;28(6):663–672. doi:10.1081/DDC-120003857
37. Andiyana Y, Suyatma NE, Suliantari S. Physico-mechanical properties of starch-based nanocomposite film incorporated with hydrothermally synthesized zinc oxide nanoparticles. *Mater Sci Forum.* 2016;872:162–167. doi:10.4028/www.scientific.net/MSF.872.162
38. Jacob S, Nair AB, Boddu SHS, Gorain B, Sreeharsha N, Shah J. An updated overview of the emerging role of patch and film-based buccal delivery systems. *Pharmaceutics.* 2021;13(8):1206. doi:10.3390/pharmaceutics13081206
39. Kardile DP, Awate PB, Bhagat VC, et al. Review on nanoparticle-loaded oral film: An innovative approach for poorly water-soluble drug delivery. *Biol Forum Int J.* 2023;15(3):138.

Impact of hepatitis C virus on *IFITM3* gene expression: A comprehensive analysis incorporating serological detection and viral load quantification via qPCR

Tabarak S. Jassim^{1,A-C,F}, Sura S. Talib^{2,B,C}, Nawar R. Jaber^{2,B,C}, Dina H. Sahib^{3,B,C,E}, Rusul W. Ali^{4,B-E}, Bahaa Al-Rubaii^{5,A,C,D,F}

¹ Department of Plant Biotechnology, College of Biotechnology, Al-Nahrain University, Baghdad, Iraq

² Biotechnology Research Center, Department of Ecology, Al-Nahrain University, Baghdad, Iraq

³ Department of Biotechnology, College of Science, University of Baghdad, Iraq

⁴ Iraqi Center For Cancer Research and Medical Genetics, Mustansiriyah University, Baghdad, Iraq

⁵ Department of Biology, College of Science, University of Baghdad, Iraq

A – research concept and design; B – collection and/or assembly of data; C – data analysis and interpretation;

D – writing the article; E – critical revision of the article; F – final approval of the article

Polymers in Medicine, ISSN 0370-0747 (print), ISSN 2451-2699 (online)

Polim Med. 2025;55(1):21–30

Address for correspondence

Bahaa Al-Rubaii

E-mail: bahaa.abdullah@sc.uobaghdad.edu.iq

Funding sources

None declared

Conflict of interest

None declared

Received on November 17, 2024

Reviewed on December 16, 2024

Accepted on December 18, 2024

Published online on June 27, 2025

Cite as

Jassim TS, Talib SS, Jaber NR, Sahib DH, Ali RW, Al-Rubaii B.

Impact of hepatitis C virus on *IFITM3* gene expression:

A comprehensive analysis incorporating serological detection and viral load quantification via qPCR. *Polim Med.* 2025;55(1):21–30. doi:10.17219/pim/199333

DOI

10.17219/pim/199333

Copyright

Copyright by Author(s)

This is an article distributed under the terms of the Creative Commons Attribution 3.0 Unported (CC BY 3.0) (<https://creativecommons.org/licenses/by/3.0/>)

Abstract

Background. Hepatitis C virus (HCV) causes long-term liver disease. Its capacity to influence the host immune system makes its pathogenesis more complicated. Targeting the *IFITM3* gene presents a promising therapeutic strategy for treating HCV infections, as it blocks the virus from entering host cells.

Objectives. This study examines how HCV viral loads affect *IFITM3* gene expression.

Materials and methods. This study included 100 patient samples diagnosed with HCV through serological methods and confirmed as positive. Then, viral and human RNA were extracted using commercial kits. The viral RNA was then quantified using one-step real-time polymerase chain reaction (qPCR), enabling an accurate assessment of viral load in the blood. Following this, human RNA was converted to cDNA and quantified using qPCR to investigate *IFITM3* gene expression.

Results. The distribution of blood groups among HCV-positive and HCV-negative samples showed that samples with the O– blood group had a significantly higher frequency of HCV positivity (18.4%) compared to the HCV-negative group (2.0%). Age analysis indicated a significant difference between HCV-positive and HCV-negative individuals with mean age of 37.8 ± 1.48 years and 44.1 ± 1.56 years, respectively. The expression levels of the *IFITM3* gene were significantly higher in the HCV-positive group (4.21 ± 1.17 fold) compared to the HCV-negative group (1.36 ± 0.157 fold), with a p-value of 0.016. A correlation analysis between *IFITM3* gene expression levels and HCV viral loads showed r-value of 0.343, indicating a moderate positive correlation, with p-value of 0.016.

Conclusions. Strong correlations observed in this study show the need for a comprehensive understanding and management approach to HCV disease. These relationships should be studied longitudinally to verify causality and assess potential interventions. *IFITM3* gene expression as a biomarker for HCV infection and disease progression warrants further investigation.

Key words: hepatitis, qPCR cirrhosis, fold, virus

Background

Hepatitis C is a significant liver diseases caused by the hepatitis C virus (HCV) that has an impact on health and mortality worldwide.¹ Unlike other types of hepatitis, HCV tends to result in chronic infection for a number of those affected. The primary mode of HCV transmission is blood exposure, which can occur through, e.g., injection drug use, improper sterilization of medical equipment or blood transfusions.²

Other important risk factors include high-risk behaviors and mother-to-child transmission during pregnancy.³ Understanding these modes of transmission plays a role in developing effective prevention strategies and early intervention measures.⁴ The symptoms and outcomes of HCV infection vary widely among individuals. While some people are able to eliminate the virus from the organism, many develop chronic infections that can progress to serious conditions such as liver cirrhosis, liver failure or hepatocellular carcinoma (HCC, a type of liver cancer).⁵

The interactions between HCV and the host immune system contribute to the wide range of disease progression.⁶ The *IFITM3* gene is one of the crucial elements in the immune system's defense against infections.⁷ The *IFITM3* gene is located on chromosome 11 and it is activated interferon signaling.⁸ Recent research has shown growing interest in its potential to reduce viral replication rates. This effect is believed to occur by blocking the viral entry into host cells, a mechanism that is activated by interferon during infections.⁹

However, researchers have proposed a hypothesis indicating that HCV influences the expression of *IFITM3* gene, which in turn may impact the development and outcome of the infection.¹⁰ Further investigation is required to comprehend the role of *IFITM3* in HCV infections.

The initial step in detecting HCV involves examining the patient's serum for the presence of HCV antibodies.¹¹ While this serological test is convenient, it is important to note that even if a patient has recovered from HCV, the antibodies may still yield a positive result. This emphasizes the necessity of additional confirmatory tests to accurately diagnose an active infection.¹²

Objectives

Monitoring HCV viral loads is essential for assessing treatment response and predicting disease prognosis.¹³ Additionally, the high sensitivity and specificity of real-time quantitative polymerase chain reaction (qPCR) make it an effective method for detecting HCV infections.¹⁴ It is important to have an understanding of how HCV impacts the expression of the *IFITM3* gene in terms of its clinical implications. This research has the potential to reveal novel targets and strategies for managing HCV infections. Exploring the relationship between HCV and *IFITM3* can

provide valuable insights into virology and immunology, ultimately enhancing our understanding of HCV pathogenesis and host defense mechanisms.

Materials and methods

Ethical approval

The current study was conducted after obtaining the ethical approval from the Human Ethical Committee of Al-Nahrain University, Baghdad, Iraq (Ref. 689, dated March 10, 2024).

Samples collection

This research was conducted at Al-Kadhmya Teaching Hospital (Baghdad, Iraq) between August 2022 and October 2023. A total of 100 samples were collected, specifically chosen based on the tests results. All participants had previously tested positive for HCV antibodies, detected using the HCV Ab Rapid Test. The serological tests used in this study were sourced from LINEAR (Barcelona, Spain). This selection process ensured that our research focused on individuals who had been serologically confirmed to have been exposed to HCV, making the findings relevant and targeted. The Anti-HCV cassette (LINEAR) was used for detection. The reagent composition included HCV test devices, which contain protein A-coated particles and HCV antigen-coated membranes.

HCV RNA extraction

The Ribo Virus (K 2/C) kit (Sacace Biotechnologies, Como, Italy) was used to extract RNA from cell fluids, following the instructions provided by the manufacturer. In a tube, 600 μ L of buffer RAV1 (Sacace Biotechnologies; containing carrier RNA) was combined with 150 μ L of serum. The mixture, along with negative controls specified using the PCR kit, was briefly mixed by pulse vortexing for 15 s, then incubated at 70°C for 5 min. If there was any turbidity after incubation, the samples were centrifuged at 11,000 \times g for 1 min. The liquid supernatant was carefully transferred to a new tube to prevent clogging during column purification. Next, 600 μ L of ethanol (96%) was added to the lysed sample. After vortexing and brief centrifugation, the mixture was applied to Ribo Virus columns placed within 2 μ L centrifuge tubes. Several wash steps were performed using buffers RAW and RAV3. Finally, RNA was eluted from the columns using RNase-free water preheated to 70°C. The resulting viral RNA was stored at -20°C until it was used for qPCR on the designated working day.

HCV real-time quantitative PCR

HCV RNA was quantitatively detected using the HCV Real-TM Quant kit (Sacace Biotechnologies). A standard

curve was generated for the quantitative determination of HCV RNA levels using qPCR (Fig. 1). This approach utilized dual-color detection to simultaneously identify HCV-specific RNA and the internal control (IC). Hot Start Taq Polymerase, M-MLV Revertase, RT-PCR-mix-1, and RT-PCR-mix-2 (Sacace Biotechnologies) were then added to the tube to create the reaction mix.

Next, 12.5 µL of the reaction mix was aliquoted into each reaction tube. After preparing the reaction tubes or PCR plate, 12.5 µL of the extracted RNA sample was transferred into the appropriate tube containing the reaction mix. Before being added, the RNA samples were meticulously re-centrifuged, ensuring that the pellet remained undisturbed, while only the supernatant was used. For qPCR, a set of standards and a negative control (NC) were prepared using the provided Quantitation Standards for HCV and IC, while TE-buffer was used for the PCR NC.

The reaction tubes were sealed and then placed into the qPCR for amplification. The process began with an initial reverse transcription step at 50.0°C for 15 min, followed by a denaturation step at 95.0°C for 15 min. The PCR amplification protocol was carried out under the specified thermal cycling conditions, which included 5 cycles of denaturation at 95.0°C for 5 s, annealing at 60.0°C for 20 s and extension at 72.0°C for 15 s. After that, there were 40 cycles of denaturation (for 5 s at 95.0°C), annealing (for 30 s at 60.0°C) and extension (for 15 s at 72.0°C). Then, the data were examined to determine the existence and amount of HCV RNA, while the IC was used to confirm the RNA extraction process and detect any potential PCR inhibition. The precision and reliability of HCV viral load measurement, which is essential for patient prognosis and tracking response to antiviral medication, were guaranteed by the implementation of ICs and strict adherence to PCR setup methods. According to clinical guidelines, a sustained virological response was defined as the lack of detectable HCV RNA 6 months after treatment termination.

Human RNA extraction

RNA was extracted from the samples using the RNeasy Micro Kit from Qiagen (Hilden, Germany). The eluted RNA was then converted into cDNA using the PrimeScript kit (Takara, Tokyo, Japan), which involved adding 2.0 µL of cDNA synthesis mix, 5.0 µL of RNA sample and nuclease free H₂O up to 10 µL for each sample. The tubes were then placed in a cycler machine, set to maintain a temperature of 37°C for 30 min. Once the 30-min incubation was complete, the cDNA was ready for use. For relative quantification of the *IFITM3* gene using qPCR, the following primer sequences were used:

Forward: 5'-TTCTGCTGCCTGGGCTTCATAG-3'

Reverse: 5'-ACCAAGGTGCTGATGTTTCAGGC-3'

For normalization of results, the *GAPDH* gene was used as a reference gene, with the following primer sequences:

Forward: 5'-GATGGCAACAATCTCCACTTTGC-3'

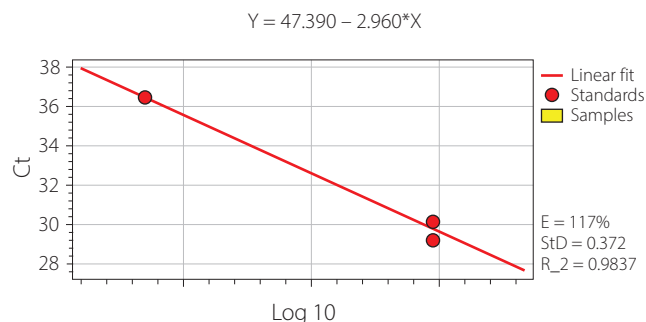


Fig. 1. Standard curve for the quantitative determination of HCV RNA levels using RT-PCR

HCV – hepatitis C virus; qPCR – quantitative real-time polymerase chain reaction

Reverse: 5'-GCCGCATCTTCTTGTGCAGT-3'.

The qPCR reaction mixture for each sample was prepared as follows: 10 µL of KAPA SYBR green FAST qPCR Universal, 0.5 of forward primer and reverse primer and 5 of previously prepared cDNA, with nuclease-free water added to a final volume of 20 µL. The prepared tubes were then placed into the thermocycler, and the amplification and detection were programmed with the following cycling conditions: enzyme activation (95°C for 10 min), then 40 cycles of denaturation 95.0° for 30 s, annealing 60.0°C for 30 s and extension 72.0°C for 30 s.

Statistical analyses

Several statistical techniques, including the χ^2 test and average with standard error (SE), and Student's t-test was used to compare 2 independent scale parameters. Regression analysis, 95% confidence intervals (95% CIs) and hypothesis testing frequently involve the mean, median and SE – 3 essential basics of inferential statistics. The HCV viral load experiment's resultant curves are represented by the standard curve for the quantitative assessment of HCV RNA levels obtained with qPCR.

Results

After completing the qPCR run of each experiment, amplification curves were generated, representing the amplification of the target sequence. Figure 2A displays the amplification curves obtained from the gene expression analysis after the qPCR run. Figure 2B illustrates the resultant curves from the HCV viral load experiment.

The investigation into the relationship between blood group, gender, age, and HCV infection status revealed several notable findings, as shown in Table 1. A total of 100 individuals were included in the study, with 49 testing positive for HCV and 51 testing negative for HCV. When examining the distribution of blood groups among the HCV-positive and HCV-negative cohorts, the χ^2 test yielded a value of 17.2, indicating a statistically significant association

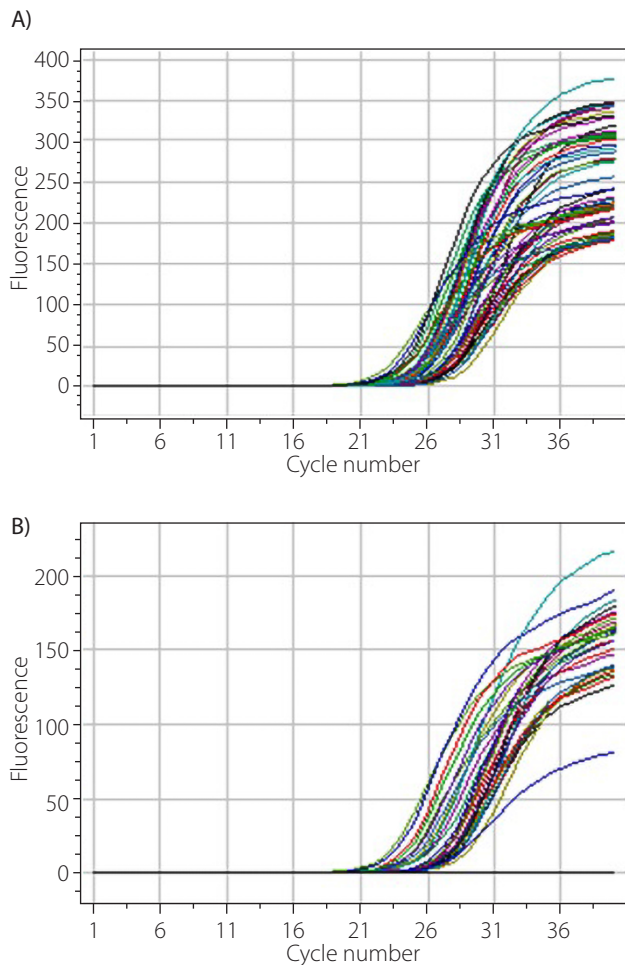


Fig. 2. Resulted amplification curves of quantitative real-time polymerase chain reaction (qPCR)

between blood group and HCV status ($p = 0.016$). Notably, the proportion of individuals with the 0– blood group was markedly higher in the HCV-positive group (18.4%) compared to the HCV-negative group (2.0%). Conversely, a lower percentage of individuals with the A– blood group were HCV-positive (14.3%) compared to HCV-negative individuals (3.9%). This suggests that certain blood groups may be more prevalent among HCV-positive population within this sample. Gender distribution between the HCV-positive and HCV-negative groups did not show a statistically significant difference ($\chi^2 = 0.642$, $p\text{-value} = 0.421$), with women representing 55.1% of the HCV-positive group and 47.1% of the HCV-negative group. The average age of HCV-positive individuals was 37.8 years (± 1.48), while the HCV-negative group had an average age of 44.1 years (± 1.56), indicating a significant difference between the 2 groups.

The significance level for this difference was $p = 0.005$, which is statistically significant, suggesting that HCV positivity is associated with a younger age in this population. The expression levels of the *IFITM3* gene were compared between individuals who tested positive for HCV ($n = 49$) and those who tested negative ($n = 51$), with the results summarized in Table 2. The mean fold expression

of the *IFITM3* gene in the HCV-positive group was significantly higher (mean = 4.21, median = 2.09, SE = 1.17) compared to the HCV-negative group (mean = 1.36, median = 0.975, SE = 0.157). The difference between the 2 groups was statistically significant, as indicated by a $p\text{-value}$ of 0.016.

The noticeable increase in the *IFITM3* expression among individuals infected with HCV indicates that this gene might have a role to play in respond to HCV infection. The higher SE observed in the HCV-positive group suggests that there is variability in *IFITM3* gene expression among these individuals, which could be influenced by factors such as the stage of infection, viral load or individual immune response.

Table 1. Distribution of samples according to blood group, gender, age, and hepatitis C virus (HCV) infection status

Parameter		HCV-positive	HCV-negative
Blood group	B+	2	10
		4.1%	19.6%
	A+	9	13
		18.4%	25.5%
	AB–	7	6
		14.3%	11.8%
	AB+	5	8
		10.2%	15.7%
	A–	7	2
		14.3%	3.9%
	B–	5	3
		10.2%	5.9%
	O+	5	8
		10.2%	15.7%
Gender	0–	9	1
		18.4%	2.0%
	total	49	51
		100.0%	100.0%
	χ^2	17.2	
	p-value	0.016	
	male	22	27
		44.9%	52.9%
	female	27	24
		55.1%	47.1%
Age	total	49	51
		100.0%	100.0%
	χ^2	0.642	
	p-value	0.421	
		37.8 \pm 1.48	44.1 \pm 1.56
		0.005	

Table 2. Comparison of *IFITM3* gene expression levels between HCV-positive and HCV-negative individuals

Group	n	Mean of <i>IFITM3</i> gene expression fold	Median	SE
HCV-positive	49	4.21	2.09	1.17
HCV-negative	51	1.36	0.975	0.157
p-value	0.016			

HCV – hepatitis C virus; SE – standard error.

The research investigated the prevalence of HCV-positive and HCV-negative samples according to the presence of other chronic diseases, as shown in Table 3. Statistical

analysis using the χ^2 test revealed a significant difference between the 2 groups ($\chi^2 = 50$, $p = 0.001$), indicating an unequal distribution of chronic diseases among individuals with and without HCV. Notably, a higher percentage (26.5%) of HCV-positive individuals were found to have alcoholic steatohepatitis (NASH) compared to only 3.9% in the HCV-negative group.

These findings suggest a potential link between HCV infection and the presence of NASH. On the other hand, both groups showed similar proportions in terms of hepatocellular carcinoma (HCC, i.e., liver cancer), with rates of 10.2% in HCV-positive individuals and 9.8% in HCV-negative individuals. This indicates that HCV presence

Table 3. Distribution of samples according to the presence of other chronic diseases

Other chronic diseases	HCV-positive	HCV-negative
Fatty liver disease (non-alcoholic steatohepatitis)	1	0
	2.0%	0.0%
Fatty liver disease (non-alcoholic steatohepatitis)	13	2
	26.5%	3.9%
Hepatocellular carcinoma (liver cancer)	5	5
	10.2%	9.8%
Cardiovascular disease	7	4
	14.3%	7.8%
Chronic kidney disease	11	4
	22.4%	7.8%
Type 2 diabetes mellitus	5	1
	10.2%	2.0%
None	1	25
	2.0%	49.0%
Essential hypertension	4	0
	8.2%	0.0%
Chronic kidney disease	2	2
	4.1%	3.9%
Essential hypertension	0	3
	0.0%	5.9%
Fatty liver disease (non-alcoholic steatohepatitis (NASH))	0	3
	0.0%	5.9%
Hepatocellular carcinoma (liver cancer)	0	1
	0.0%	2.0%
Cardiovascular disease	0	1
	0.0%	2.0%
Total	49	51
	100.0%	100.0%
χ^2	50	
p-value	0.001	

HCV – hepatitis C virus.

did not significantly impact the occurrence of liver cancer in this sample. Other notable findings include the following: Cardiovascular disease (CVD) was more prevalent in the HCV-positive group (14.3%) compared to the HCV-negative group (7.8%). Chronic kidney disease (CKD) was more common in HCV-positive individuals (22.4%) compared to HCV-negative individuals (7.8%). Type 2 diabetes mellitus was observed in 10.2% of HCV-positive individuals, compared to only 2.0% of HCV-negative individuals, suggesting a possible link between HCV infection and the development of type 2 diabetes. A significant portion of the HCV-negative group (49.0%) reported having no other chronic diseases, whereas only 2.0% of HCV-positive individuals reported no additional chronic conditions.

This analysis examines the mean HCV viral load across different blood groups, revealing variability in viral loads among them. Notably, individuals with the A- blood group exhibited a significantly higher mean viral load ($2.11E + 06$), accompanied by a large SE ($1.67E + 06$). This suggests substantial variability within this group. The large SE relative to the mean indicates that the data may be highly variable or influenced by outliers, which could impact the overall interpretation of viral load distribution across different blood groups.

The B+ blood group also exhibited a relatively high mean viral load (315.336) with a substantial SE (314.788), indicating high variability among individuals in this group. On the other hand, the A+ and AB- blood groups had the lowest mean viral loads (50.999 and 26.827, respectively) with comparatively smaller SE, suggesting a more consistent viral load among individuals in these groups (as shown in Table 4). The p-value of 0.347 indicates no statistically significant connection between blood group and HCV viral load at the alpha level of 0.05. This suggests that any observed differences in viral load across blood groups are likely due to chance rather than a real effect. However, the higher variability observed in A- and B+ blood groups may be worth further investigation. Exploring potential contributing factors such as stage of infection, history of antiviral treatment, and genetic influences on viral replication could provide deeper insights into why certain blood groups exhibit greater variability in HCV viral load.

The data analysis presented in Table 5 provides insights

Table 4. Mean and standard error (SE) of hepatitis C virus (HCV) viral load in the corresponding ABO blood group of patients

Blood group	Mean HCV viral load	SE	p-value
B+	315,336	314,788	0.347
A+	50,999	24,713	
AB-	26,827	21,575	
AB+	265,720	104,661	
A-	$2.11E + 06$	$1.67E + 06$	
B-	217,473	182,378	
O+	124,650	99,489	
O-	210,322	77,613	

into HCV viral load levels in patients with coexisting chronic conditions. The study reveals variations in viral loads across different conditions, suggesting a potential link between HCV severity and the presence of chronic diseases. Among all patients, those diagnosed with type 2 diabetes mellitus exhibited the highest average HCV viral load ($2.52E + 06$), accompanied by a large SE ($2.38E + 06$). This indicates substantial variability in viral loads among individuals with diabetes, suggesting that type 2 diabetes may influence HCV replication or disease progression. However, due to the large SE, these findings should be interpreted cautiously. The variability observed suggests that additional factors, such as disease stage, immune response or treatment history, may contribute to differences in HCV viral load among individuals with type 2 diabetes. Further investigation is needed to determine the precise nature of this relationship.

On the other hand, patients without any chronic diseases had the lowest mean viral load (455), which was significantly lower than that of individuals with comorbidities. This finding suggests that the absence of chronic diseases may be associated with a lower HCV burden. This difference could be attributed to a compromised immune system in individuals with chronic diseases, making them more susceptible to higher viral replication, and the absence of potential interactions between HCV and other

Table 5. Mean and standard error (SE) of hepatitis C virus (HCV) viral load in the corresponding other chronic diseases that the patients were suffering from

Other chronic diseases	Mean HCV viral load	SE	p-value
Fatty liver disease (non-alcoholic steatohepatitis (NASH))	269,269	99,975	0.214
Hepatocellular carcinoma (liver cancer)	238,651	124,538	
Cardiovascular disease	282,420	194,190	
Chronic kidney disease	106,805	46,017	
Type 2 diabetes mellitus	$2.52E+06$	$2.38E+06$	
None	455	347	
Essential hypertension	79,287	40,343	

diseases, which might otherwise work synergistically to worsen infection severity. For other chronic conditions, such as fatty liver disease (NASH), HCC, CVD, and essential hypertension, the mean viral loads ranged from 79.287 to 282.420. Notably, patients with NASH had a mean viral load of 269.269 with a SE of 99.975, suggesting a possible link between NASH and higher HCV viral loads. Standard errors across most conditions, except for type 2 diabetes and CVD were relatively lower compared to their means, indicating a reasonable level of confidence in the mean estimates for these conditions.

The scatter plot in Fig. 3 was used to assess the correlation between *IFITM3* gene expression levels and HCV viral loads. A correlation coefficient (r) of 0.343 indicates a moderate positive correlation, suggesting that higher *IFITM3* gene expression tends to coincide with increased HCV viral loads. The p -value of 0.016, which is below the conventional threshold of 0.05, indicates that this correlation is statistically significant and unlikely to be due to chance.

The positive correlation suggests a potential association between *IFITM3* gene expression levels and increased HCV loads. This could indicate that the *IFITM3* gene plays a role in the replication or life cycle of the HCV, or it might reflect an enhanced host response to higher viral loads. The shaded region surrounding the regression line, presumably representing the 95% CI, indicates variability in estimating *IFITM3* gene expression for any given HCV load. This variability is expected and suggests that, while an overall trend exists, individual data points may deviate due to factors not considered in our analysis.

The regression analysis was conducted to evaluate the relationship between HCV viral load and *IFITM3* gene

expression while controlling for potential confounders such as age, gender, blood group, and the presence of chronic conditions. The HCV viral load emerged as a significant predictor of *IFITM3* expression, with an estimated coefficient of 0.356 and a p -value of 0.016. This finding suggests that for each unit increase in viral load, *IFITM3* expression increases by 0.356 units, indicating a positive association between viral load and *IFITM3* gene expression.

This significant relationship underscores the potential role of viral load in modulating *IFITM3* expression levels in patients with HCV. In contrast, age did not show a significant association with *IFITM3* expression (estimate = 0.00503, p = 0.97), suggesting that age has a negligible effect in this population. Similarly, gender (male) was not a significant predictor (estimate = -3.141, p = 0.297), although the negative coefficient hints at a trend toward lower *IFITM3* expression in men, which was not statistically significant.

The analysis also examined the effect of blood group on *IFITM3* expression. While most blood groups (A+, AB-, AB+, B-, B+, O+) did not significantly affect *IFITM3* expression, blood group O- exhibited a marginally significant positive association (p = 0.073). Individuals with blood group O- might have higher *IFITM3* expression compared to those with other blood groups; however, the statistical evidence is not strong enough to draw firm conclusions. Regarding chronic conditions, type 2 diabetes mellitus emerged as a significant predictor of *IFITM3* expression, with an estimate of 5.074 and a p -value of 0.038. This indicates that individuals with type 2 diabetes tend to have higher levels of *IFITM3* expression, suggesting a potential link between metabolic disorders and the regulation of *IFITM3*. In contrast, other chronic conditions such as CKD essential hypertension, and NASH did not show significant associations with *IFITM3* expression (Table 6).

Discussion

Diagnosing and treating HCV infection is challenging because HCV can lead to cirrhosis and HCC,¹⁵ and its mutation rate and genetic variability further complicate treatment.¹⁶ It is estimated that 71 million people globally are infected with HCV, stressing the need for effective treatments and a better knowledge of its pathogenesis.¹⁷ Interferon-induced transmembrane protein 3 helps fight viral infections¹⁸ by preventing viral entry into host cells, thereby conferring resistance.¹⁹

The antiviral activity of *IFITM3* primarily stems from its ability to restrict fusion between viruses and host cell membranes – a critical step in the viral life cycle.²⁰ *IFITM3* is localized within lysosomal membranes and is believed to modify their properties, effectively blocking the release of viral genetic material into the cytosol. This function becomes particularly significant in the context of HCV, which relies on this pathway to enter hepatocytes.²¹

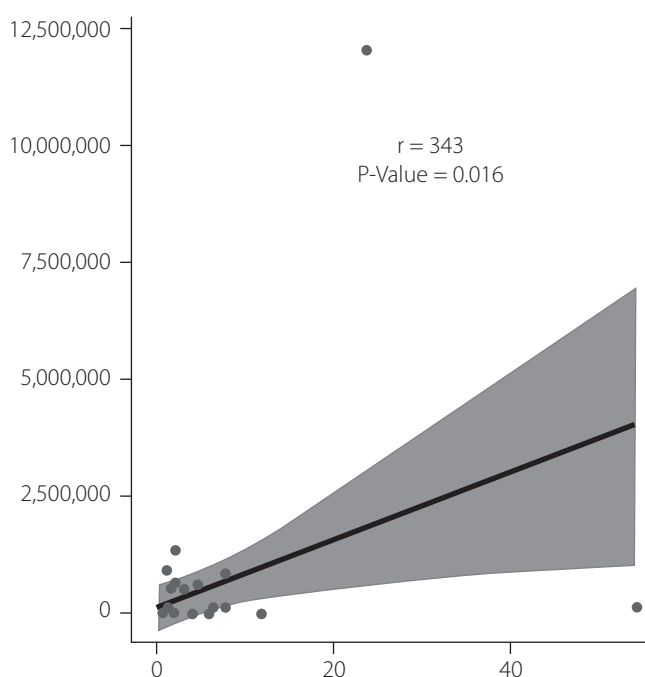


Fig. 3. Correlation between *IFITM3* gene expression levels and hepatitis C virus (HCV) viral loads

Table 6. Regression analysis representing the relationship between HCV viral load and *IFITM3* gene expression

Parameter	Estimate	SE	Statistic (t-value)	p-value
(Intercept)	2.5	8.31	0.301	0.765
HCV viral load	0.356	0.337	0.106	0.016
Age	0.00503	0.132	0.0382	0.97
Gender (male)	-3.141	2.97	-1.06	0.297
Blood group A+	1.815	5.79	0.313	0.756
Blood group AB-	-3.377	6.14	-0.55	0.586
Blood group AB+	1.368	6.54	0.209	0.836
Blood group B-	-0.625	8.37	-0.0747	0.941
Blood group B+	-0.584	6.36	-0.0918	0.927
Blood group O-	12.83	6.92	1.85	0.729
Blood group O+	-1.92	6.01	-0.319	0.752
Chronic kidney disease	4.769	4.17	1.14	0.261
Essential hypertension	-0.872	5.4	-0.162	0.873
Fatty liver disease	-0.362	4.65	-0.078	0.938
Hepatocellular carcinoma (liver cancer)	2.421	5.69	0.426	0.673
None	1.114	11.46	0.0972	0.923
Type 2 diabetes mellitus	5.074	5.72	0.887	0.382

HCV – hepatitis C virus; SE – standard error.

Recent studies have shed light on the function of *IFITM3* in HCV infection.²² Evidence suggests that upon infection, the body may upregulate *IFITM3*, which could influence viral levels and disease progression. *IFITM3* is now being considered both as a potential therapeutic target and as a marker to assess HCV infection severity and treatment response.²³ Our understanding of *IFITM3*'s role in HCV infection is still evolving, and ongoing research aims to uncover its range of antiviral properties and mechanisms. By studying how HCV interacts with factors like *IFITM3* within the body, we can develop new strategies to combat HCV and improve patient outcomes. In this study, we explored the relationship between HCV infection and various demographic and clinical factors, including blood group, gender, age, *IFITM3* gene expression, and coexisting chronic diseases.

Analysis of blood group distribution among HCV-positive and HCV-negative individuals revealed a significant association ($p = 0.016$), with blood group O- being more prevalent in the HCV-positive cohort. It is hypothesized that individuals with the O- blood group might exhibit an altered immune response, potentially affecting the expression of antiviral genes such as *IFITM3*. Given that *IFITM3* plays a crucial role in blocking viral entry into host cells, it is plausible that blood group antigens modulate interferon responses, which in turn influence *IFITM3* gene expression and viral load. However, this area warrants further investigation.

Contrary to gender, where no significant association was found ($p = 0.421$), age showed a significant difference, with the HCV-positive group being younger on average

($p = 0.005$). This information suggests that younger individuals with certain blood types may require closer monitoring of viral infections. These results align with a previous study that also found the highest prevalence of HCV infections among individuals with blood group O-.²⁴ In addition, the study observed a significant upregulation of *IFITM3* gene expression in HCV-positive individuals ($p = 0.016$), suggesting that *IFITM3* plays a role in the immune response to HCV infection. These findings are supported by previous research.²⁵

This is further supported by the positive correlation between *IFITM3* expression and HCV viral loads ($r = 0.343$, $p = 0.016$), which indicates a potential interaction between host genetic factors and viral replication dynamics. Additionally, when examining the relationship between HCV infection severity and the presence of other chronic diseases, our analysis revealed a significantly higher prevalence of conditions such as NASH, CKD and type 2 diabetes mellitus among HCV-infected individuals.

This prevalence underscores the need for comprehensive management strategies that address not only HCV but also these co-morbid conditions, which can influence disease progression and treatment responses. Nonetheless, the mean HCV viral load did not correlate with blood group ($p = 0.347$), suggesting that blood type may not directly affect viral replication in HCV pathogenesis. Given the heterogeneity in viral loads across blood types and chronic conditions, particularly the high mean viral load observed in patients with type 2 diabetes mellitus, further

research is needed to determine how these variables may impact disease severity or treatment efficacy. Additionally, the PCR method is recommended for virus identification and is widely used across microbiology and medical fields as a molecular diagnostic approach.^{26–36}

Conclusions

The impressive correlations observed in this research underscore the need for a comprehensive strategy to understand and manage HCV disease. Future investigations, particularly those employing longitudinal data, are necessary to elucidate the mechanisms behind these associations, establish causality, and assess the impact of interventions. Additionally, further study of *IFITM3* gene expression as a potential biomarker for HCV infection and progression holds considerable promise.

Data availability

The datasets generated and/or analyzed during the current study are available from the corresponding author on reasonable request.

Consent for publication


Not applicable.


Use of AI and AI-assisted technologies


Not applicable.

ORCID iDs


Tabarak S. Jassim  <https://orcid.org/0000-0003-1263-605X>

Sura S. Talib  <https://orcid.org/0009-0001-0927-8856>

Nawar R. Jaber  <https://orcid.org/0009-0002-0835-5781>

Dina H. Sahib  <https://orcid.org/0009-0006-0157-6919>

Rusul W. Ali  <https://orcid.org/0009-0000-5456-6411>

Bahaa Al-Rubaii  <https://orcid.org/0000-0003-4546-1815>

References

- Mayanja E, Luboobi LS, Kasozi J, Nsubuga RN. Mathematical modelling of HIV-HCV coinfection dynamics in absence of therapy. *Comput Math Methods Med.* 2020;2020:2106570. doi:10.1155/2020/2106570
- Warkad SD, Song KS, Pal D, Nimse SB. Developments in the HCV screening technologies based on the detection of antigens and antibodies. *Sensors.* 2019;19(19):4257. doi:10.3390/s19194257
- Cuyper L, Ceccherini-Silberstein F, Van Laethem K, Li G, Vandamme A, Rockstroh JK. Impact of HCV genotype on treatment regimens and drug resistance: A snapshot in time. *Rev Med Virol.* 2016;26(6):408–434. doi:10.1002/rmv.1895
- Negro F. Natural history of hepatic and extrahepatic hepatitis C virus diseases and impact of interferon-free HCV therapy. *Cold Spring Harb Perspect Med.* 2020;10(4):a036921. doi:10.1101/cshperspect.a036921
- Moghim M, Tavakoli F, Doosti M, Ahmadi-Vasmehjani A, Akhondi-Meybodi M. Correlation between interleukin-28 gene polymorphism with interleukin-28 cytokine levels and viral genotypes among HCV patients in Yazd, Iran. *BMC Res Notes.* 2019;12(1):626. doi:10.1186/s13104-019-4651-z
- Mosaad YM, Metwally SS, Farag RE, Lotfy ZF, AbdelTwab HE. Association between toll-like receptor 3 (TLR3) rs3775290, TLR7 rs179008, TLR9 rs352140 and chronic HCV. *Immunol Invest.* 2019;48(3):321–332. doi:10.1080/08820139.2018.1527851
- Jiang LQ, Xia T, Hu YH, et al. IFITM3 inhibits virus-triggered induction of type I interferon by mediating autophagosome-dependent degradation of IRF3. *Cell Mol Immunol.* 2018;15(9):858–867. doi:10.1038/cmi.2017.15
- Friedlová N, Zavadil Kokáš F, Hupp TR, Vojtěšek B, Nekulová M. IFITM protein regulation and functions: Far beyond the fight against viruses. *Front Immunol.* 2022;13:1042368. doi:10.3389/fimmu.2022.1042368
- Schoggins JW. Interferon-stimulated genes: What do they all do? *Annu Rev Virol.* 2019;6(1):567–584. doi:10.1146/annurev-virology-092818-015756
- Jaroszewicz J, Calle Serrano B, Wursthorn K, et al. Hepatitis B surface antigen (HBsAg) levels in the natural history of hepatitis B virus (HBV)-infection: A European perspective. *J Hepatol.* 2010;52(4):514–522. doi:10.1016/j.jhep.2010.01.014
- Freiman JM, Tran TM, Schumacher SG, et al. Hepatitis C core antigen testing for diagnosis of hepatitis C virus infection: A systematic review and meta-analysis. *Ann Intern Med.* 2016;165(5):345. doi:10.7326/M16-0065
- Sidiq Z, Hanif M, Dwivedi KK, Chopra KK. Benefits and limitations of serological assays in COVID-19 infection. *Indian J Tuberc.* 2020;67(4 Suppl):S163–S166. doi:10.1016/j.ijtb.2020.07.034
- Revie D, Salahuddin SZ. Human cell types important for hepatitis C virus replication in vivo and in vitro: Old assertions and current evidence. *Virol J.* 2011;8:346. doi:10.1186/1743-422X-8-346
- Wang Y, Jie W, Ling J, Yuanshuai H. HCV core antigen plays an important role in the fight against HCV as an alternative to HCV-RNA detection. *Clin Lab Anal.* 2021;35(6):e23755. doi:10.1002/jcla.23755
- Goto K, Roca Suarez AA, Wrensch F, Baumert TF, Lupberger J. Hepatitis C virus and hepatocellular carcinoma: When the host loses its grip. *Int J Mol Sci.* 2020;21(9):3057. doi:10.3390/ijms21093057
- Martínez I, Ryan P, Valencia J, Resino S. The challenging road to hepatitis C virus eradication. *J Clin Med.* 2021;10(4):611. doi:10.3390/jcm10040611
- Polaris Observatory HCV Collaborators. Global prevalence and genotype distribution of hepatitis C virus infection in 2015: A modelling study. *Lancet Gastroenterol Hepatol.* 2017;2(3):161–176. doi:10.1016/S2468-1253(16)30181-9
- Ahmadi I, Afifipour A, Sakhaee F, et al. Impact of interferon-induced transmembrane protein 3 gene rs12252 polymorphism on COVID-19 mortality. *Cytokine.* 2022;157:155957. doi:10.1016/j.cyt.2022.155957
- Gómez-Herranz M, Taylor J, Sloan RD. IFITM proteins: Understanding their diverse roles in viral infection, cancer, and immunity. *J Biol Chem.* 2023;299(1):102741. doi:10.1016/j.jbc.2022.102741
- Majdoul S, Compton AA. Lessons in self-defence: inhibition of virus entry by intrinsic immunity. *Nat Rev Immunol.* 2022;22(6):339–352. doi:10.1038/s41577-021-00626-8
- Palatini M, Müller SF, Kirstgen M, et al. IFITM3 interacts with the HBV/HDV receptor NTCP and modulates virus entry and infection. *Virus-es.* 2022;14(4):727. doi:10.3390/v14040727
- Unali G, Crivicich G, Pagani I, et al. Interferon-inducible phospholipids govern IFITM3-dependent endosomal antiviral immunity. *EMBO J.* 2023;42(10):e112234. doi:10.15252/embj.2022112234
- Pomar CA, Bonet ML, Ferre-Beltrán A, et al. Increased mRNA levels of ADAM17, IFITM3, and IFNE in peripheral blood cells are present in patients with obesity and may predict severe COVID-19 evolution. *Biomedicines.* 2022;10(8):2007. doi:10.3390/biomedicines10082007
- Mahnoor, Noreen M, Imran M, et al. Association of blood groups with hepatitis C viremia. *Saudi J Biol Sci.* 2021;28(9):5359–5363. doi:10.1016/j.sjbs.2021.05.062
- Narayana SK, Helbig KJ, McCartney EM, et al. The interferon-induced transmembrane proteins, IFITM1, IFITM2, and IFITM3 inhibit hepatitis C virus entry. *J Biol Chem.* 2015;290(43):25946–25959. doi:10.1074/jbc.M115.657346
- Al-Saidi M, Al-Bbana JA, Hassan E, Al-Rubaii BAL. Extraction and characterization of nickel oxide nanoparticles from Hibiscus plant using green technology and study of its antibacterial activity. *Bio-medicine.* 2022;42(6):1290–1295. https://www.researchgate.net/publication/366877028_Extraction_and_characterization_of_nickel_oxide_nanoparticles_from_Hibiscus_plant_using_green_technology_and_study_of_its_antibacterial_activity

27. Sultan RS, Al Khayali BDH, Abdulmajeed M, Al-Rubaii BAL. Exploring small nucleolar RNA host gene 3 as a therapeutic target in breast cancer through metabolic reprogramming. *Opera Med Physiol.* 2023;10(4):36–47. doi:10.24412/2500-2295-2023-4-36-47
28. Wieland S, Makowska Z, Campana B, et al. Simultaneous detection of hepatitis C virus and interferon stimulated gene expression in infected human liver. *Hepatology.* 2014;59(6):2121–2130. doi:10.1002/hep.26770
29. Mohammed RA, Al-Asady ZTS, Frayyeh MJ, Al-Rubaii BAL. The influence of radiotherapy exposure on anti-TPO Ab, anti-Tg Ab, anti-nuclear Ab, anti-DSA Ab and complete blood markers in hospital physician workers in Nuclear Baghdad Hospital. *Opera Med Physiol.* 2024;11(2):5–15. doi:10.24412/2500-2295-2024-2-5-15
30. Al-Maliki NS, Zedan ZK. miRNA-126 as a biomarker for cancer stem cells: Role in chemotherapy resistance in Iraqi patients with acute myeloid leukemia. *Al-Rafidain J Med Sci.* 2024;6(1):195–199. doi:10.54133/ajms.v6i1.577
31. Halah AL, Zainab HL, Hamzah SS, Tahreer HS, Al-Rubaii BAL. Molecular identification of intracellular survival related *Brucella melitensis* virulence factors. *Biomedicine.* 2022;42(4):761–765. https://www.researchgate.net/publication/366877028_Extraction_and_characterization_of_nickel_oxide_nanoparticles_from_Hibiscus_plant_using_green_technology_and_study_of_its_antibacterial_activity
32. Abdullah MM, AL-Rubaii BAL. Effect of Lactobacillus supernatant on swarming-related gene expression in *Proteus mirabilis* isolated from urinary tract infections. *Ukr J Nephrol Dial.* 2024;4(84):39–48. doi:10.31450/ukrjnd.4(84).2024.05
33. Ghena Jameel I, Al-Rubaii BAL. The efficiency of certain amino acids in regulating *chABC1* gene expression in *Proteus mirabilis*. *Iraqi J Sci.* 2024;65(9):4983–4992. doi:10.24996/ij.s.2024.65.9.15
34. Zbar NS, Abbas ZN, Al-Ugaili DN. Detection of streptokinase production by *Streptococcus pyogenes* using real time PCR. *Res J Pharm Technol.* 2022;15(7):3251–3254. doi:10.52711/0974-360X.2022.00545
35. Mohammed DY, Al-Maoula MS, Al-Khafaji ZH, Dwaish AS. Effect of hot alcoholic extract of algae, *Enteromorpha ralfsii* on the mortality and emergence rate of housefly *Musca domestica*. *Int J Agric Biol.* 2024;31(6):417–424. [https://api.fspublishers.org/viewPaper/66425_03%20doi%2015.2159%20IJAB-23-0326%20\(8\)%20417-424.pdf](https://api.fspublishers.org/viewPaper/66425_03%20doi%2015.2159%20IJAB-23-0326%20(8)%20417-424.pdf).
36. Zedan ZK, Salah HAA. The dysregulation of mir-21 and mir-143 as a clinical marker for cancer stem cells in tissue samples of Iraqi male patients with gastrointestinal sarcoma. *J Pharm Negative Results.* 2022;13(3):20–25. doi:10.47750/pnr.2022.13.03.004

Polyhydroxybutyrate nanoparticle improving the sensitivity of *Pseudomonas aeruginosa* to ceftriaxone and reducing the biofilm formation in vitro

Shams Ihssan Sadiq^{B,E,F}, Jenan Atiyah Ghafil^{A–F}

Department of Biology, College of Science, University of Baghdad, Iraq

A – research concept and design; B – collection and/or assembly of data; C – data analysis and interpretation; D – writing the article; E – critical revision of the article; F – final approval of the article

Polymers in Medicine, ISSN 0370-0747, eISSN 2451-2699

Polim Med. 2025;55(1):31–39

Address for correspondence

Jenan Atiyah Ghafil

E-mail: genan.atiyah@sc.uobaghdad.edu.iq

Funding sources

None declared

Conflict of interest

None declared

Received on February 24, 2025

Reviewed on March 16, 2025

Accepted on April 6, 2025

Published online on June 30, 2025

Cite as

Sadiq SI, Ghafil JA. Polyhydroxybutyrate nanoparticle improving the sensitivity of *Pseudomonas aeruginosa* to ceftriaxone and reducing the biofilm formation in vitro. *Polim Med.* 2025;55(1):31–39. doi:10.17219/pim/203765

DOI

10.17219/pim/203765

Copyright

Copyright by Author(s)

This is an article distributed under the terms of the Creative Commons Attribution 3.0 Unported (CC BY 3.0) (<https://creativecommons.org/licenses/by/3.0/>)

Abstract

Background. Polyhydroxybutyrate nanoparticles (PHB-NPs) represent a promising strategy for addressing the growing threat of bacterial resistance to antibiotics – a major concern in global public health. Despite their potential, there is a noticeable gap in the current literature regarding their ability to enhance the efficacy of existing antibiotic therapies.

Objectives. This study investigates the synergistic effect of PHB-NPs in enhancing the antibacterial activity of ceftriaxone (CRO) against *Pseudomonas aeruginosa*, with a particular focus on mitigating key virulence factors such as biofilm formation and adhesion.

Materials and methods. Polyhydroxybutyrate nanoparticles were synthesized using the pH gradient and sonication method. The antibacterial activity of PHB-NPs, CRO and the combined formulation (PHB-NP-CRO) was assessed using minimum inhibitory concentration (MIC) testing and the well diffusion method. Additionally, the effects of these formulations on *P. aeruginosa* biofilm formation on an abiotic surface (polystyrene) and bacterial adhesion to human oral mucosal epithelial cells (OMECS) were evaluated.

Results. The diameters of the prepared PHB-NPs ranged from 15 nm to 34 nm, with an average size of 28.2 ± 6.3 nm. All *P. aeruginosa* isolates were capable of biofilm production. A negative correlation was observed between the diameter of the CRO inhibition zones and the extent of biofilm formation among the 20 isolates. The MICs for PHB, PHB-NPs, CRO, and the combined formulation (PHB-NP-CRO) were 2,000, 1,000, 250, and 62.5 µg/mL, respectively. Sub-MIC concentrations (as low as 1/32 MIC) of both CRO and PHB-NP-CRO exhibited significant inhibitory effects on biofilm formation and bacterial adhesion to human OMECS ($p < 0.050$).

Conclusions. The combination of PHB-NPs with CRO significantly enhances the antibacterial activity of CRO against *P. aeruginosa*. Moreover, sub-inhibitory concentrations (sub-MICs) of both PHB-NP-CRO and CRO alone effectively reduce the bacterium's ability to form biofilms and adhere to biotic surfaces.

Key words: nanoparticles, adhesion, biofilm, ceftriaxone, polyhydroxybutyrate

Background

Pseudomonas aeruginosa is a Gram-negative opportunistic pathogen that poses a significant threat to public health. It is known for causing a wide spectrum of infections, ranging from relatively mild skin and soft tissue infections to life-threatening conditions such as pneumonia, urinary tract infections, otitis media, bloodstream infections, and sepsis.^{1–4}

The ability of *P. aeruginosa* to form biofilms, its intrinsic resistance to multiple antibiotics and its capacity to acquire additional resistance mechanisms through genetic adaptation represent key virulence factors of this bacterium.^{1–3} These characteristics make *P. aeruginosa* infections particularly challenging to treat, especially in immunocompromised patients.⁵ One of the primary strategies for eradicating *P. aeruginosa* infections involves the use of broad-spectrum antibiotics. Ceftriaxone (CRO), a third-generation cephalosporin, is among the agents that may be employed. It acts by inhibiting bacterial cell wall synthesis.³ However, the emergence of antibiotic resistance – particularly resistance to cephalosporins – poses a significant concern in the treatment of *P. aeruginosa* infections. Resistance can occur through various mechanisms, including the secretion of β -lactamases that hydrolyze the β -lactam ring of CRO, alterations in bacterial cell wall permeability and overexpression of efflux pumps.⁶ Consequently, there is an urgent need to develop strategies that enhance the antibacterial efficacy of existing antibiotics – especially in light of the rising prevalence of antibiotic resistance and the limited success in discovering new antimicrobial agents. Nanotechnology offers promising strategies to address the growing challenge of antibiotic resistance. Nanomaterials can enhance drug delivery, improve antibiotic efficacy and help overcome bacterial resistance mechanisms. Among the various nanomaterials explored, polyhydroxybutyrate (PHB) nanoparticles have emerged as a biocompatible and biodegradable option for advanced drug delivery systems.⁷

Polyhydroxybutyrate is considered a low-toxicity material, primarily due to its natural biodegradability, biocompatibility and non-toxic degradation products. It is a naturally occurring polyester synthesized by various microorganisms, including *Ralstonia eutropha* and *Bacillus* species.⁸ Numerous previous studies have explored the antibacterial properties of PHB. As a naturally occurring polyester synthesized by microorganisms, PHB is particularly attractive due to its low toxicity.⁹ Previous studies have demonstrated the antibacterial activity of polyhydroxybutyrate nanoparticles (PHB-NPs) against various bacterial species. Additionally, other researchers investigated the efficacy of CRO in treating burn wound infections caused by *P. aeruginosa*.^{9–11}

Rossi et al. incorporated polyhydroxybutyrate (PHB) with gentamicin for the treatment of *Staphylococcus* infections.¹² An earlier study demonstrated that sub-minimum

inhibitory concentrations (sub-MICs) of CRO reduced *P. aeruginosa* adhesion to human oral mucosal epithelial cells (OMECs).³ However, the antibacterial effect of combining PHB-NPs with CRO remains scarcely explored in the literature.

Objectives

This study aims to evaluate the potential of PHB-NPs loaded with CRO to enhance the antibiotic's efficacy against *P. aeruginosa* in vitro. The current research may contribute to the development of novel therapeutic strategies for combating drug-resistant *P. aeruginosa* infections and improving patient outcomes.

Materials and methods

Ethical approval

The study was approved by the Human Ethical Committee of the Department of Biology, College of Science, University of Baghdad, Iraq. An official signed approval letter was issued under Reference No. CSEC/1124/0098 on June 8, 2024.

Isolation and identification of bacteria

Infected wound samples were aseptically collected from 91 inpatients diagnosed with wound infections at Baghdad Teaching Hospital (Baghdad, Iraq). All patients had not received antibiotic treatment within 72 h prior to sample collection and provided written informed consent to participate in the study. Wound swabs were cultured on MacConkey agar (HiMedia, Mumbai, India) and incubated at 37°C for 18 h.

Non-fermenting colonies were sub-cultured onto cetrimide agar (HiMedia) for further identification. Colonies exhibiting bright fluorescent green pigmentation – attributed to pyoverdine production – with flat, spreading morphology and a smooth, mucoid texture were selected for analysis. Standard biochemical tests were performed to identify the clinical isolates. Final identification of *P. aeruginosa* was carried out using the VITEK® DensiCHEK™ instrument and fluorescence-based system (bioMérieux, Marcy-l'Étoile, France) with the ID-GNB identification card.

PHB-NPs preparation

Polyhydroxybutyrate nanoparticles were prepared and characterized following the method previously described by Ghafil and Flieh.¹³ Briefly, 0.5 g of PHB (Sigma-Aldrich, St. Louis, USA) was dissolved in 25 mL of distilled water, and the pH was adjusted to 4 using 1 N HCl. The mixture was subjected to ultrasonication at 4,500 kHz

for 30 s at 21°C. Subsequently, the pH was raised to 10 using 1 N NaOH. The solution was then shaken in a water bath shaker (Memmert GmbH, Schwabach, Germany) at 37°C for 2 h and incubated at 21°C for 18 h.

Following incubation, the pH of the solution was readjusted to 7 using 1 N HCl. The prepared PHB-NPs were characterized using atomic force microscopy (AFM; Innova® AFM; Bruker, Santa Barbara, USA). For AFM analysis, a thin film of the nanoparticles was deposited on a silica glass plate. Scanning electron microscopy (SEM) was also performed (Zeiss EVO® LS 15; Carl Zeiss AG, Jena, Germany); a glass smear of the PHB-NPs was prepared and coated with a thin layer of platinum to enhance conductivity for imaging.¹³

Kirby–Bauer method

The Kirby–Bauer disk diffusion method was employed to assess the susceptibility of *P. aeruginosa* to CRO. A bacterial suspension adjusted to a turbidity equivalent to a 0.5 McFarland standard was uniformly spread onto Mueller–Hinton agar (MHA) plates (20 mL per plate; HiMedia). Ceftriaxone disks (30 µg; Bioanalyse, Ankara, Turkey) were placed on the surface of the agar, and the plates were incubated at 37°C for 18 h.

The diameters of the inhibition zones around each CRO disk were measured and interpreted according to the Clinical and Laboratory Standards Institute (CLSI) breakpoint guidelines. Based on these standards, isolates were classified as sensitive (S), intermediate (I) or resistant (R). Notably, resistance classification was determined for CRO.¹⁴

Minimum inhibitory concentration

The microdilution technique described by Al-Mutalib and Zgair,¹⁵ was used to determine the minimum inhibitory concentrations (MICs) of PHB, PHB-NPs, CRO, and PHB-NPs-CRO against a *P. aeruginosa* strain exhibiting high resistance to CRO. Stock solutions of PHB and PHB-NPs (5 mg/mL) were prepared by dissolving 0.5 g of each in 100 mL of dimethyl sulfoxide (DMSO). Equivalent concentrations of CRO and PHB-NPs-CRO (containing 1 mg PHB-NPs and 1 mg CRO) were used for MIC determination.

Double-fold serial dilutions (100 µL) were prepared in a 96-well U-bottom microtiter plate (BIOFIL) using sterile Mueller–Hinton broth (MHB; HiMedia). The *P. aeruginosa* suspension was prepared by harvesting overnight bacterial growth, followed by washing with sterile phosphate-buffered saline (PBS; 0.1 M, pH 7.2) and centrifugation at $5,000 \times g$ for 10 min (Beckman Coulter, Brea, USA). The optical density (OD) of the resulting suspension was adjusted to 0.1 at 600 nm using a spectrophotometer (Bio-evopeak, Jinan, China).

The microtiter plates were gently shaken and incubated at 37°C for 18 h. Multiple controls were included in the experiment: 1) MHB with the bacterial isolate, 2) MHB only

(sterility control), 3) serial dilutions of PHB, 4) serial dilutions of PHB-NPs, 5) serial dilutions of CRO, 6) serial dilutions of PHB-NP-CRO, and 7) serial dilutions of DMSO. The minimum inhibitory concentration (MIC) was defined as the lowest concentration of the tested compound that completely inhibited visible bacterial growth.¹⁵

Well diffusion method

The method described by Hasan and Ghafil¹⁶ was followed to evaluate the antibacterial effects of PHB, PHB-NPs, CRO, and PHB-NPs-CRO against *P. aeruginosa* strain Pa11. A 100 µL aliquot of the standardized Pa11 inoculum ($OD_{600} = 0.1$), as prepared in section of MIC method, was uniformly spread onto MHA plates.

Five wells, each 8 mm in diameter, were created in the agar using a sterile cork borer. Each well was filled with 100 µL of the respective test solution (2,000 µg/mL) of PHB, PHB-NPs, CRO, or PHB-NPs-CRO. One well was filled with 100 µL of DMSO and served as a negative control. The plates were incubated at 37°C for 18 h. The diameters of the inhibition zones around each well were measured using a ruler. All experiments were performed in triplicate.¹⁶

Biofilm formation

The standard method described by Talib and Ghafil³ was followed to assess biofilm formation by *P. aeruginosa* strains resistant to CRO (30-µg disk). Briefly, 200 µL of sterile Tryptic Soy Broth (TSB; HiMedia) were added to the wells of a flat-bottom polystyrene tissue culture plate. A 5 µL aliquot of the standardized *P. aeruginosa* inoculum (prepared as described in MIC method) was added to each well. Plates were incubated at 37°C for 18 h. After incubation, the TSB was discarded, and the wells were gently washed 3 times with sterile distilled water to remove non-adherent cells. The plates were air-dried and stained with 200 µL of 0.4% Hucker's crystal violet solution for 15 min. Excess stain was removed by washing the wells 5 times with distilled water. After complete drying, 200 µL of anhydrous ethanol was added to each well to solubilize the bound dye. The absorbance was measured at 590 nm using a microplate reader (BioTek 800 TS; BioTek, Winooski, USA). The experiment was performed in triplicate.³ To investigate the effect of various sub-MIC concentrations of PHB, PHB-NPs, CRO, and PHB-NPs-CRO ($\frac{1}{2}$ MIC, $\frac{1}{4}$ MIC, $\frac{1}{8}$ MIC, $\frac{1}{16}$ MIC, $\frac{1}{32}$ MIC, and $\frac{1}{64}$ MIC) on *P. aeruginosa* biofilm formation, a modification of the standard biofilm assay was employed. Instead of using plain TSB, serial dilutions of each test compound at the indicated sub-MIC levels were prepared in TSB (HiMedia) and added to the wells of a flat-bottom polystyrene microtiter plate. The plates were incubated at 37°C for 18 h, after which the wells were washed 3 times with distilled water to remove non-adherent cells. The wells were then stained with 200 µL of crystal violet (0.4%) for

15 min. After thorough washing and air drying, 200 μ L of anhydrous ethanol was added to each well to solubilize the bound dye. The absorbance was measured at 590 nm using a microplate reader (BioTek 800 TS). The experiment was performed in triplicate.³

Effect of sub-MICs on adhesion to human OMECs

In this experiment, a *P. aeruginosa* strain that exhibited resistance to CRO 30- μ g antibiotic disk and produced the highest level of biofilm was selected to study the effect of various sub-MICs of PHB, PHB-NPs, CRO, and PHB-NPs-CRO ($\frac{1}{2}$ MIC, $\frac{1}{4}$ MIC, $\frac{1}{8}$ MIC, $\frac{1}{16}$ MIC, $\frac{1}{32}$ MIC, and $\frac{1}{64}$ MIC) on bacterial adhesion to human OMECs. Previously established methods were followed to culture human OMECs in vitro and to assess the influence of different antibiotic concentrations on *P. aeruginosa* adhesion to these cells.^{3,15}

Bacterial colonies were cultured in TCB (HiMedia). A standardized inoculum of *P. aeruginosa* ($OD_{600} = 0.1$) was prepared in TSB and treated with various sub-MICs ($\frac{1}{2}$ MIC, $\frac{1}{4}$ MIC, $\frac{1}{8}$ MIC, $\frac{1}{16}$ MIC, $\frac{1}{32}$ MIC, and $\frac{1}{64}$ MIC) of PHB, PHB-NPs, CRO, and PHB-NPs-CRO. The suspensions were incubated at 37°C for 18 h. After incubation, the bacterial cultures were washed 3 times with PBS (0.1 M, pH 7.2) by centrifugation at 6,000 \times g for 10 min. The resulting bacterial pellets were resuspended in fresh TSB, and the optical density was readjusted to 0.1 at 600 nm. In tissue culture tubes (Biofil, Guangzhou, China), 900 μ L of a suspension containing 1×10^5 human OMECs in Dulbecco's modified Eagle's medium (DMEM) supplemented with 10% fetal calf serum and 10 mM L-glutamine was mixed with 100 μ L of pre-treated *P. aeruginosa* ($OD_{600} = 0.1$). The tubes were incubated at 37°C for 2 h. Following incubation, the OMECs

were washed 3 times with PBS (0.1 M, pH 7.2) by centrifugation at 1,000 \times g for 8 min (Beckman Coulter) to remove non-adherent bacteria. One portion of the OMECs was stained with Leishman's stain for microscopic examination. The remaining cells were lysed using PBS containing 0.5% Triton X-100 (Sigma-Aldrich). The resulting lysate was serially diluted tenfold and plated on nutrient agar to enumerate viable adherent bacteria. The OMECs exposed to untreated bacteria to PHB, PHB-NPs, CRO, and PHB-NPs-CRO served as control groups.^{3,15}

Statistical analyses

Statistical analyses were performed and graphs generated using Origin pro 8.6 (OriginLab, Northampton, USA). Data are presented as means \pm standard error ($M \pm SE$). Differences between groups were evaluated using Student's t-test and one-way analysis of variance (ANOVA). Correlations were assessed using Pearson's correlation coefficient (r). A p-value of less than 0.05 was considered statistically significant.

Results

PHB-NP preparation

In the present study, PHB nanoparticles (P3HB-NPs) were prepared using the pH gradient combined with ultrasonication, which proved to be the most effective method for producing uniform nanoparticles. To confirm the nanoparticulate nature of the prepared material, ATM and SEM were employed, as illustrated in Fig. 1. The results indicated that the diameters of the synthesized PHB-NPs ranged from 15 nm to 34 nm, with an average size of 28.2 nm.

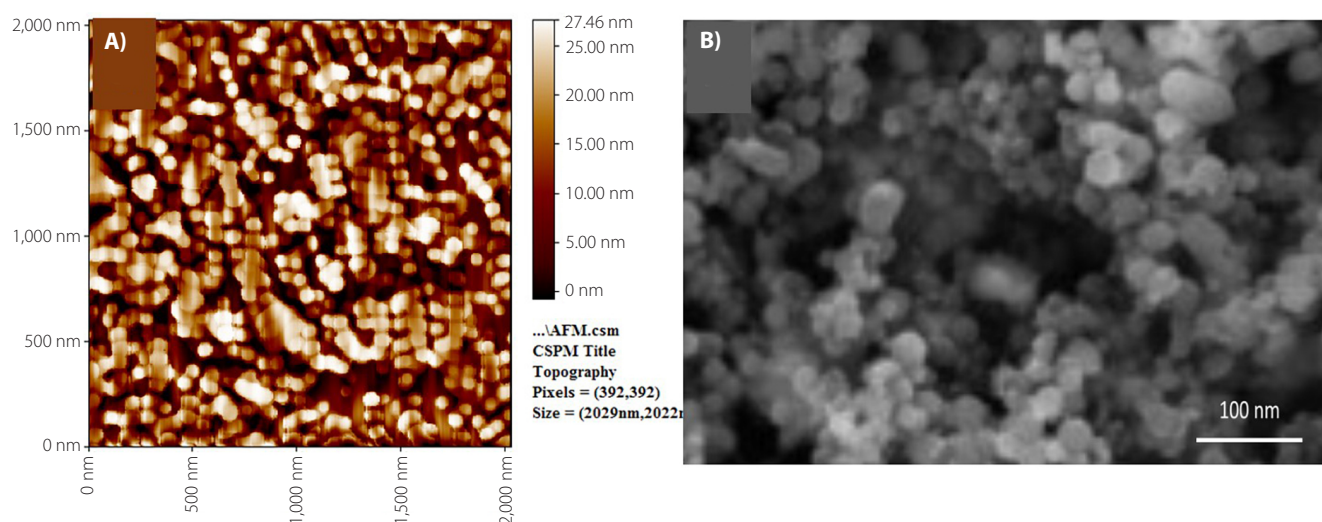


Fig. 1. A. Atomic force microscopy (AFM) 2D topography image of the polyhydroxybutyrate nanoparticles (PHB-NPs) surface layer; B. Scanning electron microscopy (SEM) image of PHB-NP layers at $\times 10,000$ magnification

Bacterial isolates

Twenty *P. aeruginosa* isolates were obtained from 91 wound swab samples collected from inpatients with severe wound infections. Initial identification was performed using microscopic examination and standard biochemical tests, followed by confirmation with the VITEK 2 system (bioMérieux). Findings indicate a high prevalence of *P. aeruginosa* in wound infections, with an isolation rate of 21.97%.

Antibiotic susceptibility and biofilm formation

The susceptibility of 20 *P. aeruginosa* isolates to CRO was assessed using the Kirby–Bauer disk diffusion method. As shown in Fig. 2, the smallest inhibition zone was observed for isolate Pa11 (9 ± 0.6 mm), followed by Pa13 (10 ± 1.01 mm) and Pa17 (10 ± 0.9 mm). In contrast, the largest inhibition zone for CRO was observed in isolate Pa10 (34 ± 4.2 mm), as shown in Fig. 2A. The levels of biofilm formation for

the 20 *P. aeruginosa* isolates are presented in Fig. 2B. Among them, Pa19 (0.31 ± 0.011) and Pa11 (0.307 ± 0.02) exhibited the highest levels of biofilm production, whereas Pa1 showed the lowest biofilm formation (0.085 ± 0.02). Among the 20 *P. aeruginosa* isolates, 7 produced strong biofilms, 10 exhibited moderate biofilm formation, and 3 were classified as weak biofilm producers. Isolate Pa11, which demonstrated the highest level of biofilm production and resistance to CRO, was selected for further experiments. In the present study, the MIC of CRO against Pa11 was determined to be $256 \mu\text{g/mL}$. Figure 3A illustrates the relationship between biofilm formation and the diameter of the inhibition zone of CRO for 20 clinical isolates of *P. aeruginosa*. A significant negative correlation was observed between biofilm-forming ability and susceptibility to CRO, as indicated by the diameter of the inhibition zones ($r = -0.78$, $p < 0.005$).

It was observed that *P. aeruginosa* isolates classified as sensitive to CRO produced significantly less biofilm ($p < 0.05$) compared to isolates exhibiting intermediate or resistant profiles. However, no significant difference in biofilm formation was found between the CRO-resistant and intermediate groups (Fig. 3B).

Susceptibility of *P. aeruginosa* to PHB-NPs and ceftriaxone

In the current study, *P. aeruginosa* isolate Pa11, which exhibited resistance to CRO and produced a high level of biofilm, was selected for further experiments. The microdilution method was used to determine the MICs of PHB, PHB-NPs, CRO, and the PHB-NP-CRO combination against Pa11. The highest MIC was recorded for PHB ($2,000 \mu\text{g/mL}$), followed by PHB-NPs ($1,000 \mu\text{g/mL}$). A notable reduction in MIC was observed for CRO alone

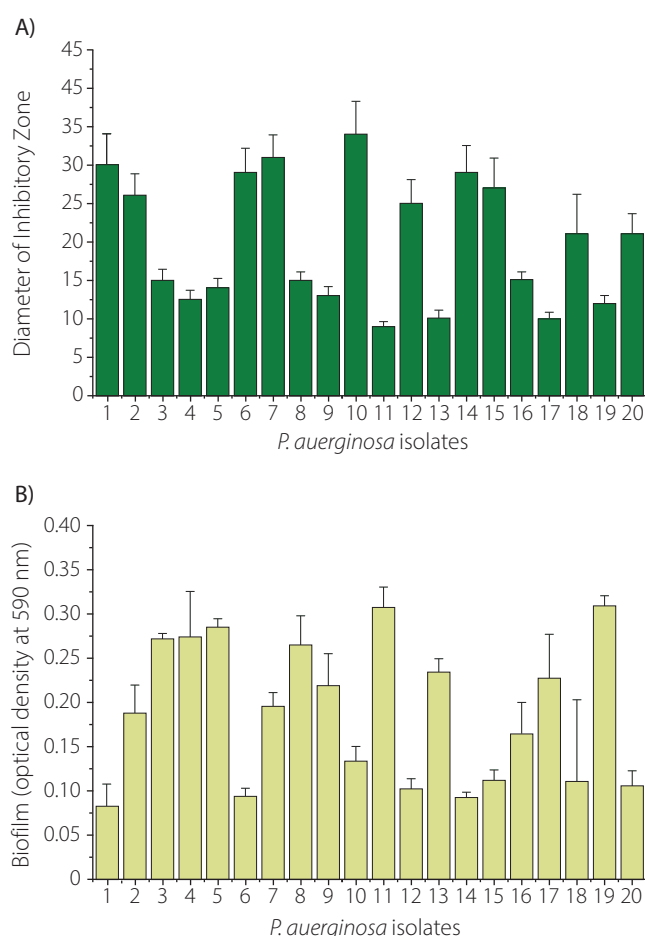


Fig. 2. A. Diameter of the inhibition zone of ceftriaxone (CRO; 30 μg) against 20 clinical isolates of *Pseudomonas aeruginosa*; B. Quantification of biofilm formation by the same isolates based on absorbance at 590 nm following staining with 0.4% crystal violet. The isolates analyzed include Pa1 through Pa20

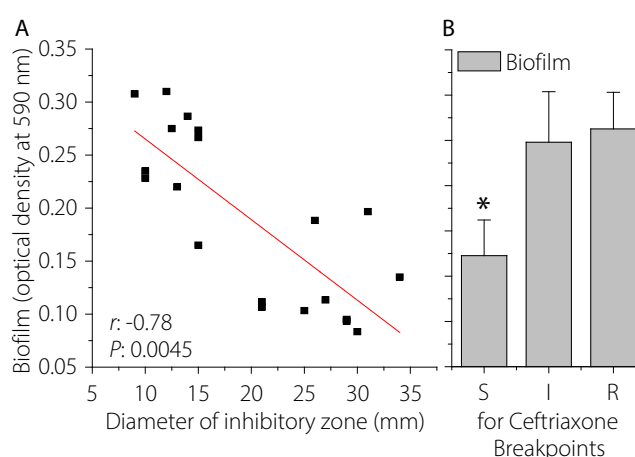


Fig. 3. A. Relationship between the diameter of the inhibition zones (in mm) of ceftriaxone (CRO) against 20 *Pseudomonas aeruginosa* isolates and their biofilm-forming ability, expressed as optical density at 590 nm; B. Comparison of biofilm formation among CRO-sensitive (S), intermediate (I) and resistant (R) isolate groups. The r coefficient indicates the Pearson's correlation coefficient. Asterisks denote statistically significant differences in biofilm formation between the sensitive group and the intermediate/resistant groups ($p < 0.05$)

(250 µg/mL), while the lowest MIC was achieved with the PHB-NP-CRO formulation (62.5 µg/mL), as shown in Fig. 4A.

Figure 4B presents the diameters of the inhibition zones produced by various treatments against *P. aeruginosa* isolate Pa11. The largest inhibition zone was observed around the well containing PHB-NP-CRO (100 µL), measuring 33.1 ± 5.13 mm, followed by CRO alone (29.2 ± 4.11 mm). In contrast, the smallest inhibition zones were recorded for PHB (9.2 ± 1.3 mm) and PHB-NPs (9.8 ± 1.9 mm). Figure 4C displays the visual representation of antibacterial susceptibility. Prominent inhibition zones were observed around the wells containing CRO and the PHB-NP-CRO formulation, indicating strong antibacterial activity. In contrast, smaller inhibition zones were noted around the wells filled with PHB and PHB-NPs. The central well, filled with DMSO, served as the negative control. These results confirm that PHB-NP-CRO exhibited the strongest inhibitory effect against *P. aeruginosa*, followed by CRO.

Effect of sub-MICs on biofilm formation

Figure 5 illustrates the effects of sub-MICs of PHB-NPs, CRO and the PHB-NP-CRO combination on biofilm formation by *P. aeruginosa* isolate Pa11. The results indicate that sub-MICs of PHB-NPs alone did not significantly inhibit biofilm formation. Sub-inhibitory concentrations ($\frac{1}{2}$ MIC, $\frac{1}{4}$ MIC, $\frac{1}{8}$ MIC, and $\frac{1}{16}$ MIC) of CRO significantly reduced biofilm formation by *P. aeruginosa* Pa11 compared to the control group pretreated with PBS ($p < 0.05$). Similarly, PHB-NP-CRO sub-MICs ($\frac{1}{2}$ MIC, $\frac{1}{4}$ MIC, $\frac{1}{8}$ MIC, $\frac{1}{16}$ MIC, and $\frac{1}{32}$ MIC) also resulted

in a significant reduction in biofilm formation compared to the PBS-treated control ($p < 0.05$). The greatest inhibition of biofilm formation was observed with sub-MICs of PHB-NP-CRO, followed by sub-MICs of CRO alone.

Effect of sub-MICs on adhesion to human OMECs

Figure 6 illustrates the impact of pre-treatment with different sub-MICs of PHB-NPs, CRO and the PHB-NP-CRO combination on the adhesion of *P. aeruginosa* Pa11 to human OMECs. No significant difference was observed in the number of adhered Pa11 cells pretreated with PHB-NPs compared to the control group (Pa11 pretreated with PBS). A significant reduction ($p < 0.05$) in the number of adhered *P. aeruginosa* Pa11 cells was observed following pre-treatment with sub-MICs of CRO ($\frac{1}{2}$ MIC, $\frac{1}{4}$ MIC, $\frac{1}{8}$ MIC, $\frac{1}{16}$ MIC, and $\frac{1}{32}$ MIC). However, no significant difference was found in adhesion when Pa11 was pre-treated with $\frac{1}{64}$ MIC of CRO ($p > 0.05$). A similar pattern was observed for Pa11 cells pre-treated with sub-MICs of PHB-NP-CRO. Figure 6A shows human OMECs with normal flat morphology and centrally located nuclei. In contrast, Fig. 6B reveals a high density of *P. aeruginosa* Pa11 adhered to OMECs following pre-treatment with PBS (control). A noticeable reduction in bacterial adhesion was observed when OMECs were exposed to Pa11 pre-treated with CRO at $\frac{1}{8}$ MIC (Fig. 6C) and PHB-NP-CRO at $\frac{1}{8}$ MIC (Fig. 6D). The present study demonstrated that the PHB-NP-CRO formulation produced the most substantial reduction in bacterial adhesion to the epithelial surface, followed by CRO alone.

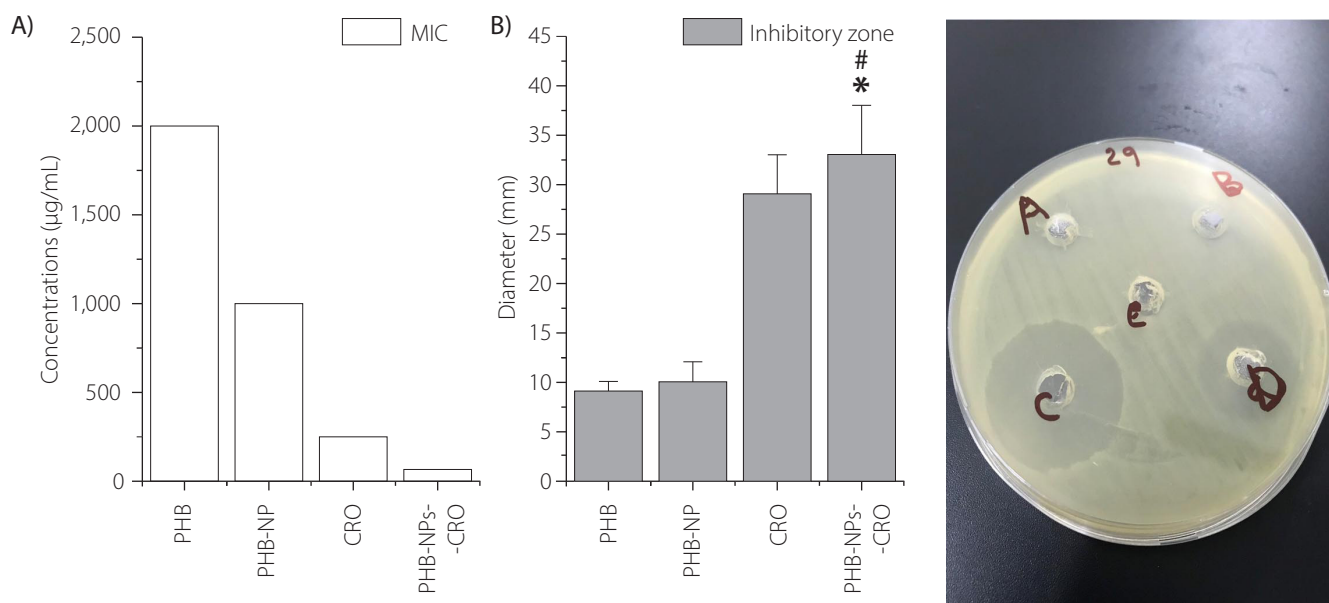


Fig. 4. A. Minimum inhibitory concentrations (MICs) of polyhydroxybutyrate (PHB), polyhydroxybutyrate nanoparticles (PHB-NPs), ceftriaxone (CRO), and the PHB-NP-CRO combination against *Pseudomonas aeruginosa* isolate Pa11; B. Diameter of the inhibition zones produced by 2000 µg of PHB, PHB-NPs, CRO, and PHB-NP-CRO; C. Representative image of a Mueller-Hinton agar (MHA) plate showing 5 wells: A – PHB, B – PHB-NPs, C – PHB-NP-CRO, D – CRO, and E – DMSO (control), each well filled with 100 µL of the respective solution

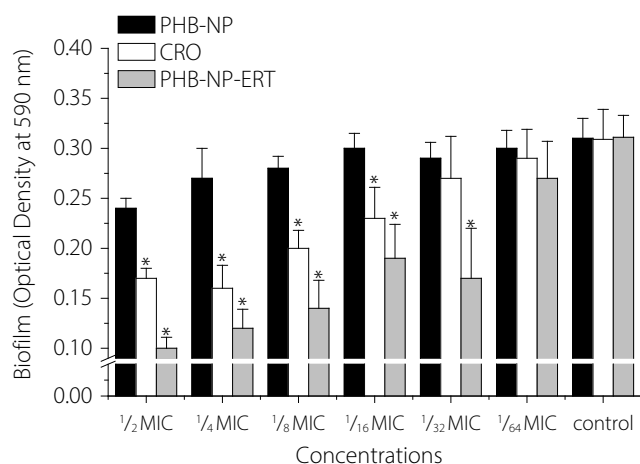


Fig. 5. Effect of different sub-inhibitory concentrations (sub-MICs: $\frac{1}{2}$ MIC, $\frac{1}{4}$ MIC, $\frac{1}{8}$ MIC, $\frac{1}{16}$ MIC, $\frac{1}{32}$ MIC, and $\frac{1}{64}$ MIC) of polyhydroxybutyrate nanoparticles (PHB-NPs), ceftriaxone (CRO) and their combination (PHB-NP-CRO) on biofilm formation by *Pseudomonas aeruginosa* isolate Pa11. Asterisks indicate statistically significant differences compared to the control group (Pa11 pretreated with PBS); $p < 0.05$ was considered statistically significant

Discussion

Infection with *P. aeruginosa* strains resistant to broad-spectrum antibiotics presents a serious challenge for clinicians.¹⁷ This is largely due to the bacterium's intrinsic resistance mechanisms and its ability to form biofilms.¹ The biofilm matrix provides protection to bacterial cells, enabling them to evade the effects of antibiotics and the host immune response.¹⁸ The resistance of *P. aeruginosa* to antibiotics – particularly to CRO, a third-generation cephalosporin – has increased markedly in recent

years.¹⁹ As a result, the development of safe and effective strategies to limit bacterial resistance has become essential. One promising approach involves the use of biocompatible materials to inhibit biofilm formation, a key factor in the persistence and resistance of bacterial infections.¹⁸

In the present study, PHB-NPs were synthesized, and their synergistic effect with CRO in reducing *P. aeruginosa* resistance and biofilm formation was evaluated. The findings demonstrated that PHB-NPs enhanced the antibacterial efficacy of CRO. Notably, sub-MICs of the PHB-NP-CRO combination significantly reduced biofilm formation and impaired *P. aeruginosa* adhesion to epithelial cells in vitro. Furthermore, the combination of CRO and PHB-NPs not only exhibited potent antibacterial activity, but also reduced bacterial virulence by inhibiting biofilm formation and adhesion to biotic surfaces, such as human OMECs. Since biofilm formation and adhesion are key virulence factors of *P. aeruginosa*, their suppression significantly enhances the therapeutic potential of this combination strategy.²⁰

Previous studies on PHB-NP synthesis reported findings consistent with the current study regarding particle size. For instance, Deepak et al. reported PHB-NP diameters ranging from 100 nm to 125 nm,²¹ while Pachiyappan et al. obtained particles with a broader size range of 50 nm to 300 nm.⁷ In contrast, the PHB-NPs synthesized in the present study exhibited significantly smaller diameters, ranging from 15 nm to 34 nm, suggesting an improvement in the efficiency of the preparation method employed. The primary applications of PHB-NPs include drug delivery,²² as well as antibacterial activity. Kiran et al. demonstrated the antibacterial efficacy of PHB-NPs against *Staphylococcus aureus* biofilms.²³ In addition,

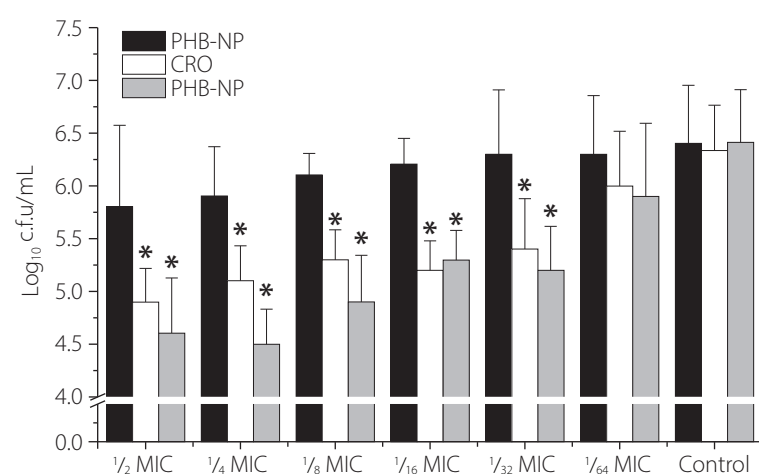
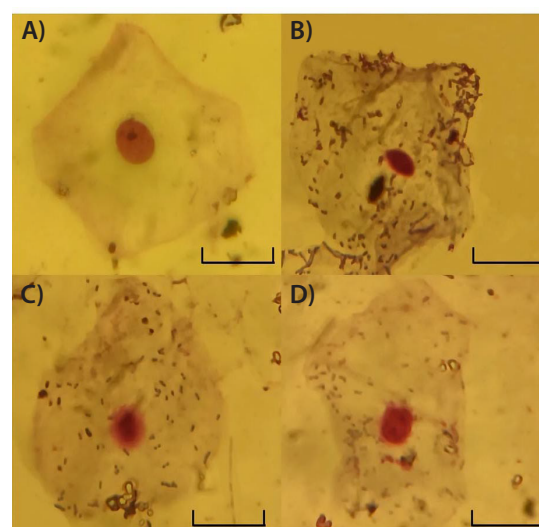


Fig. 6. Effect of pre-treatment of *Pseudomonas aeruginosa* isolate Pa11 with different sub-inhibitory concentrations ($\frac{1}{2}$ MIC, $\frac{1}{4}$ MIC, $\frac{1}{8}$ MIC, $\frac{1}{16}$ MIC, $\frac{1}{32}$ MIC, and $\frac{1}{64}$ MIC) of polyhydroxybutyrate nanoparticles (PHB-NPs) on bacterial adhesion to human oral mucosal epithelial cells (OMECS) in vitro. Asterisks indicate statistically significant differences compared to the PBS-treated control ($p < 0.05$). A. Control image of untreated human OMECs. B. Micrograph of human OMECs exposed to Pa11 pretreated with PBS; C. Micrograph of OMECs incubated with Pa11 pretreated with ceftriaxone ($\frac{1}{8}$ MIC); D. Micrograph of OMECs incubated with Pa11 pretreated with PHB-NP-CRO ($\frac{1}{8}$ MIC). Scale bars: 35 μ m



Rodriguez-Contreras reported the anticancer potential of PHB.²⁴ More recently, Hamdy et al. highlighted the utility of PHB in wound healing, tissue regeneration, and bone and tissue engineering.²⁵ Polyhydroxybutyrate is a safe, biodegradable polymer with various biomedical applications, largely attributed to its antibacterial properties.²³ The biomedical potential of PHB-NPs lies in their ability to facilitate targeted antibiotic delivery. The observed synergistic enhancement of CRO's antibacterial activity by PHB-NPs may be attributed to improved diffusion of CRO across the outer membrane of *P. aeruginosa*. Furthermore, the transformation of PHB into nanoparticle form appears to enhance its antibacterial effect when combined with CRO. PHB-NPs may interfere with quorum sensing and inhibit polysaccharide production, thereby disrupting biofilm formation and increasing bacterial susceptibility to CRO. In addition, CRO itself is known to inhibit quorum sensing mechanisms.²⁶ The nanoparticulate nature of PHB-NPs may also facilitate interactions with bacterial membranes, leading to increased membrane permeability and enhanced intracellular accumulation of CRO.²⁶ The findings of the present study highlight the promising potential of PHB-NPs in antimicrobial applications. They were shown to enhance the efficacy of CRO, enabling a reduction in the required antibiotic dosage and potentially minimizing associated side effects. This approach may offer a valuable strategy for combating broad-spectrum antibiotic-resistant *P. aeruginosa*. The observed ability of the PHB-NP-CRO combination to inhibit biofilm formation further suggests its potential use in treating biofilm-associated infections, including respiratory tract infections,^{27,28} urinary tract infections¹⁵ and medical device-related infections (e.g., catheters and prosthetic implants).²⁹ Therefore, the present study supports the use of PHB-NP-based systems as a novel approach to restoring the therapeutic efficacy of existing antibiotics against resistant bacterial strains. Based on the findings of the present study, we recommend conducting in vivo studies to further validate the observed effects. In vivo investigations are essential to evaluate the safety, efficacy and pharmacokinetic profile of the PHB-NP-CRO combination in a physiological environment. Additionally, the use of animal models and future clinical studies will be crucial in assessing the therapeutic potential, bioavailability and potential immunological responses associated with PHB-NP-CRO administration. Furthermore, evaluating the antimicrobial efficacy of PHB-NP-CRO against a broader spectrum of bacterial species, including Gram-positive and multidrug-resistant pathogens, will provide valuable insights into its potential application for the treatment of diverse infections.

Conclusions

Resistance of *P. aeruginosa* to CRO is a major public health concern. The use of safe materials that enhance the efficacy of antibiotics represents a promising therapeutic strategy. In the present study, PHB-NPs were synthesized; however, they exhibited limited antibacterial activity against *P. aeruginosa* when used alone. In contrast, the PHB-NP-CRO demonstrated a significantly enhanced antibacterial effect compared to either agent alone. The increased effectiveness of the PHB-NP-CRO formulation may be attributed to several factors, one of which, as shown in this study, is its ability to reduce biofilm formation by *P. aeruginosa*.

Data availability

The datasets generated and/or analyzed during the current study are available from the corresponding author on reasonable request.

Consent for publication


Not applicable.

Use of AI and AI-assisted technologies

Not applicable.

ORCID iDs

Shams Hssan Sadiq  <https://orcid.org/0009-0009-8413-9897>

Jenan Atiyah Ghafil  <https://orcid.org/0000-0003-1461-302X>

References

- Ghafil JA, Khadhem Al-Sudani SF, Salih Ibrahim BM, Alshahrani AM, Zgair AK. Relationship between biofilm formation of *Pseudomonas aeruginosa* and susceptibility to rifaximin and ofloxacin. *Pak J Pharm Sci.* 2024;37(6):1609–1614. PMID:39923153.
- Ghafil JA, Fliyh MT, Al-Mutalib LA. Preparing burn mouse model infected with *Pseudomonas aeruginosa*: A histopathological study. *World J Exp Biosci.* 2023;11(2):46–50. <https://wjebio.com/index.php/journal/article/view/177/143>.
- Talib MM, Ghafil JA. Effect of sub-minimum inhibitory concentrations of ceftriaxone on the *Pseudomonas aeruginosa* adhesion to human oral mucosal epithelial cells and biofilm formation to polystyrene in vitro. *Pharm Sci Asia.* 2024;51(2):180–189. doi:10.29090/psa.2024.02.24.1752
- Rolston KVI, Bodey GP. *Pseudomonas aeruginosa* infection in cancer patients: Infectious complications of cancer. *Cancer Invest.* 1992;10(1):43–59. doi:10.3109/07357909209032787
- Hernández-Jiménez P, López-Medrano F, Fernández-Ruiz M, et al. Risk factors and outcomes for multidrug resistant *Pseudomonas aeruginosa* infection in immunocompromised patients. *Antibiotics.* 2022;11(11):1459. doi:10.3390/antibiotics11111459
- Alnimr AM, Alamri AM. Antimicrobial activity of cephalosporin–beta-lactamase inhibitor combinations against drug-susceptible and drug-resistant *Pseudomonas aeruginosa* strains. *J Taibah Univ Med Sci.* 2020;15(3):203–210. doi:10.1016/j.jtumed.2020.04.004
- Pachiyappan S, Shanmuganatham Selvanantham D, Kuppa SS, Chandrasekaran S, Samrot AV. Surfactant-mediated synthesis of polyhydroxybutyrate (PHB) nanoparticles for sustained drug delivery. *IET Nanobiotechnol.* 2019;13(4):416–427. doi:10.1049/iet-nbt.2018.5053

8. Tsuge T, Hyakutake M, Mizuno K. Class IV polyhydroxyalkanoate (PHA) synthases and PHA-producing *Bacillus*. *Appl Microbiol Biotechnol*. 2015;99(15):6231–6240. doi:10.1007/s00253-015-6777-9
9. Quispe MM, Villanueva ME, Copello GJ, López OV, Villar MA. Films of poly(hydroxybutyrate) (PHB) and copper with antibacterial activity. *Polymers (Basel)*. 2023;15(13):2907. doi:10.3390/polym15132907
10. Lin X, Yin M, Liu Y, et al. Biodegradable polyhydroxybutyrate/poly-ε-caprolactone fibrous membranes modified by silica composite hydrol for super hydrophobic and outstanding antibacterial application. *J Industr Eng Chem*. 2018;63:303–311. doi:10.1016/j.jiec.2018.02.031
11. Morris WT. Effectiveness of ceftriaxone versus cefoxitin in reducing chest and wound infections after upper abdominal operations. *Am J Surg*. 1994;167(4):391–395. doi:10.1016/0002-9610(94)90122-8
12. Rossi S, Azghani AO, Omri A. Antimicrobial efficacy of a new antibiotic-loaded poly(hydroxybutyric-co-hydroxyvaleric acid) controlled release system. *J Antimicrob Chemother*. 2004;54(6):1013–1018. doi:10.1093/jac/dkh477
13. Ghafil JA, Flieh MT. Characterization of polyhydroxybutyrate nanoparticles. *Iraqi J Sci*. 2022;63(2):449–457. doi:10.24996/ijsc.2022.63.2.3
14. Weinstein MP. *Performance Standards for Antimicrobial Susceptibility Testing: Supplement M100*. 30th ed. Wayne, USA: Clinical and Laboratory Standards Institute (CLSI); 2020. ISBN:978-1-68440-067-6
15. Al-Mutalib LA, Zgair A. Effect of subinhibitory doses of rifaximin on in vitro *Pseudomonas aeruginosa* adherence and biofilm formation to biotic and abiotic surface models. *Polim Med*. 2023;53(2):97–103. doi:10.17219/pim/166584
16. Hasan AM, Ghafil JA. Study on the anti-microbial effect of sinigrin against some pathogenic bacterial species. *Bionatura*. 2022;7(4):68. doi:10.21931/RB/2022.07.04.68
17. Mohammed HA, Zgair AK. Detection of quorum sensing genes of *Pseudomonas aeruginosa* isolated from different areas in Iraq. *Iraqi J Sci*. 2022;63(11):4665–4673. doi:10.24996/ijsc.2022.63.11.5
18. Rather MA, Gupta K, Mandal M. Microbial biofilm: Formation, architecture, antibiotic resistance, and control strategies. *Braz J Microbiol*. 2021;52(4):1701–1718. doi:10.1007/s42770-021-00624-x
19. Abu El Aish KI, Alkhodary AA, Helles A, Moshtaha A, Ghanem S, Al Afifi A. Bacterial resistance to ceftriaxone in different: Specimens at governmental hospitals in Gaza Strip. *Malays J Publ Health Med*. 2023;23(1):72–81. doi:10.37268/mjphm/vol.23/no.1/art.974
20. Liao C, Huang X, Wang Q, Yao D, Lu W. Virulence factors of *Pseudomonas aeruginosa* and antivirulence strategies to combat its drug resistance. *Front Cell Infect Microbiol*. 2022;12:926758. doi:10.3389/fcimb.2022.926758
21. Deepak V, Ram Kumar Pandian SB, Kalishwaralal K, Gurunathan S. Purification, immobilization, and characterization of nattokinase on PHB nanoparticles. *Bioresour Technol*. 2009;100(24):6644–6646. doi:10.1016/j.biortech.2009.06.057
22. Prakash P, Lee WH, Loo CY, Wong HSJ, Parumasivam T. Advances in polyhydroxyalkanoate nanocarriers for effective drug delivery: An overview and challenges. *Nanomaterials*. 2022;12(1):175. doi:10.3390/nano12010175
23. Kiran GS, Jackson SA, Priyadharsini S, Dobson ADW, Selvin J. Synthesis of Nm-PHB (nanomelanin-polyhydroxy butyrate) nanocomposite film and its protective effect against biofilm-forming multi drug resistant *Staphylococcus aureus*. *Sci Rep*. 2017;7(1):9167. doi:10.1038/s41598-017-08816-y
24. Rodriguez-Contreras A. Recent advances in the use of polyhydroxyalkanoates in biomedicine. *Bioengineering*. 2019;6(3):82. doi:10.3390/bioengineering6030082
25. Hamdy SM, Danial AW, Gad El-Rab SMF, Shoreit AAM, Hesham AEL. Production and optimization of bioplastic (polyhydroxybutyrate) from *Bacillus cereus* strain SH-02 using response surface methodology. *BMC Microbiol*. 2022;22(1):183. doi:10.1186/s12866-022-02593-z
26. Naga NG, El-Badan DE, Mabrouk MEM, Rateb HS, Ghanem KM, Shaban MI. Innovative application of ceftriaxone as a quorum sensing inhibitor in *Pseudomonas aeruginosa*. *Sci Rep*. 2025;15(1):5022. doi:10.1038/s41598-025-87609-0
27. Mohapatra S, Mohanty D, Sharma S, et al. Biomedical application of polymeric biomaterial: Polyhydroxybutyrate. In: Thatoi H, Das SK, Mohapatra S, eds. *Bioresource Utilization and Management: Applications in Therapeutics, Biofuels, Agriculture, and Environmental Sciences*. Palm Bay, USA: Apple Academic Press; 2022:111–124. ISBN:978-1-00-305782-6, 978-1-77188-933-9, 978-1-77463-813-2.
28. Ali M, Zgair A. Extracellular product of *Pseudomonas aeruginosa* in growth medium is involved in the pro-inflammatory cytokine response of human oral epithelial cells in vitro. *Polim Med*. 2022;52(2):77–82. doi:10.17219/pim/155849
29. Di Domenico EG, Oliva A, Gueembe M. The current knowledge on the pathogenesis of tissue and medical device-related biofilm infections. *Microorganisms*. 2022;10(7):1259. doi:10.3390/microorganisms10071259.

The influence of selected polyoxyethylene glycols on the electrical conductivity of isosmotic and hyperosmotic sodium chloride solutions

Wpływ wybranych glikoli polioksyetylenowych na przewodność elektryczną izosmotycznych i hiperosmotycznych roztworów chlorku sodu

Maja Prajzner^{A–F}, Maria Twarda^{A–F}, Witold Musiał^{A–F}

Department of Physical Chemistry and Biophysics, Pharmaceutical Faculty, Wrocław Medical University, Poland

A – research concept and design; B – collection and/or assembly of data; C – data analysis and interpretation; D – writing the article; E – critical revision of the article; F – final approval of the article

Polymers in Medicine, ISSN 0370-0747, ISSN 2451-2699

Polim Med. 2025;55(1):41–47

Address for correspondence

Witold Musiał

E-mail: witold.musial@umw.edu.pl

Funding sources

None declared

Conflict of interest

None declared

Acknowledgements

The research was carried out in collaboration with the Student Research Club No. K130 at the Department of Physical Chemistry and Biophysics, Wrocław Medical University, Poland.

Received on November 28, 2024

Reviewed on March 17, 2025

Accepted on March 17, 2025

Published online as ahead of print on June 30, 2025

Abstract

Background. Polyethylene glycols (PEGs) are widely applied in technology of pharmaceutical products, as well as in other branches of industry. Owing to their physicochemical properties, they are particularly effective in enhancing the solubility of a wide range of drug formulations.

Objectives. The aim of the study was to evaluate the effect of PEGs on the physicochemical parameters of model systems containing different concentrations of sodium chloride (NaCl), with particular emphasis on the specific conductivity of these solutions.

Materials and methods. A series of aqueous solutions containing 0.9% and 9.0% NaCl, with increasing mass concentrations (2.0–25.0% w/w) of PEG 200 and PEG 4000, were prepared and analyzed. Their specific conductivity was tested using a CC-505 conductivity meter with an EC-70 conductivity sensor; also, densities and viscosities of the tested solutions were evaluated.

Results. The increased concentration of polymers in the system resulted in decrease of the specific conductivity and molar conductivity in each of the series of evaluated solutions. An inverse relationship occurred in viscosity measurements, which increased with increasing PEG content in the system.

Conclusions. The addition of PEG 200 and PEG 4000 to aqueous NaCl solutions affected both the specific conductivity and viscosity of these systems. Both types of polymers had similar effects on conductivity changes in 0.9% and 9.0% NaCl solutions.

Key words: polyethylene glycols, specific conductivity, molar conductivity, sodium chloride, viscosity

Cite as

Prajzner M, Twarda M, Musiał W. The influence of selected polyoxyethylene glycols on the electrical conductivity of isosmotic and hyperosmotic sodium chloride solutions. *Polim Med.* 2025;55(1):41–47. doi:10.17219/pim/203038

DOI

10.17219/pim/203038

Copyright

Copyright by Author(s)

This is an article distributed under the terms of the Creative Commons Attribution 3.0 Unported (CC BY 3.0) (<https://creativecommons.org/licenses/by/3.0/>)

Streszczenie

Wprowadzenie. Glikole polietylenowe (PEG) znajdują szerokie zastosowanie w technologii produktów farmaceutycznych, a także w innych gałęziach przemysłu. Ze względu na swoje właściwości można je stosować w celu zwiększenia rozpuszczalności różnych substancji leczniczych.

Cel pracy. Celem badań była ocena wpływu PEG-ów na parametry fizykochemiczne układów modelowych zawierających różne stężenia chlorku sodu, ze szczególnym uwzględnieniem przewodnictwa właściwego tych roztworów.

Materiał i metody. Badano serię roztworów 0,9% i 9,0% chlorku sodu w wodzie z dodatkiem PEG200 i PEG4000 o rosnących stężeniach masowych (2,0–25,0% w/w). Ich przewodność właściwą badano za pomocą konduktometru CC-505 z czujnikiem przewodności EC-70; oceniano także gęstości i lepkości badanych roztworów.

Wyniki. Zwiększone stężenie polimerów w układzie spowodowało zmniejszenie przewodności właściwej i przewodności molowej w każdej z serii ocenianych roztworów. Odwrotna zależność wystąpiła w pomiarach lepkości, która wzrastała wraz ze wzrostem zawartości glikolu polietylenowego w układzie.

Wnioski. Dodatek PEG200 i PEG4000 do wodnych roztworów chlorku sodu wpływał zarówno na przewodność właściwą, jak i lepkość tych układów. Obydwa typy polimerów miały podobny wpływ na zmiany przewodnictwa w 0,9% i 9,0% roztworach chlorku sodu.

Słowa kluczowe: glikole polietylenowe, przewodność właściwa, przewodność molowa, chlorek sodu, lepkość

Highlights

- Polyethylene glycols (PEGs) reduce conductivity in sodium chloride solutions. Increasing concentrations of PEG 200 and PEG 4000 significantly lowered the specific and molar conductivity of both 0.9% and 9.0% NaCl aqueous solutions.
- PEGs increase viscosity in saline-based pharmaceutical formulations.
Higher PEG content led to a marked rise in solution viscosity, indicating PEG's role in modifying rheological properties of NaCl systems.
- Comparative impact of PEG 200 and PEG 4000 on electrolyte behavior. –
Both PEG variants exhibited similar effects on conductivity, suggesting interchangeable application in drug delivery systems involving electrolytes.
- Optimizing drug solubility: PEG influence on physicochemical properties. The study highlights the dual role of PEGs in enhancing solubility and altering the physicochemical behavior of NaCl-based pharmaceutical preparations.

Introduction

Synthetic polymers are a very extensive group of chemical compounds that are used on a daily basis in many areas of industry, medicine and pharmacy. Detailed knowledge of the physicochemical properties of available polymers can also contribute to advancements in pharmaceutical technology. One of the frequently used groups of polymers are polyethylene glycols (PEGs). Their physical properties change with increasing molecular weight. These polymers are characterized by an increase in the melting temperature with increasing molecular weight. For example, PEGs with molecular weights between 100 and

700 are liquids, those between 1000 and 2000 are soft solids, and PEGs with molecular weights above 2000 are hard crystalline solids.¹ This property enables the formulation of semi-solid drug forms using mixtures of PEGs with different molar masses.² Owing to their characteristic properties – namely, amphiphilicity and relatively high biocompatibility – PEGs are frequently used in pharmaceutical technology, particularly to enhance the solubility of active substances in dosage forms such as tablets, capsules and ointments.¹ PEG 4000 is particularly highlighted here due to its very low toxicity and high biocompatibility; it is currently one of the most commonly used polymers for the synthesis of targeted drug delivery systems.³ Another polymer commonly used in pharmaceutical systems is PEG 200, which facilitates the formulation of homogeneous liquid preparations containing hydrophobic drug substances. Its effectiveness is attributed to its properties – PEG 200 is a low molecular weight surfactant that exists in a liquid state.⁴

The practical application of PEGs requires an understanding of their influence on the properties of administered drugs. One method for assessing this interaction is measuring the conductivity of the drug substance in a system containing the polymer. Previous studies, including those conducted by Italian researchers, have analyzed the molar conductivities of various PEGs, such as PEG 400 and PEG 2000, in the presence of sodium chloride (NaCl) solutions.⁵ Studies of this kind are particularly important due to the necessity of maintaining an isosmotic environment with the site of drug administration in certain dosage forms.⁶ The planned values of osmotic pressure can also be used in the development of new drug dosage forms intended for the controlled release of medicinal substances.⁷ In addition, conductometric techniques can subsequently be employed to study the release of substances from pharmaceutical systems containing polymeric drug carriers, representing a promising area of research.^{8,9}

Objectives

The aim of the study was to investigate the effect of selected polymers, i.e., PEG 200 and PEG 4000, on the physicochemical parameters of model systems containing 0.9% and 9.0% NaCl, and in particular to investigate the effect of these polymers on the specific conductivity of these systems. PEG 200 and PEG 4000 were selected due to their range of molar masses and melting temperatures, differing by about 100 K, and amounting to -50.0°C and 55.95°C , respectively, which ensured a different state of matter under the test conditions.^{10,11} Moreover, we aimed to build upon the results previously obtained by Italian researchers,⁵ who studied the electrical conductivity of NaCl in the presence of polymers with similar properties, and to additionally investigate the effect of higher NaCl concentrations to more precisely assess the impact of these polymers on markedly hyperosmotic NaCl solutions in future studies.

Materials and methods

Materials

The following substances were used to prepare the tested solutions: PEG 200 and PEG 4000 (for synthesis; Merck Life Science, Poznań, Poland), distilled water from a deionization station (Hydrolab HLP20UV device; Hydrolab, Straszyn, Poland) and NaCl (pure p.a.).

Methods

Preparation of solutions

The composition of the tested solutions is presented in Table 1. Four series of solutions containing a constant amount of NaCl were prepared: 2 series with 0.9 g of NaCl per 100 g of solution, and 2 series with 9.0 g of NaCl per 100 g of solution, along with reference solutions containing only NaCl at concentrations of 0.9% and 9.0%, respectively, without any polymers. Each of the test series contained 7 mixtures with PEG 200 or PEG 4000. The amounts of PEG 200 or PEG 4000 used in both variants were: 2.0, 4.0, 6.0, 10.0, 15.0, 20.0, and 25.0 g.

The molar concentration of NaCl in the tested solutions (c) was determined based on the density measurements (ρ_r) of the systems, taking into account the total mass of the solution (m_r) and the number of moles of NaCl (n), as shown in Equation 1:

$$c = \frac{n\rho_r}{m_r}$$

Table 1. Composition of the prepared solutions. The series of solutions were abbreviated according to the rule PEGXNaClY-Z, where X is the first digit from the polymer name (PEG200, X = 2; PEG4000, X = 4), Y is the percentage concentration of sodium chloride in the solution and Z is the percentage concentration of PEG in the solution.

No.	Name	NaCl [%]	PEG200 [%]	PEG4000 [%]	Water [%]
1	PEG2NaCl0.9-02	0.9	2.0	0.0	97.1
2	PEG2NaCl0.9-04	0.9	4.0	0.0	95.1
3	PEG2NaCl0.9-06	0.9	6.0	0.0	93.1
4	PEG2NaCl0.9-10	0.9	10.0	0.0	89.1
5	PEG2NaCl0.9-15	0.9	15.0	0.0	84.1
6	PEG2NaCl0.9-20	0.9	20.0	0.0	79.1
7	PEG2NaCl0.9-25	0.9	25.0	0.0	74.1
8	PEG2NaCl9.0-02	9.0	2.0	0.0	89.0
9	PEG2NaCl9.0-04	9.0	4.0	0.0	87.0
10	PEG2NaCl9.0-06	9.0	6.0	0.0	85.0
11	PEG2NaCl9.0-10	9.0	10.0	0.0	81.0
12	PEG2NaCl9.0-15	9.0	15.0	0.0	76.0
13	PEG2NaCl9.0-20	9.0	20.0	0.0	71.0
14	PEG2NaCl9.0-25	9.0	25.0	0.0	66.0
15	PEG4NaCl0.9-02	0.9	0.0	2.0	97.1
16	PEG4NaCl0.9-04	0.9	0.0	4.0	95.1
17	PEG4NaCl0.9-06	0.9	0.0	6.0	93.1
18	PEG4NaCl0.9-10	0.9	0.0	10.0	89.1
19	PEG4NaCl0.9-15	0.9	0.0	15.0	84.1
20	PEG4NaCl0.9-20	0.9	0.0	20.0	79.1
21	PEG4NaCl0.9-25	0.9	0.0	25.0	74.1
22	PEG4NaCl9.0-02	9.0	0.0	2.0	89.0
23	PEG4NaCl9.0-04	9.0	0.0	4.0	87.0
24	PEG4NaCl9.0-06	9.0	0.0	6.0	85.0
25	PEG4NaCl9.0-10	9.0	0.0	10.0	81.0
26	PEG4NaCl9.0-15	9.0	0.0	15.0	76.0
27	PEG4NaCl9.0-20	9.0	0.0	20.0	71.0
28	PEG4NaCl9.0-25	9.0	0.0	25.0	66.0
29	PEG0NaCl0.9-00	0.9	0.0	0.0	99.1
30	PEG0NaCl9.0-00	9.0	0.0	0.0	91.0

Specific and molar conductivity of the tested solutions

The specific conductivity of the systems was measured using a CC-505 conductivity meter with an EC-70 conductivity sensor ($k = 1.0 \text{ cm}^{-1}$; Elmetron, Zabrze, Poland). The molar conductivity of the solutions (Λ) was calculated based on the measurements of specific conductivity (κ) and the molar concentration of NaCl (c), as shown in Equation 2.

$$\Lambda = \frac{1000\kappa}{c}$$

Density and viscosity of the tested solutions

The other parameters, i.e., the density and viscosity of the tested systems, were measured using a Radwag AS X2 analytical balance (Radwag, Radom, Poland) with a sinker of 9.9206 cm^3 , and an Ostwald viscometer. The measurements were performed at a constant temperature of $25 \pm 0.5^\circ\text{C}$, using a thermostat.

Results

Specific and molar conductivity of the tested systems

Figure 1 shows the changes in specific and molar conductivity with increasing concentrations of PEG 200 or PEG 4000 in 0.9% or 9.0% NaCl solutions.

A clear decrease in conductivity was observed with increasing polymer concentration in the NaCl solutions. In systems containing 0.9% NaCl, the conductivity of the tested solutions decreased from 14.60 to 8.28 mS/cm with increasing concentrations of PEG 200 (Fig. 1A; NaCl molar concentration below 0.25 mol/L). In the case of PEG 4000, conductivity decreased from 14.47 to 7.47 mS/cm (Fig. 1B; NaCl molar concentration below 0.25 mol/L). Significantly higher conductivity values were observed in the 9.0% NaCl solutions, ranging from 98.90 to 53.53 mS/cm (Fig. 1A) and from 91.30 to 48.73 mS/cm (Fig. 1B), corresponding to NaCl molar concentrations above 1.5 mol/L in both cases.

In 0.9% NaCl solution, the molar conductivity values decreased from $94,238.12$ to $51,581.89 \text{ mS} \cdot \text{cm}^2 \cdot \text{mol}^{-1}$ with the addition of PEG 200 (Fig. 1C; NaCl molar concentration below 0.25 mol/L). For PEG 4000, the values ranged from $93,341.65$ to $46,305.20 \text{ mS} \cdot \text{cm}^2 \cdot \text{mol}^{-1}$ under the same conditions (Fig. 1D, NaCl molar concentration below 0.25 mol/L). In 9.0% NaCl solutions, the molar conductivity

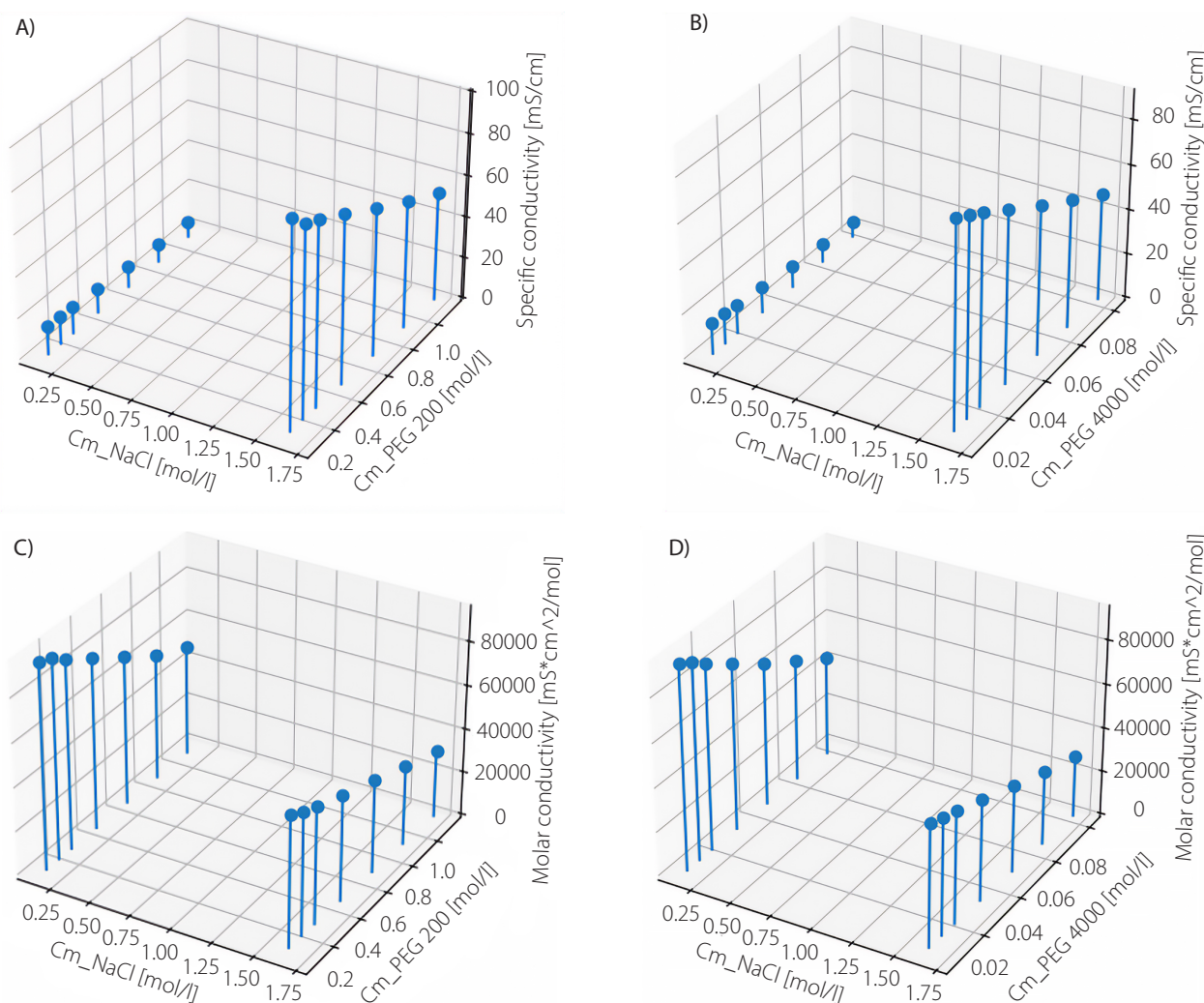


Fig. 1. The effect of polyoxyethylene glycol concentration on the specific and molar conductivity of NaCl solutions. A. Changes in the specific conductivity of NaCl 0.9% and 9.0% under the influence of polyethylene glycol (PEG) 200 addition; B. Changes in the specific conductivity of NaCl 0.9% and 9.0% under the influence of PEG 4000 addition; C. Changes in the molar conductivity of NaCl 0.9% and 9.0% under the influence of PEG 200 addition; D. Changes in the molar conductivity of NaCl 0.9% and 9.0% under the influence of PEG 4000 addition. The NaCl concentrations of 0.9% and 9.0% correspond to molar concentrations of approx. 0.15 mol/L and 1.6 mol/L, respectively, as shown in the plots

values ranged from 60,279.46 to 31,509.67 $\text{mS} \cdot \text{cm}^2 \cdot \text{mol}^{-1}$ (Fig. 1C) and from 55,665.02 to 28,562.21 $\text{mS} \cdot \text{cm}^2 \cdot \text{mol}^{-1}$ (Fig. 1D), respectively, at NaCl molar concentrations above 0.25 mol/L.

Viscosity of the tested systems

In contrast to conductivity, viscosity increased with increasing polymer concentration, as shown in Fig. 2. Small differences were observed between systems containing 0.9% and 9.0% NaCl. The viscosity of the 0.9% NaCl formulations was in the range of 1.0104–2.2642 Pa · s (PEG 200) and 1.2054–12.2376 Pa · s (PEG 4000). In the 9.0% NaCl formulations, the values were 1.0941–2.8036 Pa · s (PEG 200) and 1.2958–13.8077 Pa · s (PEG 4000).

Discussion

The influence of concentration on the specific and molar conductivity of the tested systems

The study assessed the influence of the molar concentration of PEGs, PEG 200 and PEG 4000, on the specific and molar conductivity of NaCl solutions with weight concentrations of approx. 0.9% and 9.0%, as shown in Fig. 1. The concentration of the first solution corresponded to that of physiological saline, with an osmotic pressure similar to that of body fluids. The 2nd physiological saline solution, with a tenfold higher NaCl concentration, was intended to confirm the effect of PEGs on the conductivity of the NaCl solution. It should be noted, however, that the increasing amounts of PEG 200 or PEG 4000 raised the density of the systems, resulting in a series of NaCl solutions with progressively higher molar concentrations of the salt. It was observed that, as a result of this increase in molar concentration, while maintaining the percentage concentration at 0.9%, the molar concentration rose by only 0.035–0.036 of the original value within the tested range. Therefore, this change was not significant for evaluating the effect

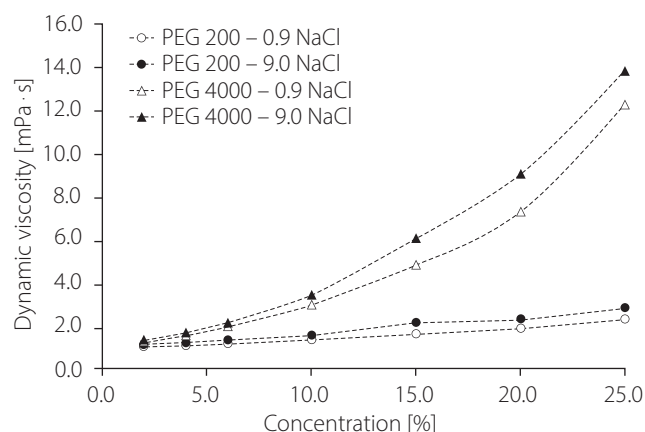


Fig. 2. Viscosity of NaCl solutions with varying concentrations of polyethylene glycol (PEG) 200 and PEG 4000

of increasing polymer concentrations on the conductivity of NaCl solutions. A similar effect was observed in the case of the 9.0% NaCl solution, where the molar concentration increased by a fraction of 0.034 in both PEG 200 and PEG 4000 systems. The highest molar concentration of NaCl was recorded for the PEG4NaCl9-25 solution (1.699 mol/L), and the lowest for the PEG2NaCl09-2 solution ($c = 0.155$ mol/L). In the case of solutions without PEG addition, these concentrations were 0.154 mol/L (PEG0NaCl09) and 1.635 mol/L (PEG0NaCl9), respectively. A significantly greater influence of the polymers on conductivity measurements was observed in the higher-concentration NaCl solutions. According to the presented results, the viscosity of the system, resulting from increasing polymer concentrations, was a key factor influencing conductivity measurements. The data demonstrated that PEG concentration has a systematic effect on both specific and molar conductivity.

The relationship between molar conductivity and electrolyte concentration

Figures 3A and 3B present the changes in molar conductivity, calculated from conductivity measurements, as a function of the elemental molar concentration of NaCl in the solutions.

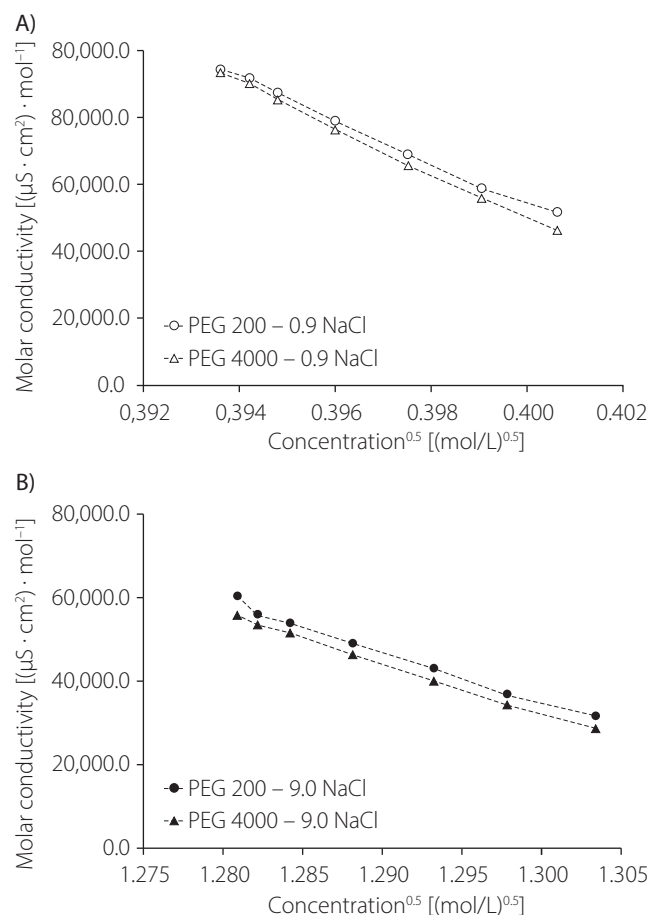


Fig. 3. The effect of polyethylene glycol (PEG) 200 and PEG 4000 on the molar conductivity of NaCl at concentrations of (A) 0.9% (approx. 0.15 mol/L) and (B) 9.0% (approx. 1.6 mol/L), presented in accordance with the Kohlrausch equation

The course of these graphs confirms that the studied systems do not deviate from the relationship proposed by Kohlrausch.¹² In this relationship, the molar conductivity of the electrolyte (Λ) is a function of concentration (c), and the limiting molar conductivity (Λ_0) is represented graphically by the y-intercept of the extrapolated curve (Equation 3). The coefficient a is characteristic of the studied system and was originally interpreted by Debye and Hückel¹³ and later reinterpreted by Onsager¹⁴:

$$\Lambda = \Lambda_0 - a\sqrt{c}$$

Extrapolating the graphs to the x-axis can provide information on the limiting molar conductivity values in the studied systems. Indeed, the cut-off points of the extrapolated courses of the abovementioned relationship are similar to each other in solutions with the same NaCl concentrations. Significantly higher values of the cut-off points were noted for lower NaCl concentrations, and the polymer with a higher molar mass favored a slight decrease in electrolytic conductivity. It should be noted that the tested range of NaCl concentrations was small and requires possible confirmation in tests conducted on a wider range of NaCl concentrations.

The influence of viscosity on the specific and molar conductivity of the tested systems

An interesting relationship was observed when comparing viscosity with specific and molar conductivity (Fig. 4AB)

Both specific and molar conductivity decreased with increasing viscosity. However, a sharper decrease was observed with PEG 200. The decrease in conductivity with increasing viscosity was less pronounced in the case of PEG 4000. This phenomenon may be attributed to differences in both the concentration and molar mass of the polymers used.

The importance of conductivity and viscosity for the practical application of the tested mixtures

The use of polyoxyethylene glycols as carriers and substrates for medicinal substances is particularly important in the context of electrical conductivity studies. Due to the need to maintain appropriate osmotic pressure in certain cases, corresponding to a 0.9% NaCl solution, conductivity can serve as an informative parameter, providing insight into the properties of such systems. In addition, PEG-water mixtures are characterized by a high potential for increasing the solubility of some chemical compounds. For example, to enhance the solubility of the non-steroidal anti-inflammatory drug etoricoxib, PEG 400 was used as a cosolvent for oral administration.¹⁵ PEG 4000 has been similarly applied to enhance

the solubility of carbamazepine,¹⁶ while PEG 6000 has been used for dihydroartemisinin.¹⁷ The increase in solubility is also important in systems characterized by a specific osmotic pressure. Hence, it was interesting to determine the value of electrical conductivity in the context of adding cosolvent polymers to an isosmotic solution.

The observed results indicate that, regardless of the type of PEG used or the NaCl concentration, molar conductivity decreases linearly with increasing electrolyte concentration. This confirms the principle of a linear relationship between the molar conductivity of a strong monovalent electrolyte and the square root of its molar concentration.¹⁸ Based on a 2007 study by Capuano et al. which examined polyoxyethylene glycols of similar molecular weight (PEG 4, PEG 400, PEG 2000), it is known that the addition of polyethylene glycol to aqueous NaCl solutions does not influence ion-ion electrostatic interactions. Taking this knowledge into account, in subsequent stages of research, it is possible to investigate, among others, the values of the limiting molar conductivity of NaCl solutions in PEG-water mixtures in a wider range of concentrations, and the effect of medicinal substances on the conductivity of such a system.⁵

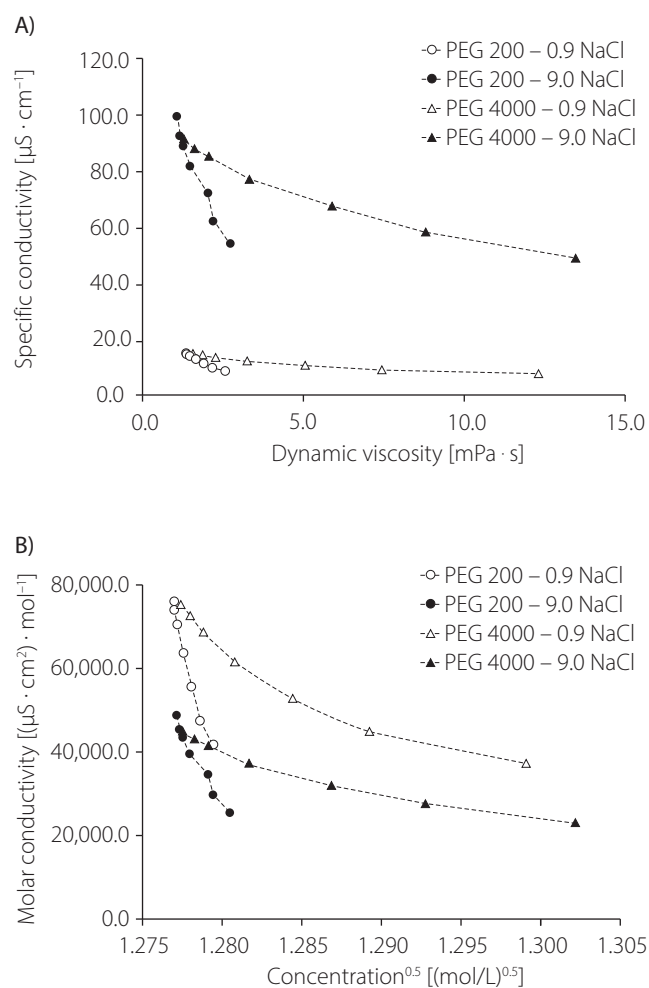


Fig. 4. Specific conductivity (A) and molar conductivity (B) as a function of viscosity

Conclusions

The addition of a polymer to a system containing NaCl at concentrations of 0.9% or 9.0% increases the solution viscosity. The increase in viscosity increases the calculated molar concentration of NaCl. With the increase in the calculated molar concentration of NaCl, the molar conductivity decreases proportionally according to the Kohlrausch equation. The rate of change in molar conductivity with the change in concentration is greater in the case of a system containing 9.0% NaCl. PEG 200 and polyoxyethylene glycol 4000 similarly influence the pattern of conductivity changes in both 0.9% and 9.0% NaCl solutions. The aim of future studies will be to determine the effect of the tested polymers on the estimated values of limiting molar conductivity.

Data availability

The datasets generated and/or analyzed during the current study are available from the corresponding author on reasonable request.

Consent for publication

Not applicable.

Use of AI and AI-assisted technologies

Not applicable.

ORCID IDs

Witold Musiał  <https://orcid.org/0000-0001-5695-5998>

References

1. D'Souza AA, Shegokar R. Polyethylene glycol (PEG): A versatile polymer for pharmaceutical applications. *Exp Opin Drug Deliv*. 2016;13(9):1257–1275. doi:10.1080/17425247.2016.1182485
2. Ende MT, Ende DJ, eds. *Chemical Engineering in the Pharmaceutical Industry: Drug Product Design, Development, and Modeling*. Hoboken, USA: Wiley; 2019. doi:10.1002/9781119600800
3. Suhail M, Chiu IH, Lin IL, Tsai MJ, Wu PC. A novel approach of polyethylene glycol-4000 hydrogels as controlled drug carriers. *Micro*. 2023;3(2):578–590. doi:10.3390/micro3020039
4. Suliman AS, Anderson RJ, Elkordy AA. Norfloxacin as a model hydrophobic drug with unique release from liquisolid formulations prepared with PEG200 and Synperonic PE/L-61 non-volatile liquid vehicles. *Powder Technol*. 2014;257:156–167. doi:10.1016/j.powtec.2014.02.048
5. Capuano F, Mangiapia G, Ortona O, d'Errico G, Sartorio R. Sodium chloride molar conductance in different poly(ethylene glycol)-water mixed solvents. *J Solution Chem*. 2007;36(5):617–629. doi:10.1007/s10953-007-9130-9
6. Roethlisberger D, Mahler HC, Altenburger U, Pappenberger A. If euhydric and isotonic do not work, what are acceptable pH and osmolality for parenteral drug dosage forms? *J Pharm Sci*. 2017;106(2):446–456. doi:10.1016/j.xphs.2016.09.034
7. Keraliya RA, Patel C, Patel P, et al. Osmotic drug delivery system as a part of modified release dosage form. *ISRN Pharmaceutics*. 2012;2012:528079. doi:10.5402/2012/528079
8. Lisik A, Musiał W. Conductometric evaluation of the release kinetics of active substances from pharmaceutical preparations containing iron ions. *Materials (Basel)*. 2019;12(5):730. doi:10.3390/ma12050730
9. Lisik A, Prescha A, Cavlaz LE, Grajeta H, Musiał W. The evaluation of alternative method of ferrous ions assessment in pharmaceutical preparations. *Monatsh Chem*. 2018;149(5):931–937. doi:10.1007/s00706-018-2147-5
10. Gómez-Merino AI, Jiménez-Galea JJ, Rubio-Hernández FJ, Arjona-Escudero JL, Santos-Ráez IM. Heat transfer and rheological behavior of fumed silica nanofluids. *Processes*. 2020;8(12):1535. doi:10.3390/pr8121535
11. Kou Y, Wang S, Luo J, et al. Thermal analysis and heat capacity study of polyethylene glycol (PEG) phase change materials for thermal energy storage applications. *J Chem Thermodyn*. 2019;128:259–274. doi:10.1016/j.jct.2018.08.031
12. Kohlrausch F. Einfache Methoden und Instrumente zur Widerstandsmessung insbesondere in Electrolyten. *Annalen der Physik*. 1880;247(12):653–660. doi:10.1002/andp.18802471205
13. Pitzer KS. Electrolyte theory: Improvements since Debye and Hückel. *Acc Chem Res*. 1977;10(10):371–377. doi:10.1021/ar50118a004
14. Onsager L. Deviations from Ohm's law in weak electrolytes. *J Chem Phys*. 1934;2(9):599–615. doi:10.1063/1.1749541
15. Nayak AK, Panigrahi PP. Solubility enhancement of etoricoxib by cosolvency approach. *ISRN Phys Chem*. 2012;2012:820653. doi:10.5402/2012/820653
16. Nair R, Gonen S, Hoag SW. Influence of polyethylene glycol and povidone on the polymorphic transformation and solubility of carbamazepine. *Int J Pharm*. 2002;240(1–2):11–22. doi:10.1016/S0378-5173(02)00083-2
17. Ansari MT, Ahmad I, Hassan SS, Tariq I, Murtaza G. Solubility enhancement of dihydroartemisinin using mixture of hydroxypropyl-β-cyclodextrin and PEG-6000. *Lat Am J Pharm*. 2014;33(13):483–491. http://www.latamjpharm.org/resumenes/33/3/LAJOP_33_3_1_19.pdf
18. Mukerjee P, Mysels KJ, Dulin CI. Dilute solutions of amphipathic ions. I. Conductivity of strong salts and dimerization. *J Phys Chem*. 1958;62(11):1390–1396. doi:10.1021/j150569a010

The impact of semisolid matrices on spreadability, rheology and celecoxib release rate

Wpływ półstałych podłoży na rozsmarowywalność, reologię i uwalnianie celekoksylu

Urszula Bąk-Kuchejda^{1,2,A–D}, Teresa Witczak^{3,B–D,F}, Mariusz Witczak^{4,B–D,F}, Anna Krupa^{1,A,C,E,F}

¹ Department of Pharmaceutical Technology and Biopharmaceutics, Jagiellonian University Medical College, Cracow, Poland

² Doctoral School of Medical and Health Sciences, Jagiellonian University, Cracow, Poland

³ Laboratory of Nanomaterials and Nanotechnology, Faculty of Food Technology, University of Agriculture, Cracow, Poland

⁴ Department of Engineering and Machinery for Food Industry, University of Agriculture, Cracow, Poland

A – research concept and design; B – collection and/or assembly of data; C – data analysis and interpretation;

D – writing the article; E – critical revision of the article; F – final approval of the article

Polymers in Medicine, ISSN 0370-0747 (print), ISSN 2451-2699 (online)

Polim Med. 2025;55(1):49–58

Address for correspondence

Anna Krupa
email: a.krupa@uj.edu.pl

Funding sources

This research was carried out in the frame of the Sonata Bis grant No. DEC-2019/34/E/NZ7/00245 financed by the National Science Centre in Poland.

Conflict of interest

None declared

Received on April 25, 2025

Reviewed on June 2, 2025

Accepted on June 9, 2025

Published online on June 30, 2025

Cite as

Bąk-Kuchejda U, Witczak T, Witczak M, Krupa A. The impact of semisolid matrices on spreadability, rheology and celecoxib release rate. *Polim Med.* 2025;55(1):49–58. doi:10.17219/pim/206077

DOI

10.17219/pim/206077

Copyright

Copyright by Author(s)

This is an article distributed under the terms of the Creative Commons Attribution 3.0 Unported (CC BY 3.0) (<https://creativecommons.org/licenses/by/3.0/>)

Abstract

Background. The results of numerous research studies published in recent years suggest that celecoxib (CEL) may be effective in the treatment of various skin disorders. However, to date, no semisolid product containing CEL has been launched.

Objectives. With a focus on the future development of topical products, we aimed to investigate the impact of different semisolid matrices on the in vitro performance of CEL.

Materials and methods. For this purpose, 1% (w/w) of the drug was suspended in 4 compounding vehicles available in Polish community pharmacies: Lekobaza (amphiphilic cream), Lekobaza Lux (hydrophobic cream), Celugel (hydrogel), and Oleogel (lipogel). Given their very different physicochemical properties, our goal was to analyze, for the first time, their influence on spreadability, viscoelastic properties and the release rate of CEL.

Results. It was found that all of the semisolid matrices were suitable as vehicles for the drug in terms of spreadability and rheological stability. The viscous properties predominated when Celugel was used as a vehicle, but when Lekobaza, Lekobaza Lux and Oleogel were tested, the elastic properties prevailed. The drug release rate was the highest when hydrophilic matrices, i.e., Celugel or Lekobaza were used, but when hydrophobic matrices such as Lekobaza Lux or Oleogel were examined, CEL was released slowly. These findings might be related not only to the properties of these matrices, but also to the design of the release study that was more suitable for evaluating the hydrophilic matrices.

Conclusions. Celugel could be particularly useful as a vehicle for CEL for the therapy of large lesions with heavy exudation, but if there is a risk of skin drying out after using the hydrogel, the use of Lekobaza can be recommended.

Key words: celecoxib, oleogel, hydrogel, cream, semi-solid drugs

Abstrakt

Wprowadzenie. Wyniki licznych badań naukowych opublikowanych w ostatnich latach, wskazują, że celekoksyb może być skuteczny w terapii chorób skóry. Jednak do tej pory nie wprowadzono do obrotu żadnego półstałego produktu leczniczego z celekoksybem.

Cel pracy. Myśląc o rozwoju półstałych produktów leczniczych z celekoksybem, przeznaczonych do podania na skórę, dokonano oceny wpływu, jaki rodzaj podłoża może mieć na właściwości aplikacyjne i uwalnianie substancji leczniczej w warunkach *in vitro*.

Materiał i metody. W tym celu 1% (w/w) celekoksylu zawieszono w czterech podłożach recepturowych, dostępnych w polskich aptekach, tj. Lekobaza (krem amfifilowy), Lekobaza Lux (krem hydrofobowy), Celugel (hydrożel) i Oleogel (lipożel). Ponieważ wykazują one bardzo zróżnicowane właściwości fizykochemiczne, po raz pierwszy dokonano oceny ich wpływu na rozsmarowywalność, właściwości lepkosprężyste i uwalnianie celekoksylu.

Wyniki. Stwierdzono, że wszystkie półstałe podłoża nadawały się jako nośniki leku pod względem rozsmarowywalności i stabilności reologicznej. Właściwości lepkie przeważały, gdy Celugel był używany jako nośnik, ale gdy testowano Lekobazę, Lekobazę Lux i Oleogel, przeważały właściwości elastyczne. Szybkość uwalniania celekoksylu była największa, gdy użyto hydrofilowe podłoża, takie jak Celugel lub Lekobazę, ale gdy badano matryce hydrofobowe, np. Lekobazę Lux lub Oleogel, uwalnianie celekoksylu następowało znacznie wolniej. Może to być związane nie tylko z właściwościami tych półstałych podłoży, ale także z metodyką zastosowaną w badaniach uwalniania. Była ona bardziej odpowiednia do oceny matryc hydrofilowych niż lipofilowych.

Wnioski. Podsumowując, Celugel może być szczególnie przydatny jako nośnik celekoksylu w leczeniu dużych zmian skórnych z silnym wysiękiem, ale jeśli istnieje ryzyko wysuszenia skóry po zastosowaniu hydrożelu, zalecane jest zastosowanie podłoża Lekobaza.

Słowa kluczowe: hydrożel, oleożel, celekoksyb, półstałe postacie leków, krem

Background

Celecoxib (CEL) is a non-steroidal anti-inflammatory drug (NSAID) that selectively inhibits cyclooxygenase-2 (COX-2), reducing the production of prostaglandins. This effect contributes to its anti-inflammatory and analgesic properties.¹ Currently, the majority of drug products containing CEL are in the form of tablets and capsules, primarily used for the oral treatment of osteoarthritis and rheumatoid arthritis symptoms in adults. The drug has also been approved for the oral treatment of dysmenorrhea and ankylosing spondylitis, an inflammatory condition affecting the joints and ligaments of the spine. In addition to these oral solid dosage forms, an oral solution of CEL for the treatment of acute migraine pain has also been introduced in recent years.^{2,3}

On the other hand, numerous reports have highlighted serious side effects associated with oral systemic therapy using CEL. These reports prompted the exploration of new clinical indications, particularly for the topical treatment of inflammatory skin disorders or local infections. Nitescu et al. focused their research on the treatment of psoriasis.^{4,5} The authors developed ointments using white vaseline, in which 1%, 2%, 4%, or 8% of CEL was suspended. Using a mouse-tail model, Nitescu et al. demonstrated that CEL had a stronger anti-psoriatic effect than diclofenac, significantly increasing mean epidermal thickness⁴ and exhibiting anti-proliferative properties, particularly when the ointment contained 4% or 8% of the drug.⁵

The functionality of CEL was also studied in the treatment of hand-foot syndrome.⁶ This is a common chemotherapy side effect that manifests as burning pain, erythema, cracking of the skin, and blistering. A stable hydrogel containing carbomer (as a matrix-forming agent), glycerin,

absolute ethanol, and PEG 400 was developed and evaluated in clinical studies. The patients applied a dose corresponding to half a teaspoon of CEL hydrogel to 1 extremity and the same amount of placebo hydrogel to the opposite extremity twice a day for 3 weeks. They were also instructed to apply a dose of Eucerin® cream 1 h after the hydrogel application, as the high ethanol content (33%) in the hydrogel could cause skin dryness. After this treatment, 60% of the patients showed at least 1 grade of improvement in their skin condition.⁶

Neelon et al.⁷ indicated that CEL's anti-inflammatory properties might be a promising strategy to accelerate burn wound healing. The use of a carboxymethyl cellulose hydrogel loaded with 5 mg/mL of CEL resulted in a higher percentage of burn wound closure compared to 3 other anti-inflammatory agents tested in parallel.⁷ Interestingly, CEL also exhibits antimicrobial activity against methicillin-resistant *Staphylococcus aureus* (MRSA). A significant reduction in the mean bacterial count was observed when a petroleum jelly loaded with 1% or 2% of the drug was applied to infected mice twice daily for 5 days.⁸

A review of the aforementioned research studies clearly demonstrates that semisolid matrices, whether hydrophilic or lipophilic, have been proposed as carriers for CEL in recent years. The choice of matrix depended on the availability of the carrier and the disease state of the skin. However, from both regulatory and technological perspectives, the type of semisolid matrix can significantly impact the ease of drug administration, usability and sensory feel (whether dry or greasy).⁹ Moreover, the rheological properties of the matrix influence the product's texture and the drug release rate, which in turn affect the drug's absorption through the skin, ensuring targeted efficacy and safety.

Objectives

However, little is known about the impact that either hydrophilic or lipophilic semisolid matrices may have on CEL release. Therefore, the aim of this study is to assess how different semisolid matrices, destined for compounding and available in Polish community pharmacies (Table 1), may alter the spreadability, rheology and release rate of CEL. We believe that the results described in this study can serve as a starting point for the further development of new semisolid dosage forms loaded with CEL, tailored to specific clinical indications.

Materials and methods

Materials

Celecoxib was obtained from STI (Poznań, Poland). Celugel and Oleogel (Actifarm, Warsaw, Poland), and Lekobaza and Lekobaza Lux (Fagron, Cracow, Poland) were used as commercial semisolid bases. Polyethylene glycol 400 (PEG 400) was provided by Chempur (Piekary Śląskie, Poland). Acetonitrile (ACN) of chromatographic gradient grade was purchased from Witko (Łódź, Poland). Purified water was prepared using a Milli-Q Elix Essential water purification system by Millipore Corp. (Merck, Warsaw, Poland).

Manufacturing of semisolid formulations

Celecoxib (1% w/w) was suspended in 4 commercial semisolid compounding bases:

- Celugel (hydrogel; Actifarm, Warsaw, Poland);
- Lekobaza (amphiphilic cream; Fagron, Cracow, Poland);
- Lekobaza Lux (lipophilic polymeric cream; Fagron);
- Oleogel (lipogel; Actifarm, Cracow, Poland).

The formulations were prepared using an automatic compounding mixer, the Gako Cito-Unguator e/s (Eprus, Bielsko-Biała, Poland). The mixing time was set to 4 min, with the mixing speed set at 1,130 rpm (level 3). For Celugel, the drug was manually combined with the carrier using a pestle and mortar to avoid aeration of the final formulation.

Spreadability

A rectangular acrylic plate (4 mm-thick) with a central orifice of 1 cm in diameter was used as a template for applying samples. The template was placed on an acrylic support plate (20 cm × 20 cm) positioned on a millimeter scale. The sample was applied into the orifice of the template, and the surface was leveled with a spatula. After removing the template, the sample was covered with another acrylic plate of known weight (282 g), onto which weights of increasing mass were placed: 100 g, 200 g and 300 g. The radii of the surface onto which the formulations were spread

Table 1. Characteristics of selected semisolid matrices destined for compounding

Brand name	General properties	Composition	Water content (%)	Indications	Examples of drugs loaded
Celugel (hydroxyethylcellulose mucilago)	hydrogel of pH = 4.5–6.0, light, non-greasy, cooling effect, rinsible with water, high mucoadhesion	water, glycerol, hydroxyethyl cellulose (HEC 10,000), sorbic acid, potassium sorbate	>80	skin and mucous membranes, burns, exudative lesions, acne	hydrocortisone, chloramphenicol, benzocaine, nystatin, metronidazole, boric acid in aqueous solutions
Lekobaza	amphiphilic cream of pH = 5.5, soft cream, easy rinsible with water, creates protective film on the skin	glycerol monostearate, white vaseline, propylene glycol, water, medium chain triglycerides, macrogol-20-glycerol-monostearate	40	skin inflammation, exudative lesions, dry skin, lichenization	salicylic acid, zinc oxide, tetracaine, lignocaine, urea, dithranol, vitamin A
Lekobaza Lux	lipophilic cream of pH = 3.5–5.0, very soft cream, creates a lubricating layer, hardly rinsible, cooling and moisturizing effect	water, triglycerol isostearate, isopropyl palmitate, liquid paraffin, polyethylene, vitamin E, potassium sorbate, citric acid anhydrous, magnesium sulfate heptahydrate, glycerol	65	inflammatory skin disorders, eczema	clotrimazole, benzocaine, urea, dimethicone, vitamin A, vitamin E, prednisolone, salicylic acid
Oleogel (gelatum basale hydrophobicum)	hydrophobic lipogel of pH = 7.0, occlusive, colorless, hardly rinsible, moisturizing effect, emolient	liquid paraffin (95%), polyethylene (5%)	0	dry and rough skin, inflammatory skin conditions, allergic reactions, itching, skin infections	boric acid, salicylic acid, dithranol, pix liquida, hydrocortisone, benzocaine, prednisolone

were measured after 1 min of loading. The results were expressed as the mean area ($n = 3$) covered by the formulation. The test was carried out under ambient conditions.

Rheology

The viscoelastic properties were characterized using an oscillatory rheometer RS 6000 (Thermo-Haake, Karlsruhe, Germany) with parallel-plate geometry. The surface of both plates was roughened to ensure adhesion between the sample and the measuring plate. The samples were applied to the plate and left for 5 min in the measuring system for stress relaxation and temperature stabilization. Subsequently, the tests were performed at 25°C. The relationship between moduli and stress was measured from 1 to 1,000 Pa at a constant frequency of 1 Hz. The linear viscoelastic region (LVR) was determined using Haake Rheowin Data Manager v. 4.93 (Thermo-Haake) by the point at which the storage modulus (G') deviated by 5% from the plateau.¹⁰ The dynamic plastic stress (τ) was determined along with the corresponding deformation (γ). The mechanical spectra from 1 to 100 s⁻¹ were recorded in the LVR at a constant deformation ($\gamma = 0.01$). The experimental data were described by power equations¹⁰:

$$G' = K' \cdot \omega^{n'}$$

$$G'' = K'' \cdot \omega^{n''}$$

where G' is the storage modulus (Pa), G'' is the loss modulus (Pa), ω is the angular velocity (s⁻¹), and K' , K'' , n' , n'' are constants.

In vitro release test

Receptor solution screening

The in vitro release tests (IVRTs) were performed under sink conditions. Given that CEL is a poorly water-soluble drug, it was necessary to optimize the composition of the receptor solution. Preliminary research indicated that mixtures composed of 20–70% (v/v) ethanol 96°, 5% (v/v) PEG 400 and water were the most promising. The equilibrium solubility of CEL was determined at 32 ± 1°C. An excess amount of the drug was added to 1 mL of the solvent mixture, and the samples were shaken at 500 rpm for at least 24 h to reach equilibrium (uniTHERMIX 2pro; Lab Logistics Group Labware, Meckenheim, Germany). Subsequently, they were centrifuged for 15 min at 13,000 rpm (uniCFUGE 5; Lab Logistics Group Labware). After dilution and filtration, the concentration of CEL dissolved was quantified using a chromatographic method (see below). Finally, the mean values from 6 measurements were calculated.

Synthetic membrane screening

The screening of artificial membranes was conducted to select the barrier material that limits the diffusion of CEL the least. The porous artificial membranes ($\varnothing = 0.45 \mu\text{m}$) made of various materials, including hydrophobic polytetrafluoroethylene (PTFE), hydrophilic polyethersulfone (PES), nylon (NY), and a dialysis membrane with a molecular weight cut-off of 14,000 Da (DIA), were tested. First, the binding of CEL to each of these membranes was analyzed. The membrane samples were immersed in 10 mL of CEL solution (20 µg/mL) in an aqueous-organic solvent mixture, chosen as the receptor solution for the IVRT. The samples were incubated at 32 ± 1°C for 12 h. After dilution, the concentration of CEL was quantified using a chromatographic method ($n = 3$).

Next, the release of CEL from a model formulation in Leukobaza was studied, with each of the aforementioned membranes placed between the donor and receptor chambers in a vertical diffusion cell (VDC). Prior to the IVRT, the membranes were presoaked for at least 12 h in either distilled water (for the DIA membrane to remove glycerol) or in the receptor solution (for PTFE, PES and NY). Further details on the test conditions are provided below.

Experimental design

The steady-state release of CEL from semisolid formulations was analyzed using a dry-heat Phoenix DB-6 six-cell manual sampling vertical diffusion system (Teledyne Hanson Research, Chatsworth, USA). The VDCs of size S, with an effective diffusional area of 1.0 cm² and a receptor chamber capacity of 16.2 mL, were used in this study. A de-aerated aqueous-organic solution composed of ethanol 96°, PEG 400 and water (45:5:50, v/v) was applied as the receptor solution. The test was conducted at 32 ± 1°C. The receptor phase medium was continuously stirred at 400 rpm using Teflon-covered magnetic stirring bars (15 × 6 mm). A 300 µL sample of the tested semisolid formulations was dosed onto the surface of a nylon membrane ($\varnothing = 0.45 \mu\text{m}$) in the donor compartment using a positive-displacement pipette (Microman E M1000E; Gilson, Villiers-le-Bel, France). Prior to assembly in the diffusion cell, the membranes were presoaked in the receptor solution for at least 12 h. The donor chambers were covered with glass covers to prevent the drying of the tested formulations. At predetermined time intervals (120, 180, 240, 300, and 360 min), 500 µL samples were withdrawn from the receptor compartment, and the volume was replaced with an equal volume of receptor solution preheated to 32°C. After dilution, the concentration of CEL released was quantified using a chromatographic method (see below).

For each cell, the amount of CEL released at each sampling time was determined in µg/cm², and the mean cumulative amount released ($n = 3$) was plotted against the square root of time. According to the USP NF-PF monograph (1724)

Semisolid Drug Products – Performance Tests, the slope of the resulting line serves as a measure of the release rate (steady-state flux).¹¹

Quantification of celecoxib

The concentration of CEL released was determined using high-performance liquid chromatography (HPLC) with an Agilent 1260 Infinity HPLC system (Agilent Technologies, Waldbronn, Germany) connected to a diode array detector (DAD). The separation of CEL was carried out with an InfinityLab Poroshell 120EC-C18 RP LC column (4.6 × 100 mm; particle size 4 µm; Agilent Technologies), along with the corresponding guard column. Prior to analysis, the samples were diluted with the mobile phase (1:1) and filtered through polytetrafluoroethylene (PTFE) membrane filters (Ø = 0.22 µm). The injection volume was 20 µL.

A mixture of ACN and DMSO (9:1, v/v) was used as a needle wash solvent. The column temperature was set to 25°C. The mobile phase consisted of ACN and water (65:35, v/v), and the flow rate was maintained at 1.0 mL/min. CEL detection was performed at 254 nm. The CEL retention time was 2.80 min, and the total method run time was 3.50 min. A stock solution of CEL (1 mg/mL) in ACN was prepared and then diluted with the mobile phase (for equilibrium solubility studies) or with a 1:1 mixture of the mobile phase and the receptor solution (for IVRT) to obtain the corresponding calibration curves. The analytical method developed for equilibrium solubility studies was linear ($r^2 = 0.9999$) within the concentration range of 0.2–12.0 µg/mL (LOD = 0.05 µg/mL, LOQ = 0.15 µg/mL), whereas for the IVRT test, it was linear ($r^2 = 0.9999$) within the concentration range of 2–80 µg/mL (LOD = 0.28 µg/mL, LOQ = 0.84 µg/mL).

Results

Spreadability

The spreadability of the tested formulations, expressed as the area covered by a known volume of the sample under a defined load, is shown in Fig. 1. As a rule of thumb, the larger the area, the better the spreadability. Among the tested semisolid matrices, the greatest area was observed for the hydrogel Celugel and the amphiphilic cream base Lekobaza, measuring $36.3 \pm 1.2 \text{ cm}^2$ and $32.2 \pm 1.2 \text{ cm}^2$, respectively. When lipophilic matrices were analyzed, the area was approximately half that of the hydrophilic matrices, with $17.9 \pm 0.8 \text{ cm}^2$ for Lekobaza Lux and $13.3 \pm 1.1 \text{ cm}^2$ for Oleogel. Moreover, suspending 1% solid CEL particles in Lekobaza Lux resulted in a further reduction in spreadability ($15.8 \pm 1.2 \text{ cm}^2$), while the spreadability of Oleogel slightly improved ($14.6 \pm 1.4 \text{ cm}^2$). However, the most significant impact was observed with CEL in the hydrogel Celugel, where

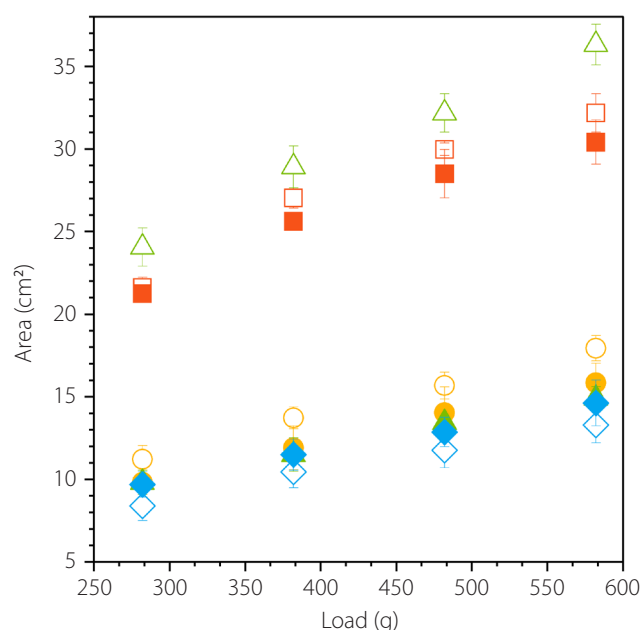


Fig. 1. Spreadability of semisolid formulations before (open symbols) and after (solid symbols) suspending celecoxib (CEL) as a function of loading. Mean \pm standard deviation (SD) ($n = 3$). The shape of the symbol corresponds to the type of matrix: Celugel (green triangles), Lekobaza (red squares), Lekobaza Lux (yellow circles), and Oleogel (blue diamonds)

the drug-loaded formulation showed nearly twice lower spreadability, i.e., $14.9 \pm 0.9 \text{ cm}^2$, compared to $36.3 \pm 1.2 \text{ cm}^2$ for the blank formulation. These data points are not visible in Fig. 1, as they are overlapped by those of Oleogel and Lekobaza Lux loaded with CEL. When CEL was suspended in the amphiphilic Lekobaza, the spreadability was only slightly reduced, with a final area of $30.4 \pm 1.4 \text{ cm}^2$.

Rheological properties

Oscillation frequency sweeps were performed to obtain information on the structural characteristics of semisolid formulations loaded with CEL, which may influence their functionality, drug release, and stability. In Fig. 2A, the viscoelastic properties as a function of frequency are presented, using a fixed oscillation amplitude within the LVR, with the corresponding empirical power law fitting parameters provided in Table 2. Figures 2B and 2C display the values of phase shift angle (δ) and loss tangent ($\tan \delta$, the damping factor), respectively. The phase angle denotes the ratio of the loss modulus (G'') to the storage modulus (G') and provides insight into the microstructure and overall viscoelastic properties of the material. A phase angle close to 0° indicates that the sample behaves as an ideal elastic solid, while a phase angle near 90° suggests it behaves as a viscous liquid.¹² For all examined formulations loaded with CEL, the phase angle ranged between 2° and 82° , which indicates that their rheological properties are suitable (0 – 90°) for spreading on the skin surface (Fig. 2B).

In the Celugel formulation loaded with CEL, the viscous

characteristics predominated ($G' < G''$, Fig. 2A & $\tan \delta = 1.2$ – 6.9). Both the storage and loss moduli increased with increasing frequency until the crossover point ($G' = G''$) at approx. 100 rad/s, indicating that the hydrogel behaves as a viscoelastic liquid. In contrast, the CEL formulation in Oleogel exhibited viscoelastic solid behavior ($G' > G''$), with high storage modulus (G') values that remained nearly constant across the entire frequency range, while the loss modulus (G'') gradually increased. Similarly, the Lekobaza Lux formulation loaded with CEL showed a predominant storage modulus ($G' \gg G''$) and exhibited the highest values among all tested formulations. Like Oleogel, the storage modulus remained almost constant across the entire frequency range. The constant G' values indicate that the formulation has a rigid structure with a yield point that was not exceeded under the applied frequency range. When the suspension of CEL in Lekobaza Lux was analyzed, the loss modulus (G'') remained constant at low frequencies, approx. 4 times lower than that of Oleogel, but began to increase when the angular velocity (ω) exceeded 10 rad/s. This suggests a transition from elastic gel-like behavior ($G' > G''$) to more viscous characteristics (viscoelastic solid). However, a crossover point was not observed. For Lekobaza loaded with CEL, the elastic properties dominated ($G' > G''$), and both moduli gradually increased with increasing frequency. The difference between the elastic modulus (G') and the viscous modulus (G'') was the smallest among all the formulations tested.

Overall, the higher values of the storage modulus compared to the loss modulus ($G' > G''$ & $\tan \delta < 1$) in CEL formulations in Lekobaza, Lekobaza Lux and Oleogel are considered favorable. These results indicate that cohesive forces predominate in these systems, reducing the risk of the drug dose dripping off the skin.¹³ Since the loss tangent values reflect the strength of the particle association in the polymeric network, it can also be concluded that, upon storage under resting conditions (mimicked by the lowest frequency of 1 rad/s), these 3 formulations exhibited the lowest $\tan \delta$ (Table 2, Fig. 2C), suggesting the strongest particle association at the microstructural level. This may ensure high long-term stability by reducing the risk of phase separation in the dense matrix.¹²

Design of IVRT

Since CEL is primarily administered orally, no compendial test exists for studying its release from semisolid matrices. Consequently, the present study began with the search for both an appropriate receptor solution and an artificial membrane to establish the conditions for IVRT. These conditions were then used to evaluate the performance of the developed topical formulations.

Given the poor solubility of CEL in water ($<5 \mu\text{g/mL}$), an aqueous-organic mixture was required as a receptor solution to maintain sink conditions. Based on published data and our preliminary solvent screening (data not shown),

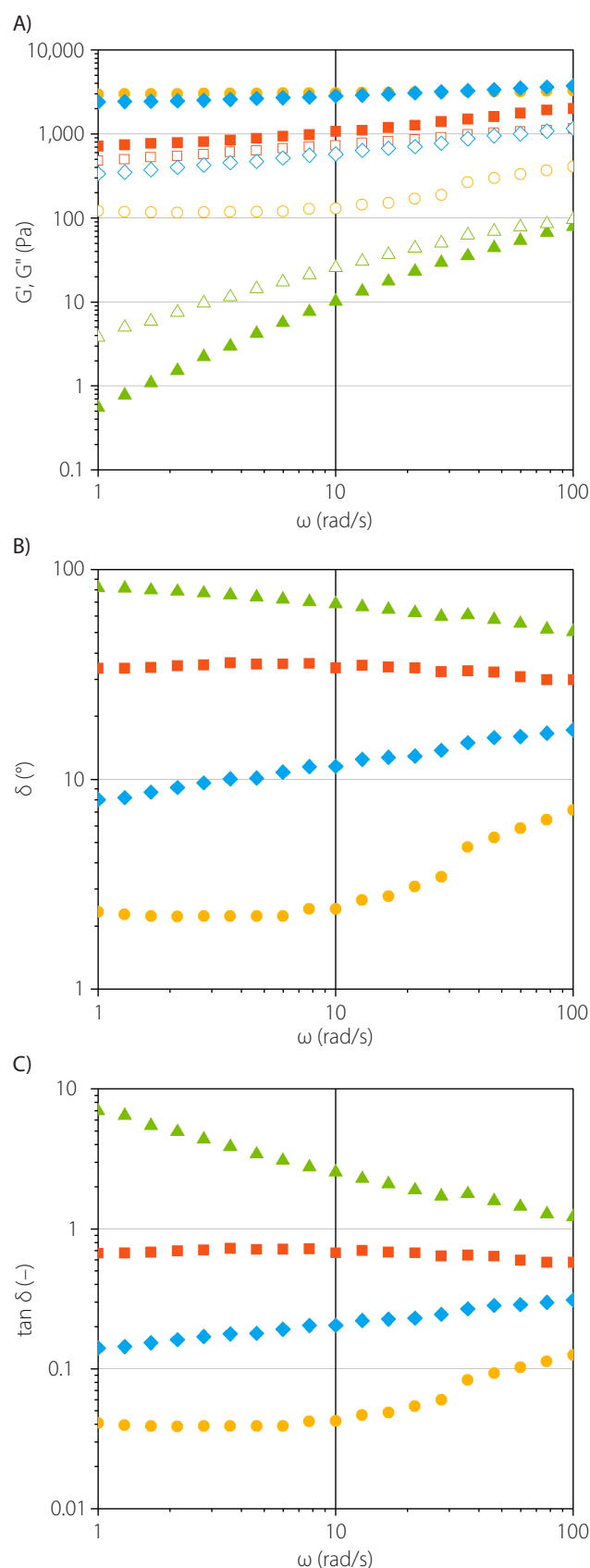


Fig. 2. A. Elastic modulus (G' , solid symbols) and viscous modulus (G'' , open symbols); B. Phase angle δ ; C. Loss tangent ($\tan \delta$) determined for semisolid formulations loaded with celecoxib (CEL) in an oscillatory sweep test at 25°C. The shape of the symbol corresponds to the type of matrix: Celugel (green triangles), Lekobaza (red squares), Lekobaza Lux (yellow circles), and Oleogel (blue diamonds)

Table 2. Mean values of oscillatory tests parameters. Amplitude sweeps: End of linear viscoelastic region linear viscoelastic region (LVR) (τ and γ). Frequency sweeps: Power law parameter fits (K' , K'' , n' and n'') and phase shift angle and tangent phase shift angle at 1 rad/s

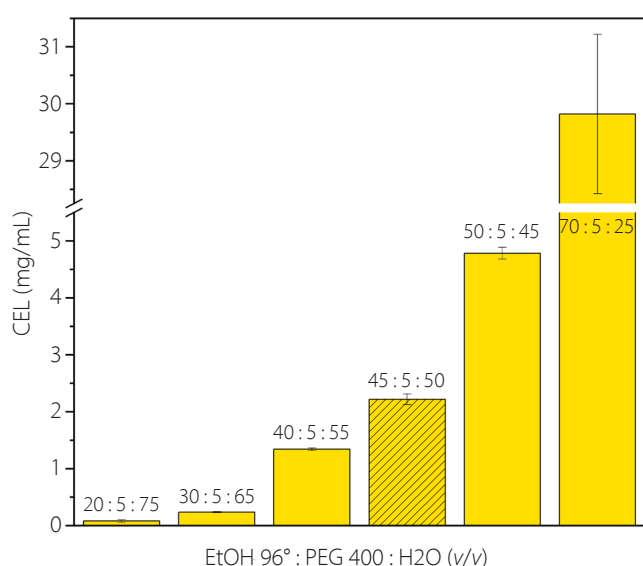
Parameter	Unit	Lekobaza Lux	Lekobaza	Celugel	Oleogel	ANOVA – p
LVR						
τ	Pa	108.2 \pm 5.8d	12.3 \pm 2.7a	28.3 \pm 0.5b	43.6 \pm 5.2c	<0.001
γ	–	0.043 \pm 0.002c	0.005 \pm 0.001a	1.421 \pm 0.033d	0.018 \pm 0.001b	<0.001
Frequency sweeps						
K'	Pa \cdot s $^{n'}$	2946.5 \pm 60.4d	651.4 \pm 24.0b	0.698 \pm 0.037a	2303.6 \pm 113.7c	<0.001
n'	–	0.021 \pm 0.002a	0.233 \pm 0.010c	1.091 \pm 0.014d	0.099 \pm 0.004b	<0.001
$r^2_{>}$	–	0.946	0.971	0.989	0.974	
K''	Pa \cdot s $^{n''}$	87.8 \pm 4.6b	471.6 \pm 36.3d	4.49 \pm 0.08a	321.8 \pm 12.0c	<0.001
n''	–	0.279 \pm 0.018b	0.197 \pm 0.010a	0.711 \pm 0.004c	0.273 \pm 0.006b	<0.001
$r^2_{>}$	–	0.784	0.997	0.990	0.991	
$\tan \delta^*$	–	0.04 \pm 0.00c	0.67 \pm 0.03b	6.93 \pm 0.78d	0.14 \pm 0.00a	<0.001
δ	°	2.34 \pm 0.15a	33.79 \pm 1.36c	81.71 \pm 0.92d	8.01 \pm 0.11b	<0.001

Mean value \pm standard deviation 3 replications). Mean values signed these same letters in particular rows are non-significantly different at the 0.05 level of confidence; *at 1 rad \cdot s $^{-1}$.

a mixture composed of water, ethanol 96° and PEG 400 was selected as the most promising. The PEG 400 concentration was kept at 5% (v/v). The effect of various ethanol 96° concentrations was evaluated to determine the optimal solvent ratio that ensures the highest equilibrium solubility of CEL. As shown in Fig. 3, drug solubility increases gradually with the concentration of ethanol 96°. However, a high concentration of ethanol in the receptor solution could potentially lead to backward diffusion into the donor chamber and may affect the integrity of the membrane. To minimize these risks, it is important to keep the ethanol concentration as low as possible. Therefore, a mixture

composed of 45% ethanol 96°, 5% PEG 400 and 50% water was selected for IVRT studies. The equilibrium solubility of CEL in this mixture at 32°C was 2.2 \pm 0.09 mg/mL.

The suitability of 4 synthetic filter membranes (0.45- μ m pore size) for the IVRT of CEL was also assessed. Initially, the binding of CEL was evaluated by measuring the recovery after soaking the membranes for 12 h in the drug solution. The recovery ranged from 99.0% to 100.7%, confirming that all membranes met the guidelines for inertness.¹⁴ Next, the impact of the filter material on the diffusion of CEL suspended in the semisolid matrix was investigated to select the material that least hindered this process. Based on screening tests showing a high drug diffusion rate from Lekobaza, this semisolid matrix was selected as the model for this part of the study. The release profiles obtained (using the receptor solution of the previously described composition), along with scanning electron micrographs of the membrane surface, are presented in Fig. 4A and Fig. 4B, respectively. The corresponding linear regression parameters are provided in Table 3. With the exception of the PES membrane, all studied filters exhibited symmetry in terms of pore size. For the PES membrane, the side with the largest pores (side A) was oriented towards the donor cell, while the side with the smallest pores (side B) faced the receptor cell (Fig. 4B). As shown in Fig. 4A, drug diffusion was least restricted when PES and NY membranes were used. The difference between the slopes for these membranes was minimal (31.00 \pm 0.44 vs 29.03 \pm 0.70), but the variation in CEL concentration released across the cells was significantly lower when the NY membrane was used instead of PES. Considering the low binding of CEL to the NY membrane (recovery of 99.8%), the high compatibility of this membrane with both the receptor solution and semisolid formulations, as well as the reduced variability in CEL diffusion, the NY membrane was

**Fig. 3.** Impact of ethanol 96° concentration on equilibrium celecoxib (CEL) solubility in aqueous-organic solutions at 32°C. Mean \pm SD (n = 6). The striped bar represents the acceptor solution

PEG – polyethylene glycol, SD – standard deviation.

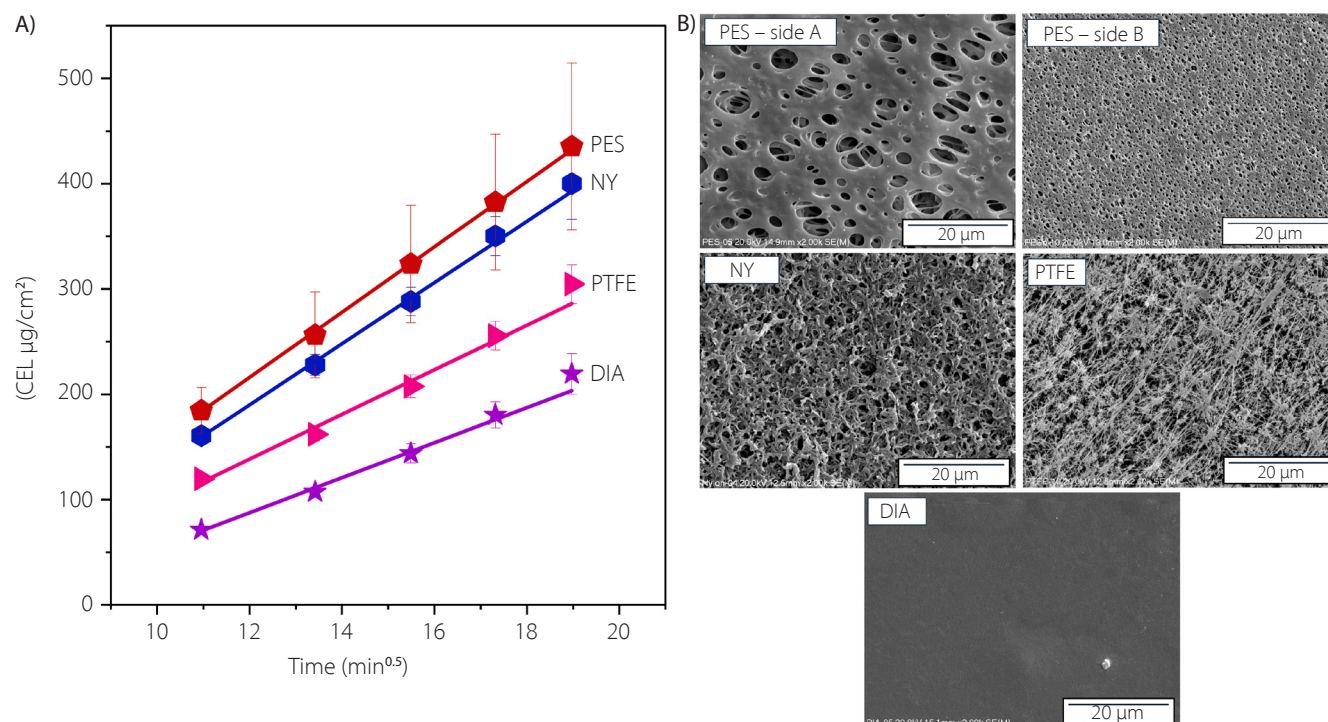


Fig. 4. A. Impact of artificial membrane on celecoxib (CEL) release from Lekobaza. Cumulative amount of CEL released is presented compared to the square root of time. Mean \pm standard deviation (SD) ($n = 3$). Solid lines show linear fit; B. Images of synthetic membrane surface captured using a scanning electron microscope (Hitachi S-4700; Hitachi, Tokyo, Japan; $\times 2000$ magnification)

PES – polyethersulfone; NY – nylon; PTFE – polytetrafluoroethylene; DIA – dialysis membrane.

selected to evaluate the performance of CEL in various semisolid matrices.

Impact of semisolid matrix on CEL release

In Fig. 5, the cumulative amount of CEL released from the developed semisolid formulations is plotted against the square root of time. The slope of this line represents the drug release rate (Table 3).¹¹ All formulations exhibited

a linear relationship between the amount of drug released and the square root of time, with correlation coefficients exceeding 0.98. This confirms that CEL release follows the Higuchi model, indicating that the release process is diffusion-controlled. After 6 h, the highest amount of CEL

Table 3. Linear regression parameters calculated from celecoxib (CEL) release profiles

Variable		Slope ($\mu\text{g}/\text{cm}^2/\text{min}^{-0.5}$)	SD	r^2
Membrane	PES	31.00	0.44	0.9994
	NY	29.03	0.70	0.9983
	PTFE	21.18	1.48	0.9856
	DIA	16.62	0.90	0.9912
Semisolid matrix	Celugel	47.71	3.37	0.9852
	Lekobaza	29.03	0.70	0.9983
	Lekobaza Lux	15.99	0.17	0.9997
	Oleogel	0.62	0.02	0.9977

SD – standard deviation; r^2 – coefficient of determination; PES – polyethersulfone; NY – nylon; PTFE – polytetrafluoroethylene; DIA – dialysis membrane.

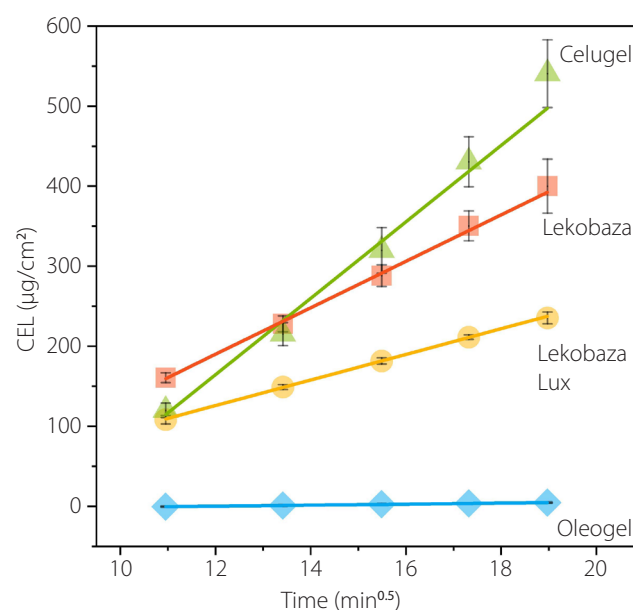


Fig. 5. Cumulative amount of celecoxib (CEL) released from semisolid formulations compared to square root of time. Mean \pm standard deviation (SD) ($n = 3$). Solid lines show linear fit

was released from the hydrophilic Celugel ($540.5 \pm 42.3 \mu\text{g}/\text{cm}^2$), followed by the amphiphilic Lekobaza ($399.9 \pm 33.8 \mu\text{g}/\text{cm}^2$). The CEL release from the lipophilic Lekobaza Lux ($235.3 \pm 7.3 \mu\text{g}/\text{cm}^2$) was nearly half that of the release from Lekobaza. When the CEL suspension in a lipophilic Oleogel matrix was studied, the amount of CEL released remained very low, even after 6 h of testing ($4.6 \pm 0.5 \mu\text{g}/\text{cm}^2$), which was more than 100 times lower compared to Celugel. These results were reflected in the slope values, which followed this order: Celugel > Lekobaza >> Lekobaza Lux >>> Oleogel. This clearly indicates that the drug's affinity to the semisolid matrix and the receptor solution governs the kinetics of CEL partitioning. Since CEL is a lipophilic drug ($\log P = 3.53$), it has a strong affinity for lipophilic vehicles, resulting in slower release rates as the lipophilicity of the matrix increases, especially when a hydrophilic receptor solution is used. Similar findings were reported by Shah et al.,¹⁵ who optimized the IVRT conditions for hydrocortisone ($\log P = 1.61$) using phosphate buffers as receptor solutions. They showed that the IVRT results correlated well with the pharmacokinetics and pharmacodynamic response when hydrophilic semisolid matrices (e.g., lotions, creams) were used as drug vehicles. However, when hydrocortisone was incorporated into a lipophilic matrix, its diffusion to the receptor solution was highly limited, and this did not correlate with the in vivo performance of the drug. To address this challenge, the authors demonstrated that saturating the synthetic membrane with a 15% solution of ethoxylated aliphatic amine in isopropyl myristate (mimicking the lipids of the skin) was critical to enhance the miscibility of the receptor solution with the matrix components. This approach led to reliable in vitro results that better reflected the in vivo performance of the drug when topical oily vehicles were used.¹⁵ In the present study, Oleogel was the most lipophilic semisolid matrix among the tested vehicles. This vehicle is immiscible with the receptor solution, which could hinder the partitioning of CEL between the matrix and the receptor solution, especially when separated by a hydrophilic synthetic membrane. A similar observation can be made for CEL release from Lekobaza Lux (lipophilic cream). The release rate was approximately twice as slow compared to when the amphiphilic cream, Lekobaza, was used.

However, the advantages of using hydrophilic matrices, such as emulgels or hydrogels, over lipophilic ointments for the cutaneous delivery of the non-steroidal anti-inflammatory drug diclofenac sodium were demonstrated by Manian et al.¹³ Diclofenac sodium, with a similar $\log P$ of 4.26 to CEL, is sparingly soluble in water, in contrast to the practically insoluble CEL. The authors found that the release rate of diclofenac sodium was the fastest from the hydrogel and the slowest from the ointment. Similar to our approach, they did not saturate the synthetic membranes with isopropyl myristate. Interestingly, their IVPT studies on human skin provided evidence that the drug permeability was greatest from the emulgel, followed

by the emulsion and the hydrogel. Notably, there was no permeation of the drug from the ointment.

These results suggest that hydrophilic vehicles, which are non-greasy and thus more acceptable to patients, could be more favorable than lipophilic matrices for topical CEL delivery. A proper design of IVRT, including the saturation of the synthetic membrane with a solvent mimicking skin lipids, seems crucial when analyzing lipophilic matrices in order to obtain reliable in vivo performance insights into the performance of poorly soluble drugs based on in vitro results. This approach will be explored in detail in our future studies.

Limitations

Taking into account the variety of new indications for celecoxib, e.g. oncological therapy, psoriasis treatment or its antimicrobial activity, the use of semisolid carriers that differ a lot in properties is proposed. However, comparing in vitro is challenging, and does not always reflect the ease of administration or therapeutic effects observed upon topical treatment. Among others, this applies to release studies (IVRT), where a design of the test in terms of the kind of a diffusion chamber, an artificial membrane, a contact area or a receptor solution can have an impact on the final results, and therefore; its combination with IVPT, microscopy and spectroscopy is necessary to better characterize in vitro a new semisolid product.

Conclusions

The choice of semisolid matrix significantly influences the spreadability, rheology and release rate of suspended CEL. Among the developed formulations, the greatest spreadability was observed when Lekobaza was used, while Oleogel exhibited the smallest spreadability. Rheological measurements indicated that all samples exhibited non-Newtonian fluid characteristics with shear-thinning properties. The comparison of oscillation frequency sweep profiles revealed that the viscous component predominated only when Celugel was used as a vehicle. When CEL was suspended in Oleogel, Lekobaza or Lekobaza Lux, the elastic properties prevailed. Despite the differences in the viscoelastic properties of the developed formulations, all of them exhibited rheological properties suitable for topical administration. The low $\tan \delta$ values typical of Oleogel, Lekobaza and Lekobaza Lux suggest their high long-term stability. The rheology and lipophilicity of the matrix influenced the CEL release rate. The drug was released rapidly from the hydrophilic Celugel matrix, which exhibited viscous liquid characteristics. However, when the formulation made with Oleogel was tested, the lack of miscibility between the matrix and the receptor solution likely hindered drug diffusion. Therefore, the design of the IVRT test, particularly for poorly soluble drugs, should ensure optimal

miscibility between matrix components and the receptor solution. The IVRT study design outlined in this research appears to be the most suitable for evaluating CEL release from hydrophilic matrices. From a clinical perspective, hydrogels are recommended for the treatment of inflammatory skin lesions with exudate, making Celugel a suitable vehicle for CEL. However, if there is a risk of skin drying due to chronic treatment, the formulation of CEL in Lekobaza cream appears to be the better option. This is particularly relevant as the high spreadability of CEL suspended in Lekobaza makes it ideal for application over large skin surfaces.

Data availability

The datasets generated and/or analyzed during the current study are available from the corresponding author on reasonable request.

Consent for publication

Not applicable.

Use of AI and AI-assisted technologies

Not applicable.

ORCID iDs

Urszula Bąk-Kuchejda  <https://orcid.org/0000-0003-0105-1419>
 Teresa Witczak  <https://orcid.org/0000-0002-4860-9718>
 Mariusz Witczak  <https://orcid.org/0000-0003-2942-8396>
 Anna Krupa  <https://orcid.org/0000-0002-0603-512X>

References

- Cohen B, Preuss CV. Celecoxib. In: *StatPearls*. Treasure Island, USA: StatPearls Publishing; 2025:Bookshelf ID: NBK535359. <http://www.ncbi.nlm.nih.gov/books/NBK535359/>. Accessed June 4, 2025.
- U.S. Food and Drug Administration (FDA). Drug Approval Package: ELYXB. Silver Spring, USA: U.S. Food and Drug Administration (FDA); 2020. https://www.accessdata.fda.gov/drugsatfda_docs/nda/2020/212157Orig1s000TOC.cfm. Accessed March 11, 2025.
- U.S. Food and Drug Administration (FDA). Elyxyb [package insert] Palo Alto, CA: SCILEX Pharmaceuticals Inc. Silver Spring, USA: U.S. Food and Drug Administration (FDA); 2020. https://www.accessdata.fda.gov/drugsatfda_docs/label/2024/212157s003lbl.pdf. Accessed March 11, 2025.
- Nițescu DAM, Păunescu H, Ștefan AE, et al. Anti-psoriasis effect of diclofenac and celecoxib using the tail model for psoriasis. *Pharmaceutics*. 2022;14(4):885. doi:10.3390/pharmaceutics14040885
- Nitescu DAM, Paunescu H, Gologan D, Mihael A, Stoian AC, Coman OA. The effect of topical celecoxib as an anti-psoriasis agent. *Maedica (Bucur)*. 2022;17(4):805–811. doi:10.26574/maedica.2022.17.4.805
- Shayeganmehr D, Ramezannia F, Gharib B, et al. Pharmaceutical and clinical studies of celecoxib topical hydrogel for management of chemotherapy-induced hand-foot syndrome. *Naunyn-Schmiedeberg's Arch Pharmacol*. 2023;396(7):1571–1581. doi:10.1007/s00210-022-02339-8
- Neelon J, Yau I, Carlsson AH, et al. Topical application of anti-inflammatory agents on burn wounds and their effect on healing. *Burns*. 2024;50(9):107290. doi:10.1016/j.burns.2024.107290
- Thangamani S, Younis W, Seleem MN. Repurposing celecoxib as a topical antimicrobial agent. *Front Microbiol*. 2015;6:750. doi:10.3389/fmicb.2015.00750
- Volontè P, Musazzi UM, Arnaboldi L, et al. Equivalence assessment of creams with qualitative differences in light of the EMA and FDA regulatory framework. *Eur J Pharm Sci*. 2024;195:106726. doi:10.1016/j.ejps.2024.106726
- Esper M, Hernández MJ, Sanz T, Salvador A. Rheological properties of emulsion templated oleogels based on xanthan gum and different structuring agents. *Curr Res Food Sci*. 2022;5:564–570. doi:10.1016/j.crfs.2022.03.001
- United States Pharmacopoeia – National Formulary (USP-NF). General Chapter (1724). Semisolid Drug Products: Performance Tests. USP-NF. In: Rockville, USA: United States Pharmacopoeia (USP); 2023. doi:10.31003/USPNF_M5695_01_01
- Adeyeye MC, Jain AC, Ghorab MKM, Reilly WJ. Viscoelastic evaluation of topical creams containing microcrystalline cellulose/sodium carboxymethyl cellulose as stabilizer. *AAPS PharmSciTech*. 2002;3(2):16–25. doi:10.1208/pt030208
- Manian M, Jain P, Vora D, Banga AK. Formulation and evaluation of the in vitro performance of topical dermatological products containing diclofenac sodium. *Pharmaceutics*. 2022;14(9):1892. doi:10.3390/pharmaceutics14091892
- U.S. Food and Drug Administration (FDA). In Vitro Release Test Studies for Topical Drug Products Submitted in ANDAs. Silver Spring, USA: U.S. Food and Drug Administration (FDA); 2022. <https://www.fda.gov/drugs/guidance-compliance-regulatory-information/guidances-drugs>. Accessed March 11, 2025.
- Shah VP, Elkins J, Hanus J, Noorizadeh C, Skelly JP. In vitro release of hydrocortisone from topical preparations and automated procedure. *Pharm Res*. 1991;8(1):55–59. doi:10.1023/a:1015826205930

Applications of biomaterials in reconstructive gynecology

Zastosowanie biomateriałów w ginekologii rekonstrukcyjnej

Radosław Blok^{1,D,F}, Grzegorz Myszczyński^{1,D,F}, Artur Wiatrowski^{1,A,B,E,F}, Marek Tomiałowicz^{1,B,C,E,F}, Maria Pomorska^{2,C,E,F}, Jerzy Florjanski^{1,A,F}

¹ University Center for Obstetrics and Gynecology, Wrocław Medical University, Poland

² Department and Clinic of Ophthalmology, Wrocław Medical University, Poland

A – research concept and design; B – collection and/or assembly of data; C – data analysis and interpretation;

D – writing the article; E – critical revision of the article; F – final approval of the article

Polymers in Medicine, ISSN 0370-0747, eISSN 2451-2699

Polim Med. 2025;55(1):59–65

Address for correspondence

Maria Pomorska

E-mail: maria.pomorska@umw.edu.pl

Funding sources

None declared

Conflict of interest

None declared

Received on January 4, 2025

Reviewed on January 29, 2025

Accepted on April 11, 2025

Published online on June 27, 2025

Abstract

This review comprehensively describes the applications of biomaterials in gynecology, focusing on their role in treating gynecological disorders, reconstructive procedures and minimally invasive surgeries. It highlights the latest advancements, such as biocompatibility, innovative implants and biodegradable materials. This article also provides information about biomaterials used for vaginal and pelvic wall reconstruction in pelvic organ prolapse patients, as well as its use in minimally invasive surgical procedures and infertility treatment (including assisted reproductive technologies (ART)). The application of biomaterials in gynecological oncology is also discussed, as biomaterials – particularly those incorporating nanotechnology – enable selective drug delivery and targeted cancer therapy.

We highlight the current clinical challenges and unmet needs while offering a forward-looking perspective on the potential of biomaterials in advancing regenerative medicine, personalized treatments and improving outcomes for women's health. We aim to provide some directions for future research and the development of novel biomaterials that can improve gynecological care.

Key words: biomaterials, regeneration, gynecology, implantation

Streszczenie

W pracy przeglądowej opisano zastosowania biomateriałów w ginekologii, ze szczególnym uwzględnieniem ich roli w leczeniu schorzeń ginekologicznych, procedurach rekonstrukcyjnych i operacjach małoinwazyjnych. W artykule przedstawiono informacje na temat biomateriałów stosowanych do rekonstrukcji ścian pochwy i miednicy u pacjentek z obniżeniem/wypadaniem narządów płciowych, a także ich zastosowania w małoinwazyjnych zabiegach chirurgicznych oraz w leczeniu niepłodności (w tym technologiach wspomaganego rozrodu). Omówiono także zastosowanie biomateriałów w onkologii ginekologicznej, ponieważ biomateriały umożliwiają selektywne dostarczanie leków i ukierunkowaną terapię przeciwnowotworową przy zastosowaniu biomateriału opartego na nanotechnologii. Artykuł podkreśla najnowsze osiągnięcia, takie jak biokompatybilność, innowacyjne implanty i materiały biodegradowalne, a także przedstawia obecne wyzwania w zastosowaniu klinicznym biomateriałów oraz potencjalne przyszłe możliwości ich zastosowania w medycynie rekonstrukcyjnej i spersonalizowanych metodach leczenia. Naszym celem było wskazanie kierunków przyszłych badań i rozwoju nowych biomateriałów, które mogą poprawić skuteczność leczenia w ginekologii.

Słowa kluczowe: biomateriały, ginekologia, regeneracja, implanty

Cite as

Blok R, Myszczyński G, Wiatrowski A, Tomiałowicz M, Pomorska M, Florjanski J. Applications of biomaterials in reconstructive gynecology. *Polim Med.* 2025;55(1):59–65. doi:10.17219/pim/203964

DOI

10.17219/pim/203964

Copyright

Copyright by Author(s)

This is an article distributed under the terms of the Creative Commons Attribution 3.0 Unported (CC BY 3.0) (<https://creativecommons.org/licenses/by/3.0/>)

Introduction

Biomaterials play a fundamental role in contemporary medicine, enabling the treatment of disorders and supporting tissue regeneration. Their wide range of applications includes surgical procedures, reconstructive interventions, minimally invasive approaches, and combined cancer therapies. The development of biomaterials is grounded in advanced knowledge of biology, chemistry and materials science, allowing for the design of materials with specific properties such as biocompatibility, mechanical strength and biodegradability. The use of biomaterials in gynecology dates back to the 1960s, when synthetic materials were first introduced for the treatment of gynecological disorders. Early implants made from metals or polymers often triggered immune reactions and complications. Advances in technology have since enabled the creation of biomaterials that better mimic natural tissues, becoming increasingly biocompatible and safe for patients.¹

Modern biomaterials used in gynecology can be categorized into the following groups:

- Synthetic polymers (e.g., polycaprolactone, polylactide): used in implants and biodegradable structures;
- Natural materials (e.g., collagen, elastin): ideal for tissue regeneration due to high compatibility with human tissues;
- Composite materials: combining the properties of synthetic and natural components for greater application flexibility.

The introduction of biomaterials into gynecological practice has significantly enhanced treatment effectiveness and patient comfort. Notable applications include: 1) synthetic surgical sutures replacing natural materials; 2) mesh implants for treating hernias, such as pelvic floor disorders in women; and 3) drug delivery systems, including biodegradable implants for hormone or chemotherapy drug release.

As research and technology progress, biomaterials in gynecology are becoming more advanced and accessible, opening new therapeutic possibilities.^{2,3}

Biocompatibility and biodegradability

Biocompatibility and biodegradability are 2 critical aspects of biomaterials in gynecology, determining their efficacy and safety. Biocompatibility refers to a material's ability to coexist with human tissues without causing adverse reactions such as inflammation, rejection or scarring. Biodegradability refers to a material's ability to break down within the body into metabolizable and excretable byproducts, thereby eliminating the need for surgical removal.⁴ Biocompatible biomaterials must meet several criteria, including:

- Biological neutrality, preventing immune responses;
- Adequate mechanical strength to provide structural stability during tissue regeneration;

- Chemical safety, ensuring no toxic degradation products.

Materials like polymer meshes and collagen implants in gynecology are designed to support tissue regeneration while minimizing infection risks.⁵ Biodegradable materials have found various and extensive applications in gynecology due to their ability to be absorbed by tissues after fulfilling their function. We can include the following examples:

- Polycaprolactone (PCL) is frequently used in implants for pelvic floor reconstruction;
- Polylactide (PLA) is mostly utilized in drug delivery systems and surgical meshes that degrade over time;
- Collagen and gelatin, which are natural polymers used in membranes that aid wound healing following gynecological procedures.

The biodegradability of these materials is particularly valuable in procedures requiring temporary mechanical support or precise drug release over time. Challenges in this field include controlling the degradation rate and preventing adverse biological reactions. Examples of widely used long-term drug delivery systems are implants and intrauterine devices releasing synthetic progesterone derivatives over 3–7 years.^{5,6}

Biomaterials used for vaginal and pelvic wall reconstruction

Biomaterials used in reconstructive surgery of the vaginal and pelvic walls can be classified into synthetic, biological and composite materials.⁷ Most frequently, biomaterials are used in pelvic floor dysfunction,^{3,8,9} and transvaginal mesh repair.³ Synthetic materials, such as polypropylene meshes, are widely used due to their mechanical strength and durability. Biological materials, such as human- or animal-derived collagen matrices (allografts and xenografts), offer superior biocompatibility and can enhance the immune response through stimulation of cytokine release and activation of immune cells.¹⁰ Composite materials combine the benefits of both synthetic and biological components to enhance biocompatibility while maintaining structural integrity. The available studies indicated that graft synthetic and biological materials could be efficiently used in pelvic reconstruction. Jeon and Bai categorized synthetic grafts into absorbable and non-absorbable types and further divided them into 4 subgroups based on their physical characteristics. In contrast, biological grafts are classified into 3 categories: autologous grafts (e.g., rectus fascia, fascia lata, vaginal mucosa), allografts (e.g., cadaveric fascia lata, dermis) and xenografts (e.g., porcine dermis, small intestinal submucosa).¹¹ Another interesting approach is to combine drug release and biomaterials. Mangır et al.¹² indicated in their research that polypropylene meshes used in pelvic floor repair may lead to severe complications. Accordingly, the authors emphasized the need for biomechanically compatible alternatives. Their study developed an estradiol-releasing electrospun PLA mesh to enhance extracellular matrix (ECM) production and angiogenesis.

Polylactic acid meshes contained varying concentrations of estradiol, and were tested in vitro and in vivo, indicating sustained estradiol release over 4 months. Finally, it was observed that the meshes promoted ECM production, including collagen I, collagen III and elastin, and doubled angiogenesis in chick models. These findings suggest that estradiol-releasing PLA meshes are promising candidates for pelvic floor repair, warranting further investigation in advanced animal models.¹² Table 1 shows the possible biomaterials used in pelvic therapy.^{7,13,14}

Despite the growing utility of biomaterials, their clinical use still presents challenges such as erosion, infection and chronic pain. These complications are well documented for polypropylene meshes, as they are the most commonly used synthetic materials in pelvic organ prolapse surgery. The occurrence rate of polypropylene mesh-related complications currently ranges from 5% to 29%. The U.S. Food and Drug Administration (FDA) has issued multiple warnings regarding the use of polypropylene mesh in pelvic organ prolapse surgery and, in 2019, officially ordered the cessation of sales of surgical mesh devices for transvaginal prolapse repair in the USA.

The underlying cause of mesh-related complications, such as erosion, infection and pain, is the tissue inflammatory response to mesh implantation. It was previously believed that the peak inflammatory response to polypropylene mesh occurs within 24–48 h after implantation, followed by a continuous decline. However, recent studies have revealed that polypropylene degradation over time promotes a persistent inflammatory response, primarily driven by neutrophil granulocytes, T-lymphocytes, and both M1 and M2 macrophages.^{15,16} Additionally, mesh degradation leads to the formation of microcracks on its surface, which favors the development of bacterial biofilms, as the mesh can be easily contaminated by vaginal microbiota. As polypropylene mesh degradation progresses over time following implantation, the local inflammatory response also intensifies, contributing to a higher incidence and severity of mesh-related complications.

Despite these risks, modern innovations, such as coated or resorbable meshes, have improved outcomes by reducing adverse effects. Future research focuses on developing bioactive materials that promote tissue regeneration and reduce complications. Recent studies suggest that patient-specific approaches may further enhance the effectiveness of biomaterials in reconstructive surgery.^{9,11,17}

Treatment and prevention of pelvic organ prolapse

As previously mentioned, biomaterials play a crucial role in providing structural support to weakened pelvic tissues, particularly in cases of pelvic organ prolapse (POP). Currently, polypropylene meshes are commonly used for surgical interventions,¹⁸ while bioengineered scaffolds and absorbable meshes are gaining attention for their reduced risk profiles. However, improved materials such as electrospun nanofibers¹⁹ and hydrogels,²⁰ offer promising alternatives for POP repair. The most important aspect of biomaterial use in POP surgery is risk prediction, particularly concerning complications such as erosion, mesh exposure and infection. Emerging strategies include the use of bioresorbable materials and tissue-engineered scaffolds that integrate with native tissues to mitigate complications. Current research emphasizes optimizing material properties such as elasticity, porosity and biocompatibility to enhance outcomes.^{21,22}

Minimally invasive surgery

In recent years, biomaterials have also been increasingly used in laparoscopic and endoscopic procedures. Such techniques, called minimally invasive gynecological procedures,²³ benefit from advanced biomaterials such as biodegradable polymers, hydrogels and lightweight meshes.¹³ These materials reduce scarring, promote healing and enhance surgical precision. Examples include absorbable fixation devices and bioadhesive materials for tissue approximation.⁹ It was noticed that biomaterials play a significant role in reducing the invasiveness of gynecological procedures. Biomaterials help reduce procedure invasiveness by promoting faster healing and minimizing postoperative complications. One study exemplified this by successfully treating Fallopian tube obstructions, a common cause of infertility, using a novel self-expandable biodegradable microstent. The authors fabricated the microstent from PLA using femtosecond laser cutting, achieving an outer diameter of 2.3 mm and precise strut dimensions of 114 µm in thickness and 103 µm in width. As was indicated, mechanical tests confirmed its ability to crimp to 0.8 mm and recover to 1.8 mm upon release, demonstrating its self-expanding properties. This proof-of-concept revealed the potential of microstent technology as a minimally

Table 1. Overview of biomaterials used in gynecological applications^{7,13,14}

Type of biomaterial	Examples	Applications	Advantages	Challenges
Synthetic	polypropylene, polyester	vaginal mesh, pelvic organ support	high durability, cost-effective	risk of erosion, infection, rejection
Biological	collagen, allografts	pelvic floor repair, prolapse repair	biocompatibility, tissue integration	limited availability, higher cost
Composite	hybrid meshes	pelvic reconstruction	improved integration and strength	complex manufacturing

invasive solution to restore the natural lumen of the Fallopian tube, offering a promising therapeutic option for infertility treatment.²⁴

Hydrogels, for instance, are used for adhesion prevention in laparoscopy, while shape-memory polymers called “smart” materials enable precise tissue reconstruction.²⁵ Tang et al. evaluated a shape memory polymer (SMP) device for Fallopian tube occlusion in a rabbit model. The device, made of poly(dl-lactic acid)-based poly(urethane urea), is a spiral-shaped cylinder that reverts to its permanent shape within 60 s at 37°C. Authors implanted their polymer in 48 rabbits. As observed, the SMP device induced aseptic inflammatory reactions and achieved complete Fallopian tube occlusion in all cases, with no resulting pregnancies. Additionally, SMP device demonstrated progressive biodegradation. This research demonstrates biodegradable and biocompatible potential of SMP devices as a possible permanent contraceptive solution.²⁶ Future innovations in this field aim to integrate nanotechnology and drug-eluting systems into surgical biomaterials.^{27–29}

Infertility treatment and assisted reproductive technologies

Biomaterials are increasingly used in assisted reproductive technologies (ART) to enhance embryo implantation and improve pregnancy outcomes. Examples include biodegradable scaffolds for endometrial regeneration, hydrogels for embryo culture and bioactive coatings for embryo transfer catheter.^{30,31}

As is known, the endometrium plays a crucial role in embryo development and pregnancy. Lin et al. used human umbilical cord mesenchymal stem cells (HUCMSCs), known for their rapid self-renewal and painless collection, in combination with spermidine (SN), a polyamine essential for cellular function, demonstrating promising potential in the repair of intrauterine adhesions. Authors explored the potential of hydrogel-loaded exosomes derived from HUCMSCs and spermidine to improve conception rates in mice model with thin endometrial lining. The obtained results revealed that HUCMS cells and SN enhanced endometrial function, with hydrogel-incorporated exosomes showing potential for intrauterine treatment and improving pregnancy outcomes.³² In another study, ECM hydrogels derived from decellularized tissues were applied for endometrial regeneration, offering potential therapeutic benefits for conditions such as Asherman's syndrome and endometrial atrophy. A proteomic analysis of porcine endometrial ECM hydrogels (EndoECM) was performed, revealing a significant presence of proteins essential for tissue repair. Authors used murine model of endometrial damage, and treated animals with EndoECM supplemented with growth factors (GFs). Improved regeneration was observed, marked by increased gland formation, cell proliferation, angiogenesis, and pregnancy rates, along with reduced collagen deposition. These findings

highlight bioengineered EndoECM hydrogels with GFs as a promising therapeutic option for endometrial-related infertility.³³

The female reproductive system is strongly dependent on the precise hormonal and uterine coordination to support implantation and fetal development, with pathologies in any organ or process potentially compromising fertility. Thus, there are potential benefits of biomaterials in embryo implantation and development, e.g., advanced biomaterials can mimic the ECM, improving the interaction between embryos and the uterine lining. The available studies highlight the role of nanofibers and growth-factor-laden hydrogels in creating an optimal microenvironment for implantation.^{27,28}

Gynecological oncology

Biomaterials are used not only for regeneration in gynecology but also in treating cervical, ovarian and other gynecological cancers. In this field, biomaterials are used mainly for drug delivery, tissue reconstruction and targeted therapy. Examples include nanoparticle-based carriers for chemotherapeutics, injectable hydrogels for localized drug release and scaffolds for reconstructive surgery.^{28,34–36}

Biomaterials enable selective drug delivery and targeted cancer therapy through the application of nanotechnology-based systems, such as liposomes and dendrimers, which allow for the precise delivery of anticancer drugs while minimizing systemic toxicity. Stimuli-responsive materials offer targeted therapies triggered by pH or temperature changes within the tumor microenvironment.³⁷ Ovarian cancer's high mortality necessitates innovative treatment strategies, including natural compound-based therapies. Thus, researchers continue to develop more promising nanocarriers to transport drug molecules more effectively. The recent study examined the anticancer effects of resveratrol (RSV)- and curcumin (CUR)-loaded in newly developed core-shell nanoparticles in ovarian cancer cell lines model (MDAH-2774, SKOV-3). Authors observed that RSV-loaded systems showed limited cytotoxicity, but CUR-loaded nanoparticles significantly reduced cell viability, with MDAH-2774 cells being more sensitive. Moreover, confocal microscopy showed enhanced cellular uptake and mitochondrial localization of CUR. These results underscore the potential of CUR-loaded nanoparticles for ovarian cancer treatment, warranting further investigation into their biological effects.³⁸ Another major challenge in ovarian cancer is the phenomenon of drug resistance, which is associated with mechanisms such as efflux transporters, apoptosis dysregulation, autophagy, and the presence of cancer stem cells. Multi-drug resistance (MDR) occurs in more than half of patients. Currently, the first-line treatments include the combination of surgery and chemotherapy, which is not effective against drug-resistant cancer in long-term therapies. One study developed an innovative nanotechnology-based targeted drug delivery system,

where hyaluronic acid-modified gold nanorods were used for functionalization of mesoporous silica nanoparticles (HA-PTX/let-7a-GNR@MSN) to deliver paclitaxel (PTX) and the microRNA let-7a. This new nanosystem specifically targeted CD44 receptors on drug-resistant SKOV3TR human ovarian cancer cells. An enhancement in tumor permeability by 150% was observed, along with effective delivery of therapeutic agents. In terms of MDR phenomenon, the results revealed a significant P-glycoprotein down-regulation, induction of apoptosis and inhibition of tumor growth, with mTOR-mediated pathways identified as key mechanisms in reversing drug resistance. Consequently, these nanoparticles demonstrated a promising strategy for overcoming MDR and improving ovarian cancer therapy.³⁹ Another promising technology worth developing is theranostic nanosystems, which combine both therapeutic and diagnostic capabilities, enabling a more efficient anticancer effect.⁴⁰ Emerging targets such as MUC16/MSLN and FOLR1 have been reported, showing promising effects in enhancing the personalization of ovarian cancer treatment. For instance, MUC16/MSLN interactions activate survival pathways in cancer cells, but anti-MSLN antibodies and engineered CAR-T cells effectively reverse these effects. Remarkably, FOLR1-targeted therapies, including ADCs and CAR-CIK cells, have proved a significant anti-tumor activity in preclinical and clinical studies. Other biomarkers, such as CHI3L1, nectin-4, CXCR4, and STAT3, also offered potential theranostic applications through targeted therapies and molecular profiling. These strategies highlight the potential for personalized, biomarker-driven approaches to ovarian cancer diagnosis and treatment, paving the way for improved outcomes.^{41,42} In summary, targeted nanoparticle-based delivery systems, including lipid, polymeric and inorganic nanoparticles, are designed to enhance specificity and efficacy in overcoming drug resistance, improve therapeutic outcomes and simultaneously serve as diagnostic tools in ovarian cancer.^{42,43}

Future perspectives on biomaterials in gynecology

Recent developments in biomaterials, including stem cell-laden scaffolds and bioactive hydrogels, have shown promising effects in regenerating endometrial tissue and repairing gynecological damage. These biocompatible materials support cell proliferation, angiogenesis and tissue integration.^{19,32} Another promising direction for development is tissue engineering involving 3D bioprinting and bioactive scaffolds to create personalized regenerative solutions. For instance, there are currently developed biomaterials that release growth factors to enhance the repair of damaged uterine tissues, offering potential treatments for conditions such as Asherman's syndrome.^{33,36} Another challenging issue is ovarian aging, characterized by the progressive decline of ovarian function with advancing age.

Biomaterial-based solutions can serve as a promising way in ovarian aging (OA). Ovarian aging involves a complex interplay of genetic, environmental and molecular factors, with several biomarkers, such as AMH, estrogen and follicle-stimulating hormone (FSH), serving as indicators of ovarian function. Biomaterials like extracellular vesicles, synthetic polymers and 3D scaffolds show the ability for development of artificial ovaries, enhancing follicular development and delivering therapeutic agents.⁴⁴ However, despite advancements, challenges are still present in clinical translation, including safety concerns, regulatory barriers and limited large-scale studies. Future perspectives should focus on integrating innovative biomaterials with advanced diagnostics like machine learning^{45,46} and molecular imaging to enhance early detection and treatment efficacy, and demonstrate full potential in gynecology.

Biomaterials in magnetic resonance imaging

The most commonly used biomaterials in pelvic organ prolapse surgery are polypropylene meshes. Polypropylene is a non-ferromagnetic material and therefore does not pose significant risks to patients in terms of heating, magnetic attraction or image distortion during magnetic resonance imaging (MRI) scans. As a non-ferromagnetic material, polypropylene implants typically do not produce significant artifacts in MRI scans. However, some implants may contain additives, such as metallic traces, which can cause mild artifacts. Additionally, the shape and size of polypropylene implants may contribute to local image distortions.

Regarding the visualization of polypropylene implants using MRI, polypropylene-based meshes do not interact with the MRI signal and therefore typically appear as areas of low signal intensity on MRI images. This can lead to difficulties in visualization of the implants, especially when the imaging focus is on the surrounding tissues.

In conclusion, polypropylene-based meshes used in pelvic organ prolapse surgery are MRI-compatible; however, mild imaging artifacts and difficulties in implant visualization may still occur.

Conclusions

Our review highlights significant developments in the applications of biomaterials for gynecological procedures, with a focus on minimally invasive surgeries, infertility treatments and gynecological oncology. As indicated, in minimally invasive procedures, biomaterials such as hydrogels and SMP show great potential for treating conditions like Fallopian tube obstructions and pelvic floor disorders, offering reduced complications and faster recovery times. The development of biodegradable and bioresorbable materials personalized to patient-specific needs is crucial for further improvements of surgical outcomes

while minimizing adverse effects. In the context of infertility treatments, new biomaterials like hydrogel-loaded exosomes and ECM scaffolds are emerging as effective solutions for regenerating damaged uterine tissues and addressing conditions such as endometrial atrophy and intrauterine adhesions. These technologies enhance tissue regeneration and implantation success rates, but more clinical trials are needed to establish their long-term efficacy. In the case of gynecological oncology, nanoparticle-based drug delivery systems provide a promising approach to overcome challenges like MDR and systemic toxicity in ovarian cancer treatments. These systems enable precise targeting of cancer cells, thereby reducing harmful side effects and improving treatment outcomes. In particular, theranostic strategies, combining diagnostic and therapeutic functions, show significant potential for personalized treatment approaches. Table 2 summarizes the applications of biomaterials in gynecology.

It can be stated that integrating biomaterial development with nanotechnology, molecular imaging, and machine learning offers a promising pathway to enhance both diagnostic and therapeutic efficacy in gynecology. However, several challenges remain, including addressing regulatory and safety concerns, ensuring cost-effectiveness and conducting large-scale clinical studies to translate these advancements into routine clinical practice. The findings emphasize the crucial role of biomaterials in advancing gynecological care and the necessity of continued interdisciplinary research to improve and expand their clinical application.

Table 2. Biomaterials in gynecology

Application	Biomaterials used	Benefits	Challenges
Minimally invasive surgery	hydrogels, SMPs	reduced invasiveness, faster healing	managing biodegradation rates
Infertility treatment	ECM scaffolds, hydrogel-loaded exosomes	tissue regeneration, improved implantation	limited clinical trials, cost
Gynecological oncology	nanoparticles, liposomes, ADCs	targeted drug delivery, reduced toxicity	overcoming drug resistance, scalability
Pelvic floor repair	PLA meshes, composite scaffolds	enhanced biocompatibility, tissue integration	risk of erosion, infection

ECM – extracellular matrix; PLA – polylactide; ADCs – antibody-drug conjugates; SMP – shape-memory polymer.

ORCID iDs

Radosław Blok  <https://orcid.org/0000-0002-0996-9454>
 Grzegorz Myszczyński  <https://orcid.org/0000-0002-1754-1140>
 Artur Wiatrowski  <https://orcid.org/0000-0001-6821-8768>
 Maria Pomorska  <https://orcid.org/0000-0001-9163-6343>
 Jerzy Florjanski  <https://orcid.org/0000-0002-4837-7953>

References

- Sadava EE, Krpata DM, Gao Y, Rosen MJ, Novitsky YW. Wound healing process and mediators: Implications for modulations for hernia repair and mesh integration. *J Biomed Mater Res*. 2014;102(1):295–302. doi:10.1002/jbm.a.34676
- Peleg D, Ahmad RS, Warsof SL, Marcus-Braun N, Sciaky-Tamir Y, Ben Shachar I. A randomized clinical trial of knotless barbed suture vs conventional suture for closure of the uterine incision at cesarean delivery. *Am J Obstet Gynecol*. 2018;218(3):343.e1–343.e7. doi:10.1016/j.ajog.2018.01.043
- Kahn B, Varner RE, Murphy M, et al. Transvaginal mesh compared with native tissue repair for pelvic organ prolapse. *Obstet Gynecol*. 2022;139(6):975–985. doi:10.1097/AOG.0000000000004794
- Oztemur J, Ozdemir S, Tezcan-Unlu H, Cecener G, Sezgin H, Yalcin-Enis I. Investigation of biodegradability and cellular activity of PCL/PLA and PCL/PLLA electrospun webs for tissue engineering applications. *Biopolymers*. 2023;114(11):e23564. doi:10.1002/bip.23564
- Wang Y, Wang Z, Dong Y. Collagen-based biomaterials for tissue engineering. *ACS Biomater Sci Eng*. 2023;9(3):1132–1150. doi:10.1021/acsbomaterials.2c00730
- Bahamondes L, Fernandes A, Monteiro I, Bahamondes MV. Long-acting reversible contraceptive (LARCs) methods. *Best Pract Res Clin Obstet Gynaecol*. 2020;66:28–40. doi:10.1016/j.bpobgyn.2019.12.002
- Ratner BD, Zhang G. A history of biomaterials. In: Wagner WR, Sakiyama-Elbert SE, Zhang G, Yaszemski MJ, eds. *Biomaterials Science: An Introduction to Materials in Medicine*. 4th ed. San Diego, USA: Academic Press (Elsevier Science & Technology); 2020:21–34. ISBN:978-0-12-816137-1, 978-0-12-816138-8.
- Wu X, Jia Y, Sun X, Wang J. Tissue engineering in female pelvic floor reconstruction. *Eng Life Sci*. 2020;20(7):275–286. doi:10.1002/elsc.202000003
- Gigliobianco G, Roman Regueros S, Osman NI, et al. Biomaterials for pelvic floor reconstructive surgery: How can we do better? *Biomed Res Int*. 2015;2015:968087. doi:10.1155/2015/968087
- Tripathi AS, Zaki MEA, Al-Hussain SA, et al. Material matters: Exploring the interplay between natural biomaterials and host immune system. *Front Immunol*. 2023;14:1269960. doi:10.3389/fimmu.2023.1269960
- Jeon MJ, Bai SW. Use of grafts in pelvic reconstructive surgery. *Yonsei Med J*. 2007;48(2):147. doi:10.3349/ymj.2007.48.2.147
- Mangir N, Hillary CJ, Chapple CR, MacNeil S. Oestradiol-releasing biodegradable mesh stimulates collagen production and angiogenesis: An approach to improving biomaterial integration in pelvic floor repair. *Eur Urol Focus*. 2019;5(2):280–289. doi:10.1016/j.euf.2017.05.004
- Jummaat F, Yahya EB, Khalil HP, et al. The role of biopolymer-based materials in obstetrics and gynecology applications: A review. *Polymers (Basel)*. 2021;13(4):633. doi:10.3390/polym13040633
- Swingle KL, Ricciardi AS, Perantau WH, Mitchell MJ. Delivery technologies for women's health applications. *Nat Rev Bioeng*. 2023;1(6):408–425. doi:10.1038/s44222-023-00040-w
- Dievernich A, Achenbach P, Davies L, Klinge U. Characterization of innate and adaptive immune cells involved in the foreign body reaction to polypropylene meshes in the human abdomen. *Hernia*. 2022;26(1):309–323. doi:10.1007/s10029-021-02396-7
- Wang H, Klosterhalfen B, Klinge U, Müllen A, Jockenhoevel S. Influence of polypropylene mesh degradation on tissue inflammatory reaction. *J Biomed Mater Res*. 2023;111(8):1110–1119. doi:10.1002/jbm.a.37494
- Amid PK, Shulman AG, Lichtenstein IL, Hakakha M. Biomaterials and hernia surgery: Rationale for using them [in Spanish]. *Rev Esp Enferm Dig*. 1995;87(8):582–586. PMID:7577108.
- Seifalian A, Basma Z, Digesu A, Khullar V. Polypropylene pelvic mesh: What went wrong and what will be of the future? *Biomedicine*. 2023;11(3):741. doi:10.3390/biomedicine11030741
- Verhorstert K, Gudde A, Weitsz C, Bezuidenhout D, Roovers JP, Guler Z. Absorbable electrospun poly-4-hydroxybutyrate scaffolds as a potential solution for pelvic organ prolapse surgery. *ACS Appl Bio Mater*. 2022;5(11):5270–5280. doi:10.1021/acsbom.2c00691
- Miller B, Wolfe W, Gentry JL, et al. Supramolecular fibrous hydrogel augmentation of uterosacral ligament suspension for treatment of pelvic organ prolapse. *Adv Healthc Mater*. 2023;12(22):2300086. doi:10.1002/adhm.202300086

21. Hernandez JL, Woodrow KA. Medical applications of porous biomaterials: Features of porosity and tissue-specific implications for biocompatibility. *Adv Healthc Mater.* 2022;11(9):2102087. doi:10.1002/adhm.202102087
22. Tamadon A, Park KH, Kim YY, Kang BC, Ku SY. Efficient biomaterials for tissue engineering of female reproductive organs. *Tissue Eng Regen Med.* 2016;13(5):447–454. doi:10.1007/s13770-016-9107-0
23. Sanna A, Sevas V, Gasparri ML, Farooqi AA, Papadia A. Introductory chapter: Advances in minimally invasive surgery. In: Sanna A, ed. *Advances in Minimally Invasive Surgery*. London, UK: IntechOpen; 2022. doi:10.5772/intechopen.100367
24. Dierke A, Borowski F, Großmann S, et al. Development of a biodegradable microstent for minimally invasive treatment of Fallopian tube occlusions. *Curr Direct Biomed Eng.* 2020;6(3):74–77. doi:10.1515/cdbme-2020-3019
25. Yakacki CM, Gall K. Shape-memory polymers for biomedical applications. In: Lendlein A, ed. *Shape-Memory Polymers*. Vol. 226. *Advances in Polymer Science*. Berlin-Heidelberg, Germany: Springer Berlin Heidelberg; 2009:147–175. doi:10.1007/12_2009_23
26. Tang S, Zhang CY, Huang MN, Luo YF, Liang ZQ. Fallopian tube occlusion with a shape memory polymer device: Evaluation in a rabbit model. *Contraception.* 2013;87(2):235–241. doi:10.1016/j.contraception.2012.07.002
27. Luo X, Jia K, Xing J, Yi J. The utilization of nanotechnology in the female reproductive system and related disorders. *Heliyon.* 2024;10(3):e25477. doi:10.1016/j.heliyon.2024.e25477
28. Lulseged BA, Ramaiyer MS, Michel R, Saad EE, Ozpolat B, Borahay MA. The role of nanomedicine in benign gynecologic disorders. *Molecules.* 2024;29(9):2095. doi:10.3390/molecules29092095
29. Bertozzi S, Corradetti B, Seriau L, et al. Nanotechnologies in obstetrics and cancer during pregnancy: A narrative review. *J Pers Med.* 2022;12(8):1324. doi:10.3390/jpm12081324
30. Francés-Herrero E, Lopez R, Hellström M, et al. Bioengineering trends in female reproduction: A systematic review. *Hum Reprod Update.* 2022;28(6):798–837. doi:10.1093/humupd/dmac025
31. Leonel ECR, Dadashzadeh A, Moghassemi S, et al. New solutions for old problems: How reproductive tissue engineering has been revolutionizing reproductive medicine. *Ann Biomed Eng.* 2023;51(10):2143–2171. doi:10.1007/s10439-023-03321-y
32. Lin X, Fang Y, Mi X, et al. Intrauterine injection of bioengineered hydrogel loaded exosomes derived from HUCM stem cells and spermidine prominently augments the pregnancy rate in thin endometrium rats. *Regen Ther.* 2024;27:63–72. doi:10.1016/j.reth.2024.02.003
33. López-Martínez S, Rodríguez-Eguren A, De Miguel-Gómez L, et al. Bioengineered endometrial hydrogels with growth factors promote tissue regeneration and restore fertility in murine models. *Acta Biomater.* 2021;135:113–125. doi:10.1016/j.actbio.2021.08.025
34. Kramer M, Criswell A, Sewell-Loftin MK. Biomaterial considerations for ovarian cancer models. *Front Mater.* 2023;10:1223276. doi:10.3389/fmats.2023.1223276
35. Cadena I, Chen A, Arvidson A, Fogg KC. Biomaterial strategies to replicate gynecological tissue. *Biomater Sci.* 2021;9(4):1117–1134. doi:10.1039/D0BM01240H
36. Yang Z, Xu H, Zhao X. Designer self-assembling peptide hydrogels to engineer 3D cell microenvironments for cell constructs formation and precise oncology remodeling in ovarian cancer. *Adv Sci (Weinh).* 2020;7(9):1903718. doi:10.1002/advs.201903718
37. Rahim MA, Jan N, Khan S, et al. Recent advancements in stimuli responsive drug delivery platforms for active and passive cancer targeting. *Cancers (Basel).* 2021;13(4):670. doi:10.3390/cancers13040670
38. Weźgowiec J, Łapińska Z, Lamch Ł, et al. Cytotoxic activity of curcumin- and resveratrol-loaded core-shell systems in resistant and sensitive human ovarian cancer cells. *Int J Mol Sci.* 2024;26(1):41. doi:10.3390/ijms26010041
39. Wang X, Xiong T, Cui M, et al. A novel targeted co-delivery nanosystem for enhanced ovarian cancer treatment via multidrug resistance reversion and mTOR-mediated signaling pathway. *J Nanobiotechnol.* 2021;19(1):444. doi:10.1186/s12951-021-01139-1
40. Pantshwa JM, Kondiah PPD, Choonara YE, Marimuthu T, Pillay V. Nanodrug delivery systems for the treatment of ovarian cancer. *Cancers (Basel).* 2020;12(1):213. doi:10.3390/cancers12010213
41. Rajapaksha W, Khetan R, Johnson IRD, et al. Future theranostic strategies: Emerging ovarian cancer biomarkers to bridge the gap between diagnosis and treatment. *Front Drug Deliv.* 2024;4:1339936. doi:10.3389/fddev.2024.1339936
42. Nimmagadda S, Penet MF. Ovarian cancer targeted theranostics. *Front Oncol.* 2020;9:1537. doi:10.3389/fonc.2019.01537
43. Miller EM, Samec TM, Alexander-Bryant AA. Nanoparticle delivery systems to combat drug resistance in ovarian cancer. *Nanomed Nanotechnol Biol Med.* 2021;31:102309. doi:10.1016/j.nano.2020.102309
44. Wu M, Guo Y, Wei S, et al. Biomaterials and advanced technologies for the evaluation and treatment of ovarian aging. *J Nanobiotechnol.* 2022;20(1):374. doi:10.1186/s12951-022-01566-8
45. Wu C, Xu Y, Fang J, Li Q. Machine learning in biomaterials, biomechanics/mechanobiology, and biofabrication: State of the art and perspective. *Arch Computat Methods Eng.* 2024;31:3699–3765. doi:10.1007/s11831-024-10100-y
46. Mohammed FA, Tune KK, Mohammed JA, Wassu TA, Muhie S. Early cervical cancer diagnosis with SWIN-transformer and convolutional neural networks. *Diagnostics (Basel).* 2024;14(20):2286. doi:10.3390/diagnostics14202286

Impact of polymerization reaction conditions on the stability of naproxen sodium

Wpływ warunków reakcji polimeryzacji na stabilność naproksenu sodowego

Agnieszka Gola^{1,A–F}, Adrianna Złocińska^{2,B–D}

¹ Department of Physical Chemistry and Biophysics, Faculty of Pharmacy, Wrocław Medical University, Poland

² Laboratory of Elemental Analysis and Structural Research, Faculty of Pharmacy, Wrocław Medical University, Poland

A – research concept and design; B – collection and/or assembly of data; C – data analysis and interpretation;

D – writing the article; E – critical revision of the article; F – final approval of the article

Polymers in Medicine, ISSN 0370-0747 (print), ISSN 2451-2699 (online)

Polim Med. 2025;55(1):67–71

Address for correspondence

Agnieszka Gola

E-mail: agnieszka.gola@umw.edu.pl

Funding sources

None declared

Conflict of interest

None declared

Acknowledgements

The authors would like to express their gratitude to Prof. Witold Musiał for his substantive support and invaluable assistance in the realization of this work.

Received on February 20, 2025

Reviewed on March 4, 2025

Accepted on March 5, 2025

Published online on March 28, 2025

Cite as

Gola A, Złocińska A. Impact of polymerization reaction conditions on the stability of naproxen sodium. *Polim Med.* 2025;55(1):67–71. doi:10.17219/pim/202644

DOI

10.17219/pim/202644

Copyright

Copyright by Author(s)

This is an article distributed under the terms of the Creative Commons Attribution 3.0 Unported (CC BY 3.0) (<https://creativecommons.org/licenses/by/3.0/>)

Abstract (in English)

Background. “Smart” polymers with reversible responsiveness to temperature stimuli are among the most promising carriers for controlled drug delivery, as temperature is a critical physiological factor within the human body. The majority of studies on the coupling of polymers with active substances have employed the method of attaching the drug to the polymer after its synthesis. The direct addition of the drug during the polymerization process has not been attempted, primarily due to concerns about the potential degradation of the active substance under harsh reaction conditions, such as elevated temperature and the presence of free radicals.

Objectives. This study aimed to evaluate the stability of a selected model drug – naproxen sodium (NAP), under extreme synthesis conditions, thereby providing insights into its resilience in such an environment.

Materials and methods. The Thermo Scientific Dionex UltiMate 3000 system was utilized for the chromatographic analyses. The separations were carried out on a Phenomenex Kinetex 2.6 µm, C18 100A, 150 × 2.1 mm column at 30°C. A high-performance liquid chromatography (HPLC) assay was carried out using gradient elution with a flow rate 0.4 mL/min and mobile phase of water 0.1% formic acid (A) and acetonitrile 0.1% formic acid (B) with the detector set at the wavelength of 254 nm.

Results. Chromatographic analysis showed new peaks indicating decomposition on NAP in ambient temperature in the presence of 2,2′-azobis(2-methylpropionamidine) dihydrochloride (AIBA).

Conclusions. Our findings indicate that NAP cannot be combined with the polymer during the polymerization process in extreme conditions of synthesis, specifically at temperatures of 70°C and in the presence of radicals, without undergoing decomposition. Nevertheless, further trials and tests are necessary to substantiate this hypothesis. One potential avenue for further investigation would be trials with alternative radical initiators, such as potassium persulfate (KPS).

Key words: naproxen sodium, 2,2′-azobis(2-methylpropionamidine) dihydrochloride, high-performance liquid chromatography (HPLC)

Abstract (in Polish)

Wprowadzenie. „Inteligentne” polimery wykazujące odwracalną reaktywność na bodźce temperaturowe są uważane za jedno z najbardziej obiecujących nośników do kontrolowanego dostarczania leków, ponieważ temperatura jest krytycznym czynnikiem fizjologicznym w organizmie człowieka. W większości badań dotyczących łączenia polimerów z substancjami aktywnymi stosowano metodę przyłączania leku do polimeru po jego syntezie. Nie podejmowano prób bezpośredniego dodawania leku podczas procesu polimeryzacji, głównie ze względu na obawy o potencjalną degradację substancji czynnej w ostrych warunkach reakcji, takich jak podwyższona temperatura i obecność wolnych rodników.

Cel pracy. Celem badania była ocena stabilności wybranego leku modelowego – naproksenu sodowego (NAP) – w ekstremalnych warunkach syntezy.

Materiał i metody. Do analiz chromatograficznych wykorzystano system Thermo Scientific Dionex UltiMate 3000. Separację przeprowadzono na kolumnie Phenomenex Kinetex 2,6 μm , C18 100A, 150 \times 2,1 mm w temperaturze 30°C. Badanie HPLC przeprowadzono przy użyciu elucji gradientowej z szybkością przepływu 0,4 ml/min i fazy ruchomej składającej się z kwasu mrówkowego 0,1% w wodzie (faza A) oraz kwasu mrówkowego 0,1% w acetonitrylu (faza B) z detekcją przy długości fali 254 nm.

Wyniki. Analiza chromatograficzna wykazała obecność nowych pików wskazujących na rozkład NAP w temperaturze otoczenia w obecności dichlorowodoru 2,2'-azobis(2-metylopropionamidyny) (AIBA).

Wnioski. Wyniki badań wskazują, że NAP nie może być łączony z polimerem podczas procesu polimeryzacji prowadzonego w ekstremalnych warunkach syntezy, w szczególności w temperaturze 70°C i w obecności rodników, ponieważ ulega degradacji. Niemniej jednak konieczne są dalsze próby i testy w celu potwierdzenia tej hipotezy. Jednym z potencjalnych kierunków dalszych badań byłyby próby z alternatywnymi inicjatorami rodnikowymi, takimi jak nadsiarczany potasu (KPS).

Key words (in Polish): naproksen sodowy, dichlorowodorek 2,2'-azobis(2-metylopropionamidyny), wysokosprawna chromatografia cieczowa (HPLC)

Background

Polymers, particularly thermosensitive polymers, serve as a crucial class of drug carriers, enabling both the transportation of active ingredients and their controlled release. This capability significantly enhances the therapeutic efficacy and bioavailability of drugs. Polymers in drug delivery systems enable the modification of release profiles to meet specific therapeutic requirements.¹ The growing use of thermosensitive polymers in advanced drug delivery systems is driven by their biocompatibility, biodegradability and ability to undergo structural or property changes in response to temperature fluctuations.^{2–4} These polymers can remain insoluble at body temperature but undergo structural transitions upon heating, leading to controlled drug release.⁵ In most cases, drugs are incorporated into thermosensitive polymers after polymerization. This method stabilizes both the carrier and the active ingredient, minimizing the risk of chemical reactions that could compromise drug efficacy and polymer integrity.^{6,7} Additionally, this approach allows for precise control over the structure and properties of both the carrier and the drug substance, which is essential for ensuring safety and therapeutic efficacy.

An alternative approach, which is less common, involves incorporating the active ingredient during the polymerization process. This approach is less frequently employed due to the inherent risks associated with uncontrolled reactions that may result in drug or polymer degradation.^{8,9} Nevertheless, this method may confer advantages in the creation of more integrated systems that facilitate enhanced stability and control of drug release.^{10,11} However, it is imperative

to exercise caution when selecting monomers and polymerization techniques in order conditions to minimize the risk of drug degradation.¹²

The advent of modern polymerization techniques allow for more precise adjustments, promoting safer and more efficient drug–polymer binding at the polymerization stage under controlled conditions.^{13–16} Nevertheless, in order to develop stable and safe thermosensitive polymeric systems with enhanced stability and safety, it is essential to gain insight into the nature of drug–polymer interactions and their behavior in complex biological environments. This would facilitate the full realization of the polymer potential of these systems in the context of medicine.^{17,18}

Objectives

The objective of this study was to evaluate the chemical stability of naproxen sodium (NAP) under extreme conditions commonly encountered during synthesis processes. Specifically, the study aimed to investigate the compound's behavior at an elevated temperature of 70°C and in the presence of radicals generated by 2,2'-azobis(2-methylpropionamidine) dihydrochloride (AIBA), a thermal radical initiator. These conditions simulate a high-stress environment that could potentially lead to the degradation of NAP. The study seeks to provide insights into the resistance of NAP to thermal and radical-induced degradation, facilitating the optimization of synthesis protocols and ensuring product quality. Retention times will serve as the basis for qualitative analysis.

Materials and methods

Reagents: NAP was a free sample from Hasco-Lek S.A. (Wrocław, Poland), while 97% AIBA was purchased from Sigma-Aldrich (Sternheim, Germany). The deionized water ($<0.06 \mu\text{S cm}^{-1}$) was filtered using an HLP 20 system with a $0.22 \mu\text{m}$ microfiltration capsule (Hydrolab, Straszyn, Poland). It met the requirements of the PN-EN ISO 3696:1999 standards for analytical laboratories. All chemicals and solvents were used as received without further purification or modification. Chromatographic solvents used were formic acid (Sigma-Aldrich), acetonitrile (Sigma-Aldrich) and demineralized, bi-distilled water. The Thermo Scientific Dionex UltiMate 3000 system (Thermo Scientific Dionex, Sunnyvale, USA), equipped with an LPG-3400SD pump module, WPS-3000TSL autosampler, and TCC-3000SD column oven, a UV DAD-3000 detector, RI RefractoMax 521 refractometric detector, and FLD-3400RS fluorescence detector were utilized for the chromatographic analyses. The separations were performed on an Phenomenex Kinetex $2.6 \mu\text{m}$, C18 100 Å, $150 \times 2.1 \text{ mm}$ column at a temperature of 30°C . A high-performance liquid chromatography (HPLC) assay was carried out using gradient elution with a flow rate 0.4 mL/min and mobile phase of water 0.1% formic acid (phase A) and acetonitrile 0.1% formic acid (phase B) with the detector set at the wavelength of 254 nm . A $5\text{-}\mu\text{L}$ sample was injected into the column, with a total run time of 13 min . The subsequent gradient elution began with 35% mobile phase B, maintained for 2 min . Then, mobile phase B was increased to 95% over 5 min and held at this level for an additional 2 min . From the 9^{th} to the 10^{th} min, the gradient returned to 35% mobile phase B, where it remained stable until the 13^{th} min.

Results and Discussion

Aqueous solutions of NAP, AIBA and a NAP/AIBA mixture were analyzed using HPLC. Chromatographic analysis was conducted on samples prepared at room temperature and on samples subjected to 70°C for 2.5 h . Table 1 and Fig. 1 show the retention times for the systems under examination.

The NAP chromatogram obtained at room temperature showed no new peaks, but a slight shift towards a higher retention time. This shift may be attributed to intermolecular interactions and subtle alterations in the analyte's structure induced by elevated temperature. In aqueous media, NAP is susceptible to hydrolysis.¹⁹ However, at neutral or alkaline pH, the rate of hydrolytic degradation is relatively low.²⁰ Nevertheless, an increase in temperature can facilitate hydrolysis. Furthermore, elevated temperatures can also induce the breakdown of the aromatic ring, but this process is significant at temperatures above 100°C .²¹ Moreover, a comparison of the chromatograms of NAP and AIBA to chromatogram of the NAP/AIBA mixture at room

Table 1. Retention time of the peaks exceeding a relative area of 2%

Compounds/mixtures - aqueous solutions	Retention time [min] after exposure conditions	
	ambient temperature	70°C , 2.5 h
NAP	1.130	1.167
AIBA	0.770	not tested
NAP + AIBA	0.813	0.820
	5.547	0.953
	6.450	5.553
		6.460

NAP – naproxen sodium; AIBA – 2,2'-azobis(2-methylpropionamidine) dihydrochloride

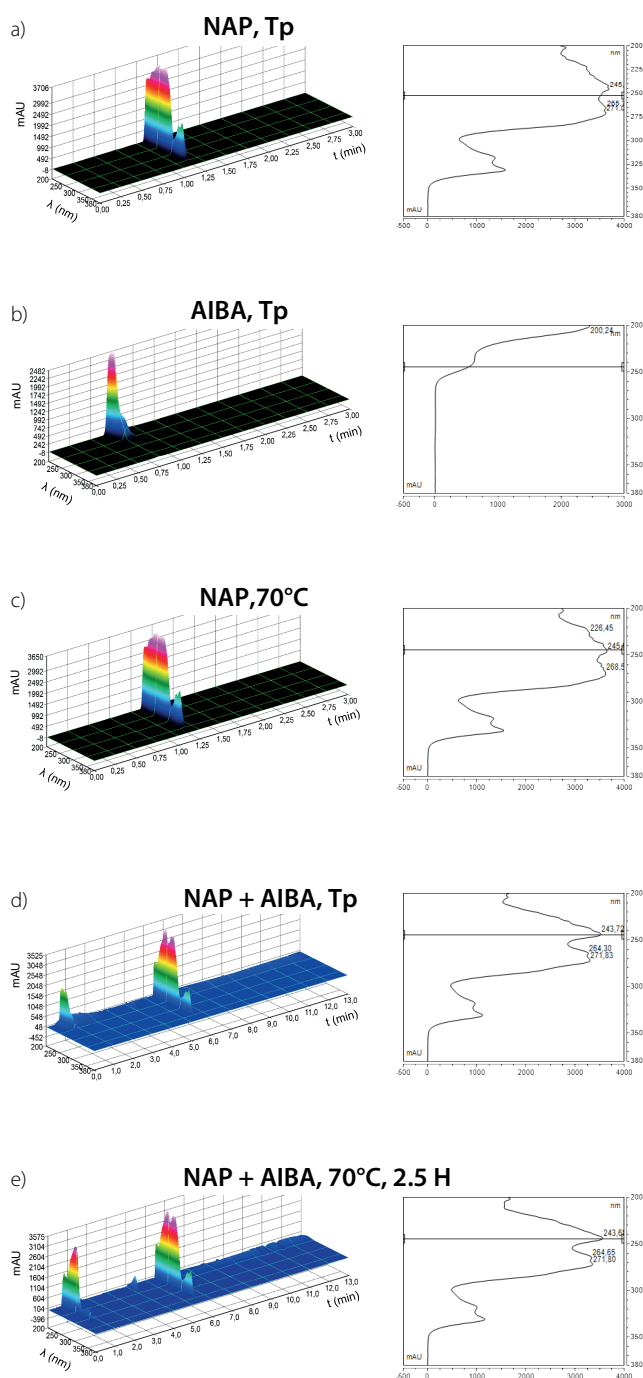


Fig. 1. 3D plots of analyzed systems

temperature revealed the absence of the NAP peak and the emergence of new peaks, indicative of NAP degradation or formation of new products. This observation suggests that NAP is unstable at room temperature in the presence of the radical initiator AIBA, even prior to radical formation. This behavior may indicate particular chemical interactions between NAP and AIBA, resulting in the formation of complexes or the initiation of a process by trace amounts of radicals. The formation of complexes between AIBA and NAP is theoretically possible. Some authors have used AIBA in synthesis, incorporating the drug into the polymeric matrix during the synthesis process. However, in this study, the direct potential interaction between AIBA and the drug was specifically evaluated.²² AIBA is a hydrophilic compound with 2 amide groups, capable of hydrogen bonding and electrostatic interactions in an aqueous environment. Moreover, in solution, AIBA can exist in an ionized form, consisting of chloride ions and protonated amide groups.

Naproxen sodium is a compound containing a carboxylate group (ionized in basic or neutral media) and an aromatic ring, enabling it to engage in both π - π interactions and hydrogen bonding. It can therefore be inferred that electrostatic interactions may occur between the ionized carboxylate group of NAP and the protic groups of AIBA.

It is also possible for a hydrogen bond to form between the amide group of AIBA and the carboxylate group of NAP. Furthermore, the aromatic ring of NAP may engage in hydrophobic interactions with non-polar AIBA fragments. As a polar solvent, water can solvate both AIBA and NAP, thereby reducing the likelihood of interactions between the two.

However, in the presence of ions (Cl^- from AIBA or Na^+ from NAP), specific complex interactions may take place. In contrast, the likelihood of trace amounts of AIBA radicals forming at room temperature is low, as their generation requires homolytic cleavage of the $\text{N}=\text{N}$ bond at temperatures in the range of 60–80°C. Additionally, photochemical decomposition is a possible mechanism,²³ but since the sample was not exposed to direct or prolonged UV radiation, this factor can be considered negligible.

Conclusions

The results suggest that NAP may not be a suitable candidate for incorporation during the polymerization process. Chromatographic analysis revealed the emergence of new peaks even at room temperature in the presence of AIBA, indicating NAP decomposition and the formation of new products. However, further research and additional experimental trials are required to gain a comprehensive understanding of the underlying mechanisms and the processes involved.

Data availability

The datasets generated and/or analyzed during the current study are available from the corresponding author on reasonable request.

Consent for publication


Not applicable.

Use of AI and AI-assisted technologies

Not applicable.

ORCID iDs

Agnieszka Gola –  <https://orcid.org/0000-0001-8034-5663>

Adrianna Złocińska –  <https://orcid.org/0000-0003-2540-7571>

References

- Kumari A, Yadav SK, Yadav SC. Biodegradable polymeric nanoparticles based drug delivery systems. *Colloids Surf B Biointerfaces*. 2010;75(1):1–18. doi:10.1016/j.colsurfb.2009.09.001
- Yu Y, Cheng Y, Tong J, Zhang L, Wei Y, Tian M. Recent advances in thermo-sensitive hydrogels for drug delivery. *J Mater Chem B*. 2021;9(13):2979–2992. doi:10.1039/D0TB02877K
- Khan B, Arbab A, Khan S, et al. Recent progress in thermosensitive hydrogels and their applications in drug delivery area. *MedComm Biomater Appl*. 2023;2(3):e55. doi:10.1002/mba2.55
- Sung YK, Kim SW. Recent advances in polymeric drug delivery systems. *Biomater Res*. 2020;24(1):12. doi:10.1186/s40824-020-00190-7
- Abuwatfa WH, Awad NS, Pitt WG, Hussein GA. Thermosensitive polymers and thermo-responsive liposomal drug delivery systems. *Polymers (Basel)*. 2022;14(5):925. doi:10.3390/polym14050925
- Martinez Espinoza MI, Gül S, Mugnaini L, Cellesi F. Oligo(ethylene glycol) methacrylate copolymer-modified liposomes for temperature-responsive drug delivery system. *Molecules*. 2024;29(23):5511. doi:10.3390/molecules29235511
- Gong J, Hou L, Ching YC, Ching KY, Hai ND, Chuah CH. A review of recent advances of cellulose-based intelligent-responsive hydrogels as vehicles for controllable drug delivery system. *Int J Biol Macromol*. 2024;264:130525. doi:10.1016/j.ijbiomac.2024.130525
- Janrao C, Khopade S, Bavaskar A, Gomte SS, Agnihotri TG, Jain A. Recent advances of polymer based nanosystems in cancer management. *J Biomater Sci Polym Ed*. 2023;34(9):1274–1335. doi:10.1080/09205063.2022.2161780
- Koide H, Yamaguchi K, Sato K, et al. Engineering temperature-responsive polymer nanoparticles that load and release paclitaxel, a low-molecular-weight anticancer drug. *ACS Omega*. 2024;9(1):1011–1019. doi:10.1021/acsomega.3c07226
- Idumah CI. Recently emerging advancements in polymeric nanogel nanoarchitectures for drug delivery applications. *Int J Polym Mater Polym Biomater*. 2024;73(2):104–116. doi:10.1080/00914037.2022.2124256
- Gradzielski M. Polyelectrolyte-surfactant complexes as a formulation tool for drug delivery. *Langmuir*. 2022;38(44):13330–13343. doi:10.1021/acs.langmuir.2c02166
- De Leo V, Milano F, Agostiano A, Catucci L. Recent advancements in polymer/liposome assembly for drug delivery: From surface modifications to hybrid vesicles. *Polymers (Basel)*. 2021;13(7):1027. doi:10.3390/polym13071027
- Alhewaitay AM, Khan I, Buabeng ER. Advancements in polymer science: Synthesis, characterization, and biomedical applications of homopolymers and copolymers. *Open J Polym Chem*. 2024;14(3):167–198. doi:10.4236/ojpcchem.2024.143008

14. Matyjaszewski K. Atom transfer radical polymerization (ATRP): Current status and future perspectives. *Macromolecules*. 2012;45(10):4015–4039. doi:10.1021/ma3001719
15. Sun W, Liu W, Wu Z, Chen H. Chemical surface modification of polymeric biomaterials for biomedical applications. *Macromol Rapid Commun*. 2020;41(8):1900430. doi:10.1002/marc.201900430
16. Ansari MJ, Rajendran RR, Mohanto S, et al. Poly(N-isopropylacrylamide)-based hydrogels for biomedical applications: A review of the state-of-the-art. *Gels*. 2022;8(7):454. doi:10.3390/gels8070454
17. Tian ML, Zhou JF, Qi X, Shen R. Thermo-sensitive hydrogel and their biomedical applications. *IOP Conf Ser Earth Environ Sci*. 2021;714(3):032062. doi:10.1088/1755-1315/714/3/032062
18. Fan R, Cheng Y, Wang R, et al. Thermosensitive hydrogels and advances in their application in disease therapy. *Polymers (Basel)*. 2022;14(12):2379. doi:10.3390/polym14122379
19. Venkatarao P. Novel validated stability-indicating UPLC method for the estimation of naproxen and its impurities in bulk drugs and pharmaceutical dosage form. *Sci Pharm*. 2012;80(4):965–976. doi:10.3797/scipharm.1207-12
20. Songnaka N, Sawatdee S, Atipairin A. Stability-indicating HPLC method for determination of naproxen in an extemporaneous suspension. *Res J Pharm Technol*. 2018;11(10):4332. doi:10.5958/0974-360X.2018.00793.X
21. Medeiros RS, Ferreira APG, Cavaleiro ETG. Thermal behavior of naproxen and ketoprofen nonsteroidal anti-inflammatory drugs. *J Therm Anal Calorim*. 2020;142(2):849–859. doi:10.1007/s10973-020-09389-1
22. Zhang Z, Wang B. Synthesis of highly efficient D-naproxen imprinted polymer and investigation of their specific performance. *J Appl Polym Sci*. 2009;113(2):1050–1062. doi:10.1002/app.30048
23. Parys W, Dołowy M, Pyka-Pająk A. Rapid TLC with densitometry for evaluation of naproxen stability. *Processes*. 2020;8(8):962. doi:10.3390/pr8080962

